Detailed source term estimation of the atmospheric release for the Fukushima Daiichi Nuclear Power Station accident by coupling simulations of atmospheric dispersion model with improved deposition scheme and oceanic dispersion model

G. Katata[1], M. Chino[1], T. Kobayashi[1], H. Terada[1], M. Ota[1], H. Nagai[1], M. Kajino[2], R. Draxler[3], M. C. Hort[4], A. Malo[5], T. Torii[6] and Y. Sanada[7]

[1]{Japan Atomic Energy Agency (JAEA), Tokai, Naka, Ibaraki, 319-1195, Japan; now at Atmospheric Environmental Research, Institute of Meteorology and Climate Research, Karlsruhe Institute of Technology, Germany}

[2]{Meteorological Research Institute, Japan Meteorological Agency (JMA), Tsukuba, Ibaraki, 305-0052, Japan}

[3]{Air Resources Laboratory, National Oceanic and Atmospheric Administration (NOAA), University Research Court College Park, Maryland, 20740, USA}

[4] {Met Office, Exeter, Devon, EX1 3PB, United Kingdom}

[5] {Canadian Meteorological Centre (CMC), Dorval, Quebec, H9P 1J3, Canada}

[6]{JAEA, Chiyoda, Tokyo, 100-8577, Japan}

[7]{JAEA, Fukushima, Fukushima, 960-1296, Japan}

Correspondence to: G. Katata (katata.genki@jaea.go.jp)

Abstract

Temporal variations in the amount of radionuclides released into the atmosphere during the Fukushima Daiichi Nuclear Power Station (FNPS1) accident and their atmospheric and marine dispersion are essential to evaluate the environmental impacts and resultant radiological doses to the public. In this paper, we estimate the detailed atmospheric releases during the accident using reverse estimation method which calculates the release rates of radionuclides by comparing measurements of air concentration of a radionuclide or its dose rate in the environment with the ones calculated by atmospheric and oceanic transport,

dispersion and deposition models. The atmospheric and oceanic models used are WSPEEDI-II (Worldwide version of System for Prediction of Environmental Emergency Dose Information), and SEA-GEARN-FDM, both developed by the authors. A sophisticated deposition scheme, which deals with dry and fogwater depositions, cloud condensation nuclei (CCN) activation and subsequent wet scavenging due to mixed-phase cloud microphysics (in-cloud scavenging) for radioactive iodine gas (I_2 and CH_3I) and other particles (CsI, Cs, and Te), was incorporated into WSPEEDI-II to improve the surface deposition calculations. The results revealed that the major releases of radionuclides due to the FNPS1 accident occurred in the following periods during March 2011: the afternoon of 12 March due to the wet venting and hydrogen explosion at Unit 1, midnight of 14 March when the SRV (Safely Relief Valve) was opened three times at Unit 2, the morning and night of 15 March, and the morning of 16 March. According to the simulation results, the highest radioactive contamination areas around FNPS1 were created from 15 to 16 March by complicated interactions among rainfall, plume movements, and the temporal variation of release rates. The simulation by WSPEEDI-II using the new source term reproduced the local and regional patterns of cumulative surface deposition of total ^{131}I and ^{137}Cs and air dose rate obtained by airborne surveys. The new source term was also tested using three atmospheric dispersion models (MLDP0, HYSPLIT, and NAME) for regional and global calculations and the calculated results showed in good agreement with observed air concentration and surface deposition of ^{137}Cs in East Japan.

1 Introduction

A significant amount of radioactive material was accidentally emitted into the atmosphere from the Fukushima Daiichi Nuclear Power Station (hereafter referred to as FNPS1) due to the catastrophic earthquake and tsunami on 11 March 2011. This caused radiological contamination not only around FNPS1 but over a wide region of Japan (NRA, 2012a). To assess the magnitude of the accident and radiological doses, an accurate estimation of the source term of the radionuclides discharged into the atmosphere is required.

After the accident, the source term of total ^{131}I, which includes all the chemical forms of ^{131}I (hereinafter ^{131}I) and ^{137}Cs was estimated by authors from the Japan Atomic Energy Agency (JAEA) using a reverse estimation method (UNSCEAR, 2014). This method calculates the release rates of radionuclides (Bq h^{-1}) by coupling the atmospheric dispersion simulation made with a unit release rate (1Bq h^{-1}) with environmental monitoring data. The ratio of the

monitoring data to the dispersion calculation provides an estimate of the source term. Chino et al. (2011) carried out the first estimation of the source term of ^{131}I and ^{137}Cs from 12 March to 5 April 2011. Katata et al. (2012a) estimated a more detailed source term for 15 March 2011 when the highest radiological polluted area was created. Katata et al. (2012b) revised the source term of Chino et al. (2011) for the early phases (12 to 14 March 2011) of the accident. Terada et al. (2012) assembled the above source terms and slightly refined the release rate after 16 March and extended it to 1 May 2011 (hereinafter the last source term in Introduction). They also showed the regional and local atmospheric dispersion patterns of the radionuclides for March 2011.

The last source term has been validated using atmospheric dispersion simulation results compared with the environmental data which were not used for the source term estimation (e.g., daily fallout and surface deposition) and by comparison with other source terms created using different approaches and datasets. Terada et al. (2012) showed that WSPEEDI-II could reproduce most of observed daily fallout in Eastern Japan from 20 to 31 March within a factor 10 using the last source term. Later on, Morino et al. (2013) carried out atmospheric dispersion simulations using several source terms and found that when the last source term was used, the surface deposition pattern of ^{137}Cs in Eastern Japan was reproduced with higher accuracy than when using any of the other source terms. Draxler et al. (2014) showed that five different atmospheric dispersion and meteorological models overall reproduced regional patterns in observed ^{137}Cs deposition and air concentration of ^{131}I and ^{137}Cs when using the last source term. Meanwhile, Hirao et al. (2013) also estimated the source term using an inverse estimation method (UNSCEAR, 2014) by coupling their atmospheric dispersion model with air concentration and daily fallout data in Eastern Japan. Their result agreed with the last source term for many of the large emission events despite using different sets of monitoring data, further supporting the reliability of the last source term. Saunier et al. (2013) and Winiarek et al. (2014) also estimated the source term for the major releases of 14 and 15 March 2011 by inverse estimation methods using air dose rate and daily fallout data, and the airborne survey of ^{137}Cs surface deposition in Eastern Japan. Their results were comparable to the last source term for those periods.

While the last source term has been supported by the many studies summarized above, three major improvements are required to determine a more precise source term. First, the deposition scheme of WSPEEDI-II needs to be modified to improve the atmospheric

dispersion simulation that affects the accuracy of the source term estimation. The previous scheme employed constant values for the dry deposition velocities and a simple exponential function of precipitation intensity for the wet scavenging coefficients, which are also widely used in the deposition schemes of many other atmospheric dispersion models (Table 1). However, this scheme is insufficient to simulate complicated processes of dry deposition on various surface characteristics and wet scavenging due to mixed phase cloud microphysics (in-cloud scavenging). For example, Morino et al. (2013) showed the prediction accuracy of the surface deposition pattern of ^{137}Cs in Eastern Japan strongly depended on the wet scavenging coefficient. Fogwater deposition is also completely missing in any of the current atmospheric dispersion models (Table 1). Thus, we introduce a new scheme consisting of comprehensive parameterizations for dry, wet, and fogwater depositions of gaseous and particulate radionuclides based on existing modeling approaches into WSPEEDI-II (hereafter the modified WSPEEDI-II).

Table 1

Second, the last source term was computed using environmental monitoring data collected over the land areas of Eastern Japan. However, when plumes flowed directly toward Pacific Ocean, the release rates were simply interpolated between the estimated values during on-shore flow. The first results of the source term estimation using both atmospheric and oceanic dispersion models by Kobayashi et al. (2013) revealed that the model calculation with the last source term underestimated the seawater surface concentration of ^{134}Cs in Pacific Ocean. However, their atmospheric dispersion simulation using the source term modified by oceanic data overestimated deposition amounts over the land because their correction was applied for both off-shore and on-shore flow cases. The overestimation of the deposition amount over the land areas of Japan has also been reported by Morino et al. (2013) when using the source term estimated by global simulations with the air concentration data sampled at the Comprehensive Nuclear-Test-Ban Treaty Organization (CTBTO) stations (Stohl et al., 2012). The surface deposition of ^{137}Cs was also clearly overestimated in regional calculations. Thus, only the release rates of the plumes which directly flowed toward the ocean should be re-computed using the coupled simulation of the atmospheric and oceanic dispersion models. For other cases the source term is estimated using only the environmental data collected over the land.

Finally, in the last source term, the release rates in the early phase of the accident have been estimated primarily using the air dose rate data observed far from the FNPS1 due to the lack of routine operating equipment (e.g., stack monitors, radiation and meteorological stations) within 20 km from the station (Katata et al., 2012a, b). Three years after the accident, additional environmental monitoring data from 12 to 31 March 2011 have become available including the air dose rates measured within 20 km from FNPS1 (Fukushima Prefecture, 2012), a detailed ^{131}I deposition map around the station (Torii et al., 2013), and dust sampling (US DOE, 2011; NRA, 2012b). This enables us to make a more detailed estimation of the atmospheric releases during the accident using the reverse estimation method by combining the modified WSPEEDI-II results with these additional monitoring data.

Thus, the present study aims to determine the detailed source terms of ^{131}I and ^{137}Cs during the FNPS1 accident with the reverse estimation method (section 2.1) combining the above new data (section 2.2) and simulations using WSPEEDI-II with a modified deposition scheme (Appendix A) and an offline coupling of the atmospheric and oceanic dispersion models (section 2.3). The estimation result of the source term is presented in chapter 3. The estimated source term is validated by comparing the atmospheric transport and deposition simulations by modified WSPEEDI-II with airborne monitoring data of air dose rate and surface deposition of ^{131}I and ^{137}Cs in Eastern Japan (subsection 4.1.1). Moreover, the source term is independently evaluated based on the simulations of different atmospheric dispersion models by demonstrating model-observation comparisons in atmospheric concentration and surface deposition over regional and global scales (subsection 4.1.2). Finally, the difference between the new source term and those from prior studies is discussed based on the simulation results (section 4.2).

2 Material and methods

2.1 Source term estimation method

A typical approach to estimate the source term is by coupling environmental measurements of radionuclides with simulations of their atmospheric dispersion using a reverse or inverse estimation method (UNSCEAR, 2014).

A reverse estimation method evaluates the release rates of radionuclides by comparing measurements of air concentration of a radionuclide or dose rate in the environment with calculated one by atmospheric transport, dispersion and deposition models (ATDM) for a unit

release of a radionuclide. The release rate is estimated by the ratio of the measurement to calculation result. This simple comparison without consideration of the uncertainty of the ATDM results may cause the large errors, and, consequently, expert judgment is essential to correct the discrepancy between the measurement and calculation.

An inverse estimation method evaluates the release rates in an objective way using an algorithm to minimize the differences between calculated and measured air concentrations or dose rates. This method is mathematically sophisticated and technical errors are explicitly considered. However, to return the highest quality estimates, a large number of measured values of air concentrations or dose rates in time and space and high-accuracy meteorological fields for the ATDM simulations are required. The accuracy of meteorological field is essential, particularly if this method is applied to local-scale dispersion simulations with a point source. The uncertainties caused by lack of above requirements can reduce if a priori release rates are provided from other estimations.

This paper aims at estimating the highest quality source term which will contribute to the accurate assessment of radiological impacts from local to regional scales. For this purpose, measurements of air concentrations or air dose rates in the local area are used if available rather than more distant data. The merit of using local data is that it is easy to find the correlation between a specific release and the increase of air concentration at measurement point from atmospheric transport simulation by the ATDM, because sharp peaks of both measured and calculated values appearing in the local area clearly show the arrival and departure of the plume. For most comparisons, air concentrations of radionuclides are normally used. However, in the case of the FNPS1 accident, time dependent air concentrations in the local area from 11 to 31 March were measured at Japan Atomic Energy Agency (hereinafter JAEA-Tokai) located at 100 km south of FNPS1. Other groups provided a small amount of dust sampling data using monitoring cars at various points mainly after 20 March. Furthermore, due to change of wind direction, there were several days when no plume was monitored at the measuring points in the local area. For the source term estimation during those days, air dose rates are used as the second choice, which means that the data available for comparison are a mixture of air concentrations and air dose rates in time. Meteorological measurements in the local area around FNPS1during this period, which are necessary to ensure the accuracy of meteorological input to ATDM, are also limited because the observation systems were inoperative due to the earthquake and tsunami.

Considering the above conditions, we used the reverse estimation method to estimate the source term following our previous studies before we newly try the inverse estimation method. It is better to use the same method and show the difference between our old and new estimations resulting from the utilization of additional data and modification of the deposition scheme. This result is expected to become a priori source term for the inverse estimation method in future studies.

Figure 1 depicts the flowchart of the source term estimation based upon coupling the simulations of the atmospheric and oceanic dispersion models. First, the release rates of the plumes discharged from FNPS1 are estimated by combining the atmospheric dispersion calculation and the data of radionuclide air concentrations and dose rates measured over the land areas of East Japan (subsection 2.1.1). When the plume directly flowed toward the Pacific Ocean, the release rates are initially determined by temporally interpolating two available values just before and after this period. Then, only the interpolated values are revised by coupling a combination of models of atmospheric and oceanic dispersion and the Pacific Ocean sea surface concentrations (subsection 2.1.2). The role of the atmospheric dispersion model is to provide the oceanic dispersion model with an estimate of the radionuclide deposition to the sea surface.

Figure 1

2.1.1 Source term estimation by using data over the land

The release rates of individual radionuclides are estimated by the reverse estimation method following our previous work (Chino et al., 2011; Katata et al., 2012a, b), i.e., coupling environmental monitoring data with atmospheric dispersion simulations, assuming a unit release rate (1 Bq h^{-1}). Release rates are obtained as the ratio of measured to calculated air concentrations of nuclide *i* at the sampling points, as follows:

$$Q_{i,t} = M_{i,t} / C_{i,t} , \quad (1)$$

where $Q_{i,t}$ is the release rate (Bq h^{-1}) of nuclide *i* when discharged into the atmosphere during the time segment *t* with a constant release rate, $M_{i,t}$ the measured air concentration (Bq m^{-3}) of *i* in the plume released during the time segment *t* and $C_{i,t}$ the dilution factor (h m^{-3}) of *i*, which

is equal to the calculated air concentration of *i* in the plume released during the time segment *t* at the measurement point calculated under the assumption of a unit release rate. This method, using air concentration data, is more reliable than the methods using air dose rates because it does not require an additional assumption on the composition of the radionuclides contributing to the dose rates.

Depending on the number of available data, we estimated release rates using Eq. (1) as follows: The number of dust sampling data in the Fukushima Prefecture was limited and, furthermore, the concentration data relevant to a specific plume was usually one and at most two or three (see subsection 2.2.1) data points. Exceptionally, the data at JAEA-Tokai provided temporal variation of air concentrations throughout the period. First, when only one data point is available for the specific plume, we simply use Eq. (1). Second, if concentration values available for the source term estimation were simultaneously observed at more than two sites, release rates were determined by averaging the source term estimated at all sites. If the time dependent air concentrations measured at one location (JAEA-Tokai) were available for comparison, the peak values from both the measurement and calculation were used in Eq. (1).

Since the uncertainty of model simulation is the primary cause of the discrepancy in the spatiotemporal distribution of the plume between measurements and simulations, the above procedures cannot be applied systematically, and the correction of this discrepancy by 'expert judgment' is necessary to reduce the impact of model uncertainty on the source term estimation. The process is to check all available measurements to see if the plume is reproduced appropriately or not for comparing calculations with the measurements, and to determine if the discrepancy is caused mainly by errors in the calculated wind direction. If the plume flow direction is clearly different from the measured wind direction, the calculated plume is rotated to match the measured wind direction and Eq. (1) is applied. The use of peak values corrects any discrepancy in the timing of the arrival of the peak air concentrations between measurements and simulations (at JAEA-Tokai). We assume that the peak values of measurements and simulations are comparable even though the timing or temporal pattern of the arrival of the peak is different because the central plume axis passes across the sampling point differently between measurements and simulations.

When air concentration data are not available, the release rates are estimated by comparing the observed spatial patterns and/or temporal changes of air dose rates. To use air dose rates,

the fractional composition of major radionuclides must be assumed. However, for measured concentrations of noble gases, a primary component of the composition was not available in the local area. Thus, we do not use the peak values of air dose rates during the passage of plume containing noble gases, but use the slopes of the air dose rate after the passage of the peak which is due to the radionuclides on the ground surface (i.e., ground-shine) for the source term estimation. The procedure to determine the composition is described in subsection 2.3.3. This method is applied to estimate the release rate in the afternoon of 12 March when the venting and hydrogen explosion occurred at Unit 1, and in the morning of 15 March to the noon of 16 March. First, the temporal changes of air dose rates from ground-shine at the measurement points are estimated by the modified WSPEEDI-II for a unit release. Then, the release rate (Bq h^{-1}) is computed from the ratio of the measured ground-shine to calculate one. Here, we find the appropriate observed point which can be used for the source term estimation by looking for when and where the specific plume increases air dose rate by the simulation of the WSPEEDI-II. For the estimation of the source term during 15–16 March, we need to determine the "net" increase of ground-shine due to the deposition of the objective plume, because the monitored air dose rates due to the ground-shine are influenced by multiple deposition events (i.e., deposition from the past plumes). The net increase is then estimated by subtracting the effect of the past plumes from the ground-shine after the passage of the objective plume.

2.1.2 Source term estimation by using data over the ocean

This estimation is applied to only the periods when the plume flowed toward the ocean, while our previous work (Kobayashi et al., 2013) estimated the release rates throughout the simulation period using the oceanic monitoring data. The judgment of whether the plume during each segment directly flowed toward the ocean is done by evaluating the simulation of the modified WSPEEDI-II, observed wind direction, and monitoring data on the land. Two sets of off-line coupling simulations of modified WSPEEDI-II and SEA-GEARN-FDM are carried out: one simply uses the source term estimated by the method in subsection 2.1.1 (hereinafter "New-land" source term) throughout the calculation period, and the other uses the release rates for each time segment separating the New-land source term into an arbitrary number of segments. In both cases, the input data of daily cumulative deposition of ^{134}Cs on sea surface to SEA-GEARN-FDM are supplied from the WSPEEDI calculations using the New-land source term.

In the first simulation, the comprehensive correction index of the New-land source term at the sampling point j (R_j) can be calculated as follows:

$$R_j = N_j / D_j \,, \tag{2}$$

where N_j and D_j are the measurements and SEA-GEARN-FDM calculations of sea surface concentration of ^{134}Cs (Bq L^{-1}) at the sampling point j over the Pacific Ocean, respectively. Instead of ^{137}Cs, we used ^{134}Cs as a standard radionuclide because imprints of former atmospheric nuclear tests were detected in the seawater sample of ^{137}Cs. Note that, from a preliminary comparison between measurement points of sea surface concentration of ^{134}Cs and the oceanic dispersion area simulated using the source term of direct releases of ^{134}Cs from FNPS1 into the ocean, we chose only observational points for ^{134}Cs that are not affected by the direct release for the source term estimation.

In the second simulation, the sea surface concentration $O_{j,t}$ (Bq L^{-1}) of ^{134}Cs at the sampling point of j that originated from the discharge of time segment t can be calculated using SEA-GEARN-FDM in a manner similar to the first simulation. If the total number of time segments is represented as nt, the contribution ratio of t at the sampling point of j, $P_{j,t}$, can be defined as the ratio of calculated sea surface concentration for the time segment of t to that for the whole simulation period, expressed as:

$$P_{j,t} = \frac{O_{j,t}}{\sum_{t=1}^{nt} O_{j,t}} = \frac{O_{j,t}}{D_j} \,. \tag{3}$$

Here, a large value of $P_{j,t}$ indicates a large contribution of the release for the time segment t to the concentration at the sampling point j accumulated for whole simulation period, i.e., D_j in Eq. (2). The correction index S_t of the New-land source term for t is expressed by weighting the contribution ratio $P_{j,t}$ at sampling point of j:

$$S_t = 10^{\sum_{j=1}^{np}\left(P_{j,t}\cdot \log_{10} R_j\right)/\sum_{j=1}^{np} P_{j,t}} \,, \tag{4}$$

where np is the total number of sampling points (46 in this study). By using Eq. (4), the new release rate of ^{134}Cs for the segment t, $U_{i,t}$ (Bq h^{-1}), is finally obtained by multiplying the release rate of ^{134}Cs for the same time segment in the New-land source term, $Q_{i,t}$, with the correction index, S_t:

$$U_{i,t} = Q_{i,t} S_t \,. \tag{5}$$

For other radionuclides, release rates are calculated by multiplying $U_{i,t}$ of Eq. (5) with the time interpolated composition ratio of each nuclide to ^{134}Cs for the New-land source term.

2.2 Observational data

2.2.1 Observational data for source term estimation over the land

The datasets of dust sampling and air dose rates (ground-shine) used for the source estimation over the land (subsection 2.1.1) are summarized in Tables 2 and 3, respectively. The location maps of sampling points are illustrated in Fig. 2. For the period of 12 March and 15–16 March 2011, the release rates are estimated primarily using ground-shine data observed by portable monitors (Fukushima Prefecture, 2011a, b; Ibaraki Prefecture, 2011; Tochigi Prefecture, 2011; TEPCO, 2011a) and at automatic monitoring posts (Fukushima Prefecture, 2012) located at 22–81 km and 4–21 km downwind from FNPS1, respectively. For other periods, we use the dust sampling data of ^{131}I and ^{137}Cs in Fukushima Prefecture (TEPCO, 2011a; NISA 2011; NRA, 2011, 2012b; US DOE, 2012) and at JAEA-Tokai in Ibaraki Prefecture (Ohkura et al., 2012) (Fig. 2). Here, the dust sampling in Fukushima Prefecture was carried out by limited number of monitoring cars and consequently, the data are not continuous in time and there are only a few data points each day. At JAEA-Tokai, which is the closest monitoring station of FNPS1, high-resolution temporal variations of air concentrations including both gaseous and particulate forms of ^{131}I was observed continuously. Compared with our previous studies (Katata et al., 2012b; Terada et al., 2012), the data of air dose rate within 20 km from FNPS1 (Fukushima Prefecture, 2012) and dust sampling (US DOE, 2011; NRA, 2012b) are used for the first time in this study.

Table 2

Table 3

Figure 2

2.2.2 Observational data for source term estimation over the ocean

For the source term estimation method over the ocean (subsection 2.1.2), we used two datasets of sea water concentration of ^{134}Cs sampled from 14 April to 3 May 2011 at the

north-western north Pacific region (450–2000 km from FNPS1, Honda et al., 2012) and from 2 April to 17 May 2011 over a much larger north Pacific region (300–8400 km from FNPS1, Aoyama et al., 2012), respectively. Figures 3a and b depict the location of all sampling points over the Pacific Ocean.

Figure 3

2.2.3 Observational data for verification of source term

For verification of the source term, the cumulative surface deposition of ^{137}Cs over East Japan measured by the aerial radiological survey of 31 May 2012 (NRA, 2012a) is used. The observed surface deposition map of ^{131}I near the plant on 1 April 2011 reconstructed by Torii et al. (2013) is also compared with the calculated one. For the evaluation of the release rates during the early stages of the accident, we use the aerial survey of total air dose rate on 17–19 March 2011 (US DOE/NNSA, 2011). Furthermore, in the atmospheric dispersion analysis, we mainly focus on temporal variations in air concentration sampled at the CTBTO stations (CTBTO, 2011) and four stations in the United States: Sacramento California, Melbourne Florida, Sand Point Alaska, and Oahu Hawaii (Fig. 3a), where the plume was detected in the early stages of the accident.

2.3 Models and simulation settings

2.3.1 Models

The emergency response system's atmospheric dispersion model (WSPEEDI-II) and an oceanic dispersion model (SEA-GEARN-FDM) are used to estimate the source term. WSPEEDI-II combines two models: a non-hydrostatic atmospheric dynamic model (MM5, Grell et al., 1994) and a Lagrangian particle dispersion model (GEARN, Terada and Chino, 2008). MM5 predicts three-dimensional fields of wind, precipitation, diffusion coefficients, etc. based upon the atmospheric dynamic equations at an appropriate spatial and temporal resolution, by using nested domains. GEARN calculates the advection and diffusion of radioactive plumes, radioactive decay, dry and wet deposition onto the ground surface, and air

dose rate from radionuclides in the air (cloud-shine) and ground-shine. GEARN can predict the atmospheric dispersion on both local and regional domains simultaneously by considering in- and out-flow between the domains. The areas of two GEARN domains are the same as the MM5 nested domains. The performance of this system was evaluated by its application to the field tracer experiment over Europe, ETEX (Furuno et al., 2004), the Chernobyl accident (Terada et al., 2004; Terada and Chino, 2005, 2008), and the FNPS1 accident (Katata et al., 2012a, b; Terada et al., 2012). A detailed description of the models is provided in Terada et al. (2004) and Terada and Chino (2005).

In the present study, the deposition scheme of WSPEEDI-II is modified to improve the atmospheric dispersion simulation and hence the resulting accuracy of the source term estimation. The scheme consists of parameterizations for dry deposition, wet deposition (in-cloud and below-cloud scavenging; CCN activation and scavenging in mixed phase clouds), and fogwater deposition of gaseous and particulate radionuclides based on existing modeling approaches. Details in the scheme are described in Appendix A.

SEA-GEARN-FDM is a finite difference model used to simulate radionuclide transport in ocean (Kawamura et al., 2014). The model calculates the temporal variation of sea surface concentration of ^{134}Cs (half-life = 2.1 years). Horizontal turbulent mixing is modeled using the Smagorinsky formula (Smagorinsky, 1963). For vertical mixing fluxes, an empirical value of eddy diffusivity in the mixing layer (4.0×10^{-3} m^2 s^{-1}) is adopted at all model grid points throughout the simulation period. SEA-GEARN-FDM uses the 10-day mean ocean current fields from the ocean–atmosphere global model K7 (Sugiura et al., 2008). The K7 model is a fully coupled global General Circulation Model (GCM) developed by the Data Research Center for Marine–Earth Sciences, Japan Agency for Marine–Earth Science and Technology (JAMSTEC/DrC). The coupled GCM is composed of the Atmospheric GCM for the Earth Simulator (AFES; Ohfuchi et al., 2004) and the Ocean–Sea Ice GCM for the Earth Simulator (OIFES; Masuda et al., 2006). The AFES and OIFES have horizontal grid resolutions of T42 (approximately 2.8°×2.8°) and 1°×1° with 24 and 45 vertical layers in σ coordinates, respectively. The four-dimensional variation method is used to execute reanalysis data in K7.

2.3.2 Simulation settings

The study area covers regional and northern-hemispheric areas around FNPS1 (Fig. 3). The simulation conditions of modified WSPEEDI-II are summarized in Table 4. Two sets of meteorological input data, a Grid Point Value (GPV) of the Global Spectral Model for Japan region (GSM) and the Meso-Scale Model (MSM) provided by the Japan Meteorological Agency (JMA) are used for initial and boundary conditions of MM5. MSM which covers Japan with a finer resolution is adopted for the reverse estimation over the land and GSM over the globe to the estimation over the ocean. A four-dimensional data assimilation method is also employed by using the GPV data, observed wind data at FNPS1 and FNPS2 (TEPCO, 2011b, c), and surface weather stations to improve the prediction accuracy of the meteorological fields around FNPS1. While most of model settings were similar to Katata et al. (2012b), the revised approach uses the more sophisticated Reisner graupel microphysics parameterization (Reisner et al., 1998) of MM5 to simulate the precipitation and ice physics. When compared to the observed rainfall amount in Fukushima Prefecture (Fig. S1), the new calculations are overall the same as or sometimes better than Katata et al. (2012b) and Terada et al. (2012). During 15–17 March 2011, the model also reproduces the upper-air observations of wind and air temperature above 400 m at Ibaraki Prefecture (Fig. S2). The simulation by the modified WSPEEDI-II (hereinafter the WSPEEDI-II simulation in chapters 2 and 3) for the source term estimation over the ocean is conducted using the GPV of the GSM by JMA. Time steps of MM5 and GEARN are set to 120 s and 60 s, respectively.

The time step in SEA-GEARN-FDM calculations is set to 60 minutes. The calculation period of SEA-GEARN was from 12 March to 30 June. The horizontal spatial resolution of the model was set to 1°×1° with 45 vertical layers. The deposition amounts calculated by the WSPEEDI simulation were given to the surface layer of SEA-GEARN-FDM every 24 h.

2.3.3 Source assumption

During the accident, radioactive nuclides were discharged into the atmosphere by various processes, venting, hydrogen explosion, and continuous leakage from the reactor buildings. A more complete analysis of the features of releases related to the events in the reactor is still under investigation. Note that the time zone used in the following sections is Japan Standard Time (JST = UTC + 9 h).

Under such situations, the fractional composition of major radionuclides, the chemical form of radionuclides, the release period, i.e., the starting and ending points of each release and release height, are assumed as follows.

The fractional composition of major radionuclides contributing to the ground-shine, e.g., ^{131}I, ^{132}Te(^{132}I), ^{133}I, ^{134}Cs and ^{137}Cs, is determined based on various measurement datasets over East Japan : METI (METI, 2011a), FNPS1, FNPS2 (TEPCO, 2011a), MEXT (NRA, 2011b), MEXTsea (NRA, 2011b), DOE (US DOE, 2011), JAEA-Tokai (Ohkura et al., 2012; Furuta et al., 2011), KEK (KEK, 2011), RIKEN (Haba et al., 2012), JCAC (Amano et al., 2012), and Tokyo Metropolitan Government (Tokyo Metropolitan Government, 2011). These radionuclides are selected based on their relative contribution to the total composition and their dose conversion factor. Figure 4 depicts the radioactive ratios for all dust sampling data. In Figs. 4a and b, the decay curves for the radioactive ratio of total inventory of Units 1 to 3 (Table 5) of ^{133}I/Total ^{131}I and ^{132}Te/^{137}Cs are also plotted. When unit release rate is applied for ^{131}I, the ratio of other radionuclides to ^{131}I is determined as follows. The temporal change of the ratio of ^{133}I/^{131}I is determined by the decay curve as shown in Fig. 4a. The ratio of ^{137}Cs to ^{131}I can be determined from the data for most of the simulation periods (Fig. 4c). The ratio of ^{137}Cs to ^{131}I at the released time should be different from that at the measurement time because of radioactive decay during the transport of the plume and the difference of deposition processes of both nuclides in the environment. However, the transport time period between the FNPS1 and the monitoring points used to determine ^{137}Cs/^{131}I ratio (Fig. 4c) are within about 10 hours and sufficiently small compared with decay constants of both nuclides (Table 5). Thus, we only consider the latter effect to adjust the ratio obtained at the measurement points to that at the release point.

The ratio of ^{134}Cs is given to be equal to that of ^{137}Cs. Although there is no a priori reason why the ratio of ^{132}Te/^{137}Cs is almost correlated with the decay curve, the ratio of ^{132}Te to ^{137}Cs exponentially decreased from approximately 20 on 12 March, as shown in Fig. 4b. Thus, we also use the decay curve to estimate the ratio of ^{132}Te/^{137}Cs. ^{132}I (half-life = 2.3 h) is treated as ^{132}Te progeny nuclide and assumed to be radioactive equilibrium with ^{132}Te (half-life = 3.2 d).

Consequently, the ratio of ^{131}I:^{132}Te (^{132}I):^{133}I:^{134}Cs:^{137}Cs when we determine the source term by using air dose rates from ground-shine is set to 1:1.5:1.1:0.1:0.1 in the afternoon of 12 March. From the morning of 15 March to the noon of 16 March, 1:0.8-0.9:0.1-0.2:0.1:0.1 is

set from 4 to 20:00 of 15 March, 1:0.2:0.09-0.1:0.014:0.014 from 20:00 of 15 March to 6:00 of 16 March, and 1:0.6-0.7:0.08:0.1:0.1 from 6:00 to 11:00 of 16 March.

Concerning the chemical form, the ratio of gaseous and particulate ^{131}I is also determined from air concentration data collected at JAEA-Tokai (Ohkura et al., 2012), although this ratio varies widely depending on the observation points (Tsuruta et al., 2012). As mentioned above, we correct the $^{137}Cs/^{131}I$ ratio at JAEA-Tokai to that at the release point considering the history of air mass by simulation model which can treat the difference of deposition process of gaseous and particulate. Because there are no observed data on the ratio of elemental iodine (I_2) and organic iodine (CH_3I), the ratio of gaseous CH_3I to I_2 is assumed to be constant of 0.6 throughout the simulation period according to the method of RASCAL 4.0 (US NRC, 2012). The determination of the ratio of I_2, CH_3I, and particulate iodine mentioned above has uncertainty. Because the deposition mechanisms for these three types of iodine are different in the environment, the estimation of the iodine source term is affected by this uncertainty. ^{132}Te should be a particulate in the atmosphere, similar to ^{134}Cs and ^{137}Cs, according to the observational data of Ohkura et al. (2012) (Fig. 4b).

The starting and ending points of each release are determined by the following method. During the period from the early morning of 12 March to the evening of 14 March, the release periods for the venting from Units 1 and 3 reported by TEPCO (TEPCO, 2011a) are determined by the periods of the decreases of the drywell (DW) pressure and those for hydrogen explosions tentatively 30 min. As mentioned in section 3.2, these release periods are partially verified by comparing the calculation results of WSPEEDI-II with monitoring data. In other period, the continuous leakage from Units 1 and/or 3 due to the increases of pressure in the containment vessels are assumed because even for the period when the special events were not reported, air dose rates near the boundary of FNPS1increased when the measurement point was located at downwind. Concerning the release height, the venting is assumed from the stack, a height of 120 m above the ground level, hydrogen explosion a volume source whose size is determined from the movies, and other leakages from the building from a height of 20 m.

During the period from 21:00 of 14 March to 4:00 of 15 March, the safety relief valve (SRV) was opened three-times to decrease the pressure of the reactor pressure vessel (RPV) at Unit 2 and, according to these operations, the environmental monitoring data clearly showed the increases of air concentration and air dose rates at downwind. Thus, we assume the three

releases at the periods which are the same as those corresponding to decreases in the RPV pressure. The release is assumed to occur from the stack via the RPV.

From 4:00 of 15 March to 11:00 of 16 March, although it was expected from environmental monitoring data that a number of large releases occurred, the reason is still not clear. Thus, the source term is estimated in detail by the comparison of calculation results for a unit release every hour to several hours with relevant increases of air dose rates. Concerning the release height, the release from the Unit 2 building is assumed until 16:00 of 15 March. After 16:00 of 15 March to 6:00 of 16 March, the mixture of releases from Unit 2 building and Unit 3 stack is assumed because the venting at Unit 3 started at 16:01 of 15 March. Since the ratio of release amounts from Units 2 and 3 is not clear, the vertical line source from 20 m to 120 m height is applied.

After 17 March, wet venting operations at Unit 3 on 21:30 of 17 March, 5:30 of 18 March, and 11:25 on 20 March was reported (TEPCO, 2011a). However, except for these venting operations, the events which caused the atmospheric releases are not clear. For this period, Tanabe (2012) discussed the possibility of a core fuel materials re-melt at Units 3 and 1 on 21 March and 22–23 March, respectively, due to a water shortage to cool the molten cores. The white and gray smokes observed at Unit 3 at 15:55 on 21 March and at 16:20 on 23 March indicate possible fires (Prime Minister of Japan and His Cabinet, 2011; TEPCO, 2011a). These events probably caused the release from the building. Thus, we assume the continuous releases except for the period of venting operations. The duration of the continuous release is roughly estimated by assuming that the certain release rate continued from/to the middle of released times of sampled air used for the source estimation. Because the sampling time irregularly changed day by day, the duration for continuous release of specific release rate is consequently different as shown in Fig. 5. Thus, this difference in release periods has no physical meanings after 17 March.

3 Source term estimation and local-scale dispersion analysis

The estimated source term is shown in Table 6 and the temporal variation of the release rates are depicted in Fig. 5. The release rates shown in Table 6 and Fig. 5 are not decay normalized values to the shutdown time but are valid at the release time. The events in the reactors (TEPCO, 2011a, 2012; Tanabe, 2012) are also shown in Fig. 5, but it is not clear from the

reverse estimation that the events written in Fig. 5 mainly caused the atmospheric releases, particularly after 15 March. The estimated values show total release rates from Units 1 to 3.

The major differences of the estimated source term in this study from our previous work (Terada et al., 2012) are described below.

Table 6

Figure 5

3.1 Afternoon of 12 March

In the afternoon of 12 March, the wet venting started at 14:00 and the extreme decrease of the pressure of the primary containment vessel of Unit 1 (PCV-U1) from 14:00 to 15:00 indicated atmospheric discharges of radionuclides. The source term estimation for this venting is possible using data from an automatic monitoring post at Kamihatori (5 km northwest from FNPS1). The hourly averaged air dose rates increased to 1590 μGy h^{-1} from 14:00 to 15:00, and then rapidly decreased (Fig. 6a). The WSPEEDI simulation shows that this high air dose rate was due to the large releases during the wet venting of Unit 1. The estimated release rates were 2.9×10^{15} and 2.9×10^{14} Bq h^{-1} for ^{131}I and ^{137}Cs, respectively. In Fig. 6a, the red line is the result of the WSPEEDI simulation using the estimated source term. The timing of a peak appearance by the plume arrival and the values of the ground-shine shown as a slow decrease in air dose rates after the peak agreed well with the observation. This shows that the source term estimated from the ground-shine is appropriate. The temporal variation of air dose rates every ten minutes at Kamihatori (Fukushima Prefecture, 2012) shows that high dose rates continued for approximately one hour. This means the release period of one hour determined from the decrease of DW pressure is appropriate.

Figure 6

The hydrogen explosion of Unit 1 at 15:36 also discharged a huge amount of radionuclides into the atmosphere. According to the WSPEEDI simulation, the radioactive plume flowed toward the north-northwest, which drastically increased the air dose rates at automatic monitoring posts of Shinzan (3.9 km north-northwest) and Namie (8.6 km north-northwest), and Kiyohashi (8.2 km north) and Minamisoma (24.9 km north-northwest) in Fukushima Prefecture from 17:00 and 20:00, respectively. In our previous work (Katata et al., 2012b), the

source term for this hydrogen explosion was estimated by using air dose rates measured by portable monitors on 13 March. However, the measurement was done by NaI(Tl) scintillation counter limited to measure up to 30 μGy h^{-1} and, as a result, only the edge of the deposition area could be measured. Thus, in this study, we used the additional data using the ionization chamber at Shinzan, located along the contamination band after the hydrogen explosion. The estimated release rates from 15:30–16:00 were 1.4×10^{16} and 1.4×10^{15} Bq h^{-1} for ^{131}I and ^{137}Cs, respectively. In Fig. 6b, the red line of the WSPEEDI simulation also agreed with the observed peak appearance and ground-shine. These increases of air dose rates due to the hydrogen explosion were also observed by airborne survey within 5-km from FNPS1 (Fig. 7), which showed the narrow contamination band to the north-northwest direction of FNPS1 in both air dose rate and ^{137}Cs deposition. Since large increases of air dose rates were not recorded in the areas from north-northwest to north directions of FNPS1 after 13 March, this contamination band over the monitoring post of Shinzan must have been due to the dry deposition of radionuclides discharged during the hydrogen explosion. Figure 6c compares the distribution of air dose rates in the daytime of March 13 between the WSPEEDI simulation and observations by the portable monitors as mentioned above. While the calculated result is slightly shifted to the west due to the delay of the wind shift comparing with observed wind shift, both results show the similar distribution pattern of the ground-shine. The contamination band was narrow despite the fact that wind direction data at FNPS1 (TEPCO, 2011b) rapidly changed in a clockwise direction during that period. This indicates that the major release due to hydrogen explosion was instantaneous.

Figure 7

3.2 13 March– Evening of 14 March

Venting operations were conducted to decrease the pressure of PCV-U3 at 9:24 and 12:30 on 13 March. The WSPEEDI simulation shows that the plume almost flowed toward the ocean in this period. According to the simulation, although the plume sometimes flowed over the coastline of Fukushima Prefecture or stagnated around FNPS1 due to calm conditions, only a very small number of monitoring posts near the coast caught the movement of the plume (Fukushima Prefecture, 2012). The estimation result shows that the large releases due to wet

venting continued until 23:00 on 13 March on the order of 10^{14} and 10^{13} Bq h^{-1} for ^{131}I and ^{137}Cs, respectively.

Despite several venting operations at Unit 3 on 13 and 14 March, a hydrogen explosion occurred at Unit 3 at 11:01 on 14 March (Fig. 5). In previous work, the source term for this hydrogen explosion was just assumed as same as that of the explosion at Unit 1 on 12 March, because the wind was toward the Pacific Ocean and no measurement data were available. In this study, we could estimate it using the sea-water concentration data over the ocean. According to our estimation, the release rates of ^{131}I and ^{137}Cs were 3.7×10^{15} and 3.7×10^{14} Bq h^{-1} for about 30 minutes, respectively, which are slightly smaller than those of the hydrogen explosion at Unit 1 (section 3.1). Here, the release period is still assumed as same as the explosion at Unit 1.

3.3 Night of 14 March– Early morning of 15 March

Figures 8a and b depict the time evolutions of the pressure of the reactor pressure vessel (RPV) at Unit 2, air dose rates, and air concentrations measured at the south area of FNPS1. During this period, dry venting was tried at Unit 2, but it is not clear that the venting succeeded. The safety relief valve (SRV) was also opened at 21:00 and 23:00 on 14 March and at 1:00 on 15 March to decrease the pressure of RPV and, as a result, the pressure decreased after these operations (Fig. 8a). If a meltdown had already occurred in Unit 2, the vapor containing radionuclides would flow to the PCV and raise the possibility of atmospheric releases with the operation of SRV. In this period, the WSPEEDI simulation shows that the plume flowed toward the south to south-southwest and the observed air dose rates at FNPS2 (11.4 km south) and Kitaibaraki (80 km south), and air concentrations of ^{131}I and ^{137}Cs measured at JAEA-Tokai (100 km south) showed three-time increases with time (Fig. 8b). Based upon the downwind distances from FNPS1 and the wind speed data, the time of the peak appearances at these three monitoring points are reasonably explained by the releases when the SRV was opened (Figs. 8a and b). In our source term estimation, the release rates in this period gradually increased with time from 2.4×10^{14} to 2.3×10^{15} Bq h^{-1} and from 1.6×10^{13} to 3.9×10^{14} Bq h^{-1} for ^{131}I and ^{137}Cs, respectively. In previous work, the source term for this period was almost constant in time. In this study, the detailed source term in time is estimated based on the detailed analysis of the relation between the incident in the reactor and

temporal variation of environmental data. These results indicate that the three times major releases in our source term estimation occurred due to SRV openings.

Figure 8

3.4 Morning of 15 March– Early morning of 16 March

Figures 9a and b show the temporal change of the DW pressure at Units 2 and 3 and air dose rates observed at automatic monitoring posts around the plant. Temporal variations of the vertically accumulated air concentration and precipitation bands in the WSPEEDI simulation are shown in Fig. 10.

In the morning of 15 March, the pressure of PCV-U2 decreased between 7:00 and 12:00. This decrease corresponded with the extreme increase of air dose rate (peak approximately 1.5×10^4 μGy h^{-1}) observed at the main gate from 7:00 to 10:00, clearly indicating a huge release into the atmosphere. According to the WSPEEDI simulation, the plume discharged in the morning first flowed toward the south-southwest and then gradually changed direction clockwise. Around the area of FNPS1, the observed air dose rates was still 41 and 19 μGy h^{-1} at the two monitoring posts of Yonomori (7.3 km south-southwest) and Matsudate (14.2 km south-southwest) at 7:00 on 15 March, respectively. Subsequently the following monitoring points detected higher air dose rates: 390 μGy h^{-1} at Ohno (4.9 km west-southwest) at 11:00, and 232 μGy h^{-1} at Yamada (4.1 km west-northwest) at 13:00 (Fig. 9b). The WSPEEDI simulation shows these high air dose rates were due to this huge amount of release in the morning (Fig. 10a). Furthermore, the WSPEEDI simulation shows the plume discharged in the morning encountered a rain band along the Naka-Dori including Koriyama (58 km W) and Shirakawa (81 km WSW) (Fig. 10a) and the north and northwest areas of FNPS1 including Fukushima (62.7 km NW) and Iitate (38.9 km NW) in the afternoon (Fig. 10b). The release rate from 7:00 to 11:00 is estimated on the order of 10^{15} and 10^{14} Bq h^{-1} for ^{131}I and ^{137}Cs, respectively. The air dose rate map from ground-shine observed by the airborne survey of 17–19 March (US DOE/NNSA, 2011) is shown in Fig. 11a. This figure shows that the high dose rate zone due to dry deposition to the southwest is narrow suggesting that the period of the large release in the morning did not continue for a long time.

Figure 9

Figure 10

Figure 11

After the major release in the morning of 15 March, the pressure of the DW at Unit 2 decreased continuously from the afternoon to the evening (Fig. 9a). According to the WSPEEDI simulation, a southeasterly wind transported radionuclides emitted during this period toward Iitate and Fukushima directly and resulted in wet deposition to the northwest of the plant, as discussed in Katata et al. (2012a). However, by our estimates, the release rates are not as high during the morning releases (Table 6). This result is different from our previous study (Katata et al., 2012a), in which a large amount of release was estimated during the period from 13:00 to 17:00. Due to an increase of the wet scavenging coefficient in the modified deposition scheme (Fig. A2b), the calculated air dose rates due to wet deposition of the plume released during the morning can almost represent the measured ones at Iitate and Fukushima without the additional deposition from the plume released in the afternoon (subsection 4.1.1, Fig. 12). Figure 12 shows temporal changes in air dose rate in Fukushima prefecture from 15 to 20 March. The measured air dose rates at Fukushima and Iitate areas (Figs. 12c and d) also shows that a large increase in the air dose rates did not appear at two points. Afterward, the air dose rates largely increased around 13:00–14:00 on 15 March (Fig. 12). One possible reason that a large increase did not appear at two monitoring points might be that most of the radionuclides deposited before the air mass arrived there. However, because rain bands coming from the northwest during the afternoon of 15 March caused precipitation around Iitate area from 16:00with a very small intensity of approximately 1 mm h^{-1} (Fig. S1). Moreover, Ohno (4.9 km WSW from the site) had no rainfall until the night (Fig. S1). These facts suggest that the plume discharged in the afternoon should produce less amount of (dry) deposition along the pathway from the FNPS1 to the northwest direction. Therefore, the plume can reach Iitate and increase air dose rate due to wet deposition if a large amount of radionuclides were discharged during the afternoon.

Figure 12

The second huge increase of the release rate was estimated during the period from 18:00 of 15 March to 1:00 of 16 March with the maximum values from 22:00–23:00 on 15 March of 1.0×10^{16} and 3.4×10^{14} Bq h^{-1} for ^{131}I and ^{137}Cs. During the evening of 15 March, wet venting was conducted at Unit 3, corresponding to the decline in DW pressure at Unit 3 from 16:05 (Fig. 9a). Afterward, wet venting was carried out at Unit 3 several times, and the decline in DW pressure finally stopped around 6:00 on 16 March. At the same time, the DW pressure dropped steeply at Unit 2 from 18:00 on 15 March to 2:00 on 16 March. These facts imply that the large release rate estimated during the evening originated from Units 2 and 3. The WSPEEDI simulation shows that, after the plume flowed clockwise from the west to northwest direction in the afternoon, it reached Namie (8.6 km north-northwest) at 21:00 on 15 March, and then the flow direction switched to counter-clockwise. At midnight on 15 March, the wind direction was from the east and the rain band approached FNPS1 from the northwest (Figs. 10c and d), suggested by both the WSPEEDI simulations and the meteorological data at Ohno (Fig. S1). Furthermore, the air dose rates observed at monitoring posts on 16 March drastically increased to 1020 μGy h^{-1} at Yamada at 0:00, 173 μGy h at Ono at 1:00, and 44.5 μGy h^{-1} at Matsudate at 3:00 (Fig. 9b). Thus, the release in the night on 15 March is considered to have created the highest dose rate zone in the western area close to FNPS1 between Yamada and Ohno, as shown by 5-km airborne survey (Fig. 7). At these locations, decreases of air dose rates after the passage of the plume were small (Fig. 9b), indicating that this high dose rate zone was created by wet deposition. The 5-km airborne survey showed two clear high-contaminated bands to the west of FNPS1 between Yamada and Ohno. This indicates the short-term variation in release rates during the period, while the temporal and spatial resolutions of the WSPEEDI simulation are not sufficiently fine to resolve these bands completely.

Our results of the source term estimation and the WSPEEDI simulation from 15–16 March reveal that the highest contamination areas around the FNPS1 were not continuous but consisted of two parts; i.e., the northwest contamination area extended to long distance mainly created by the release in the morning of 15 March, and the west and west-southwest areas near the site contaminated by the high-concentration plume discharged during the night of 15 March (Fig. S3). This conclusion is also supported by the 5-km airborne survey (Fig. 7) showing the contamination areas near the site distributed not to the northwest direction but the west-northwest and west directions of FNPS1. Although the contamination areas around the FNPS1 are known to have been created on 15-16 March by wet deposition as concluded in

Chino et al. (2011), Katata et al. (2012a), and later studies (Mathieu et al., 2012; Srinvas et al., 2012; Korsakissok et al., 2013; Morino et al., 2013; Winiarek et al., 2014), our result indicates that the formation processes were quite complicated and the above two contaminated areas in different directions of FNPS1 were created at different time periods.

Figures 11b and c show the deposition distributions of ^{131}I and ^{137}Cs in the area within 80-km from FNPS1 observed by the airborne survey. The figures show that the distribution patterns of both radionuclides are slightly different, e.g., the large deposition area of ^{137}Cs is limited to the narrow band to the northwest and south directions, while that of ^{131}I is distributed toward the west and southwest areas within 10 km from FNPS1. As discussed above, according to the WSPEEDI simulation, the major deposition in the west and southwest areas was probably created by wet deposition of the high-concentration plume released during the night on 15 March when the rain band overlapped with the plume. The WSPEEDI simulation also shows that this plume gradually flowed to the south of FNPS1 and reached JAEA-Tokai in the morning of 16 March (Fig. 10d). As described in subsection 2.3.3, the ratio of ^{131}I/^{137}Cs=60 sampled at JAEA-Tokai in the morning of 16 March was clearly higher than that of ^{131}I/^{137}Cs=7.7 on 15 March (Ohkura et al., 2012). Although this ratio at the release point decreased to 30 in the morning of 16 March in the WSPEEDI simulation due to the difference of deposition processes of iodine and cesium in the environment, it can still be concluded that the high-concentration plume discharged in the night was iodine-rich, resulting in the large deposition of ^{131}I near the plant compared with that of ^{137}Cs. One possible reason for the change in the ratio of ^{131}I/^{137}Cs at JAEA-Tokai from 15 and 16 March is that, according DW pressure data (Fig. 9a), the source was from Unit 2 in the morning of 15 March and Units 2 and 3 in the night of 15 March to the early morning of 16 March.

3.5 Morning – Noon of 16 March

In this period, the pressure decrease was reported at Unit 3 from 9:00 to 11:00 (Fig. 9a). In addition, the white smoke from the building of Unit 3 was also observed at 8:30 on 16 March (TEPCO, 2012). The WSPEEDI simulation shows that the plume released during the decrease of the DW pressure flowed toward the Pacific Ocean in the morning, and then it returned to the inland around noon. This movement of plume probably caused large increases of air dose rates to 33 and 324 μGy h^{-1} at Matsudate and Ohno at 11:00 and 12:00 on 16 March,

respectively (Fig. 9b). In this study, the data from Ohno was used for the source term estimation. The estimated release rate increased to 2.8×10^{15} and 2.8×10^{14} Bq h^{-1} for ^{131}I and ^{137}Cs, respectively.

4 Discussion

4.1 Verification of source term

In this section, we first tested the new source terms for ^{137}Cs and ^{131}I with the modified WSPEEDI-II and compared the results over local- and regional-scales to the airborne survey's surface deposition and air dose rate data. These comparisons were made between four simulation cases with combinations of original or modified WSPEEDI-II and the source term from this study or Terada et al. (2012). Then, the new source term was further tested using different atmospheric dispersion and meteorological models over regional- and global-scales to evaluate its reliability for general atmospheric dispersion model studies during the FNPS1 accident.

4.1.1 Validation using WSPEEDI-II

Air dose rate at ground monitoring points.

Figure 12 shows the temporal changes in the air dose rates from four simulations at selected monitoring points in Fukushima Prefecture from 15 to 19 March. By using the new source term, the calculated ground-shine shown as slow-slope after the peak due to the large deposition event of 15–16 March agreed with observed data within a factor of 2 at most of the monitoring points. At Hirono (21.4 km south) and Kawauchi (22 km west-southwest) (Figs. 12a and b) affected by dry deposition from the night of 14 March to the morning of 15 March, respectively (sections 3.3 and 3.4), observed air dose rates were reproduced by using new source term. A similar improvement of the simulation results when using the new source term can be found in the dry deposition during the afternoon of 12 March (Figs. 6a and b). These results indicate that the use of additional monitoring data near the plant (Fukushima Prefecture, 2012) in the new source term is needed to reproduce the ground-shine due to dry deposition during the FNPS1 accident.

Increases of ground-shine at Fukushima (63 km northwest) and Iitate (39 km northwest) (Figs. 12c and d) were not perfectly reproduced using any combinations of models and source terms. Since both sites were affected by wet deposition in the afternoon of 15 March (section 3.4), uncertainties of source term and wet deposition scheme still remain during the afternoon of 15 March. Nevertheless, the calculated ground-shine at both sites agreed better with observed one when using the new source term. Moreover, the increase of air dose rate around 14:00 on 15 March was accurately reproduced in the modified WSPEEDI-II simulation due to higher scavenging coefficient in the new deposition scheme (Fig. A2b). The greatest ground-shine was observed at Kawafusa (20 km northwest) and Yamada (4.1 km west-northwest) from the evening to the midnight of 15 March due to wet deposition. The high doses at both sites were accurately reproduced by the modified WSPEEDI-II simulation with new source term (Fig. 12f), while the doses were clearly underestimated in all other combinations. Therefore, both revision of the source term and the wet deposition scheme play an important role in this period.

Regional deposition of ^{137}Cs over East Japan.

Figure 13 illustrates the regional deposition of ^{137}Cs by combinations of original and modified WSPEEDI-II and the two source terms. The original WSPEEDI-II simulation using source term of Terada et al. (2012) showed some disagreement in the surface deposition of ^{137}Cs between observations from the airborne survey (Fig. 13e) and the calculations at several areas over East Japan (Fig. 13a). When using the new source term, as shown in Fig. 13b, this issue was slightly resolved in the original WSPEEDI simulation; the overestimation of surface deposition from the north part of Fukushima Prefecture to Miyagi Prefecture partially disappeared. The modified WSPEEDI-II using the source term of Terada et al. (2012) is also effective in eliminating the overestimation in this region (Fig. 13c). Furthermore, the modified model reproduced the contaminated areas observed in the airborne survey in Tochigi and Gunma Prefectures and Naka-Dori in the middle of Fukushima Prefecture. This result indicates that the modification of wet deposition scheme is more effective in the regional-scale simulation than the new source term. Uncertainties of rainfall (Fig. S1) and wet deposition in the above regions and Kanto area in the modified WSPEEDI-II simulations are discussed in Supplement, and should be analyzed in more detail in the future. Finally, the best performance for deposition pattern was obtained in the modified WSPEEDI-II simulation

with the new source term (Fig. 13d). These results show that the enhancement of the scavenging coefficient in the modified wet deposition scheme (Fig. A2b) plays an important role in the improvement of the regional-scale simulations that are mainly characterized by wet deposition.

Local depositions of ^{131}I, ^{137}Cs, and air dose rate over Fukushima Prefecture.

Figures 11d-f show the spatial distributions of the air dose rate and cumulative surface deposition of ^{137}Cs and ^{131}I around FNPS1 calculated by the modified WSPEEDI-II using the new source term. Comparisons of these figures with the observations (Figs. 11a-c) show that the model reproduced the deposition patterns of each radionuclide; i.e., the large deposition area of ^{137}Cs is limited to the northwest direction of FNPS1 compared with that of ^{131}I which has a larger southern component. The improvements resulting from both the revisions of WSPEEDI-II and the source term become apparent when comparing four simulation cases of surface deposition (Figs. 14 and 15). The two calculations using the source term of Terada et al. (2012) (Figs. 14a and c) showed a large overestimation of ^{137}Cs deposition near Fukushima (63 km northwest). This over-prediction is reduced by calculations using the new source term because of a decrease of release rate in the afternoon of 15 March (Fig. 14c). However, the highest contaminated zone to the northwest of FNPS1 was still significantly underestimated in all three cases (Figs. 14a-c). This under-prediction was reduced using the modified WSPEEDI-II and the new source term (Fig. 14d) due to higher scavenging coefficient of ^{137}Cs in the new deposition scheme (Fig. A2b). Thus, both revisions of the deposition scheme and the source term are required for more accurate simulation of the ^{137}Cs deposition.

Figure 14

Figure 15

In the ^{131}I deposition simulations using the original WSPEEDI-II (Figs. 15a, b), the high contaminated areas spread to the west of FNPS1 more broadly as indicated by the airborne observations (Fig. 11c). This result suggests that the new source term, which increases in the ratio of ^{131}I to ^{137}Cs around midnight on 15 March (section 3.4) reproduced the difference in

the observed deposition patterns between both radionuclides in the original WSPEEDI-II simulation. However, both calculation results also show general overestimation of observed ^{131}I deposition (Figs. 15a and b). This issue was solved in the modified WSPEEDI-II simulations with the new source term (Fig. 15d) and by using smaller scavenging coefficient for gaseous ^{131}I in the model (Fig. A2b). Therefore, we have a conclusion similar to that of the ^{137}Cs deposition simulation results, that both revisions of the wet deposition scheme and the source term are important to reproduce the local-scale ^{131}I deposition pattern.

In addition to the surface deposition, the spatial patterns in calculated and observed air dose rates due to the ground-shine just after the formation of the highest contamination areas near FNPS1 (17–18 March) were compared in Figs. 11a and d. The modified WSPEEDI-II simulation using the new source term reproduced the high dose rate zones observed at the monitoring posts and the airborne survey from 17–19 March. The good performance for the dose calculations indicate that the modifications to the deposition scheme and source term are reasonable, particularly for ^{132}Te and ^{131}I, which are the major contributors to the ground-shine in the early phases of the accident.

Statistical comparisons.

Figure 16 shows the scatter plots of the surface deposition of ^{131}I and ^{137}Cs, and air dose rate in the modified WSPEEDI-II simulation using the new source term. Overall, the model reproduced the high contamination areas over regional- and local-scales within a factor 10. The statistical comparisons for four calculation cases are summarized in Table 7, while comparisons of the air concentration of ^{131}I and ^{137}Cs at various monitoring sites in East Japan are also summarized in Table S1. In general, the original and modified WSPEEDI-II simulations using the new source term reproduced each observational dataset with a higher correlation coefficient ($CC \geq 0.53$) than those using the source term of Terada et al. (2012). Statistics of fractional bias (FB) and normalized mean square error (NMSE) for ^{131}I deposition were significantly improved in modified WSPEEDI-II calculations that included the effect of gaseous ^{131}I on the scavenging coefficient (Fig. 15d). On the other hand, the scores of CC, FB, and NMSE values in Tables 7 and S1 were sometimes worse when using new source term, although the improvements in the modified WSPEEDI-II simulation with the new source term were apparent in visual comparisons (Figs. 13-15). Introducing

physically consistent schemes may not always improve statistical scores because, in some cases, simple parameterizations can readily improve statistical scores by tuning less number of parameters compared with more sophisticated ones. To obtain the better performance of the new scheme, additional improvements related to wet deposition may be required; e.g., the accurate meteorological field calculated by spectral cloud microphysics modules or data assimilation techniques for cloud/rain observation data, and the online coupling simulation of meteorological and atmospheric dispersion models. While there are no clear differences in FA2, 5, and 10 among four simulation cases, most of data points (76–89%) of air dose rate and cumulative surface depositions calculated by the modified WSPEEDI-II with new source term were within a factor 5. Therefore, it can be concluded that our modified deposition scheme and emission estimates for the major releases during the FNPS1 accident are reasonable.

Figure 16

Table 7

4.1.2 Validation using several regional and global atmospheric dispersion models

To evaluate the new source term independently of the one dispersion model used to develop the source term, numerical simulations from three atmospheric dispersion models (MLDP0, D'Amours et al., 2010; HYSPLIT, Draxler and Rolph, 2012; and NAME, Jones et al., 2007) were compared to observations using our new source term estimates. These model simulations, organized by the World Meteorological Organization (WMO, 2014), were initially conducted prior to our study to assist the Scientific Committee on the Effects of Atomic Radiation (UNSCEAR, 2014) in its dose assessment efforts. The WMO sponsored calculations were all done in 3-hour time segments using a unit source emission rate, which permitted their use with the new source term. The calculations from the above mentioned three models as well as several others are available on-line (NOAA, 2014) where any source term combination can be interactively evaluated and compared with observations.

The simulation settings of the deposition scheme in each atmospheric dispersion model are summarized in Table 1. Meteorological data from the Meso-Scale Model (MSM) were provided by the Japan Meteorological Agency (JMA) at three-hourly intervals at a 5-km

horizontal resolution and were used to drive the three dispersion models. A one-domain calculation covering East Japan was carried out for each model run from 11–31 March 2011. Details of the simulation settings are available in Draxler et al. (2014). Both the MLDP0 and NAME calculations were the original WMO (2014) calculations. However, the HYSPLIT calculation settings were changed from the original calculation to turn off the use of the vertical motion field from MSM. In addition, in the original HYSPLIT simulations the wet deposition is calculated using both in-cloud and below-cloud scavenging processes. The in-cloud scheme was based upon an empirically derived scavenging ratio based on the ratio of pollutant concentration measurements in rain to air, while the below-cloud process was parameterized through a decay process defined by a time constant. The modified scavenging scheme used here is a simplified version of the previous HYSPLIT scheme and it now uses the same time constant decay process for both in-cloud and below-cloud removals. The numerical formulation for removal processes is similar to that in the NAME model. Both the original and modified NOAA calculations are available on-line (NOAA, 2014). Two source terms, Terada et al. (2012) and this study, averaged at 3-hour intervals, were used for the emission scenarios.

Figure 17 shows the temporal changes in air concentrations of ^{137}Cs at JAEA-Tokai (Fig. 2a) in the simulations using the three WMO models. Modeled results using either of the two source terms generally reproduced the observed time trends of air concentrations and the high values observed on 15, 16, 20–21, and 30 March.

Figure 18 shows the spatial distributions of the cumulative ^{137}Cs surface deposition over East Japan calculated using three WMO models. The improvement when using the new source term compared with Terada et al. (2012) is obvious in the deposition pattern as well as the WSPEEDI-II calculations shown previously (subsection 4.1.1). For example, the calculated large deposition areas extending from the north part of Fukushima Prefecture to Miyagi Prefecture, not observed by the airborne survey (NRA, 2012a), significantly decreased when using the new source term because of a decrease of release rates during the afternoon of 15 March. This is also apparent in the scatter plots (Fig. 19), which show overestimation in the range of measured surface deposition between 10–1000 kBq m^{-2} for all model results using the source term of Terada et al. (2012). Furthermore, utilization of the new source term clearly increased the calculated deposition amounts in the areas to the northwest of FNPS1 (Fig. 18) which matched to airborne observations (Fig. 11b). As discussed above, we can see

the improvement of the WMO model results similar to WSPEEDI-II calculations when using the new source term, indicating that the new source term is also effective in atmospheric dispersion simulations of the FNPS1 accident using other models.

Figure 17

Figure 18

Figure 19

To test the new source term for the plumes flowing over the ocean, the global simulation results from HYSPLIT were compared with measurements at several locations over the Pacific, the Americas, and Europe. It is useful to validate the new source term estimated by not only monitoring data over the land but also sea water concentration of ^{134}Cs. The global HYSPLIT simulations had previously been described by Draxler and Rolph (2012). The model configuration used here is identical to the revised WMO regional calculations discussed previously except that the calculations consisted of six hour time segments. The calculations used the 0.5-degree horizontal resolution meteorological data from NOAA's Global Forecast System (GFS), consisting of a series of 0 to +6 h forecasts available on GFS native model sigma levels (56) with meteorological fields available every three hours. The concentration grid was global at 1-degree horizontal resolution with a vertical extent of 500 m. The global measurement data used for the evaluations consisted of the United States' National Data Center (US NDC, 2011) and Health Canada's Radiation Monitoring (HCRM, 2011) stations in the Comprehensive Test Ban Treaty Organization's (CTBTO) network, the U.S. Environmental Protection Agency's Radiation Monitoring Network (RADNET, 2011), and selected stations in Europe run by various national authorities (Masson et al., 2011).

Figure 20 shows the time series of ^{137}Cs air concentrations at a few selected locations in North America, Hawaii, Alaska, Ireland, and Canada representing the emissions from FNPS1 that flowed over the Pacific Ocean and arrived during the early phases of the accident. As shown in the figure, there is a good agreement in the first arrival time of the plume and overall the general time trends were reproduced by HYSPLIT using the new source term. Scatter diagrams of the observed and calculated air concentrations for the global scale results using HYSPLIT with the new source term are depicted in Fig. 21. A large part of data points for both radionuclides are within a factor of 10. Whilst uncertainties of the model, such as the ratio of ^{131}I/^{137}Cs for major releases during the early stages of the accident, the model's deposition parameters, and the comparison with other global modeling results (Stohl et al.,

2012; Christoudias and Lelieveld, 2013; Evangeliou et al., 2013), should be further evaluated in future, we can conclude from these results that the new source term is also appropriate for the global-scale atmospheric dispersion studies of the FNPS1 accident.

Figure 20

Figure 21

4.2 Comparison in source terms

Figures 22 and 23 show the source terms estimated in the present study and those from prior studies (Terada et al., 2012; Stohl et al., 2012; Hirao et al., 2013; Saunier et al., 2013; Winiarek et al., 201). In terms of the land contamination, the most important result of this study is that the highest release rates shifted from the afternoon to the evening and nighttime of 15 March (section 3.4). As a result, the period of the major release is estimated and is coincident with the wet venting at Unit 3 and/or DW pressure deficits at both Units 2 and 3 reported on 15–16 March (Fig. 8), though it is not clear from our estimation if the release was major or not. This result is the complete opposite of all the previous studies based on the inverse estimation methods using regional (Hirao et al., 2013; Saunier et al., 2013), global (Stohl et al., 2012), and daily fallout and surface deposition datasets (Winiarek et al., 2014).

There are several reasons for the improved estimation of this major release. First, the results of local-scale simulations with much higher spatial resolution (1-km) were compared with the automated monitoring data of air dose rate close to FNPS1 (Fig. 3b) that were not available for any of the past studies. These were particularly effective to find this release and determine the timing and release rates. Second, we modified the wet scavenging scheme to increase wet deposition, particularly for conditions with low cloud water content (Fig. A2b). This caused an increase of the modeled ground-shine at Fukushima and Iitate and also decreased the release rate in the afternoon on 15 March because the previous model's under-prediction no longer needed to be compensated by an increased emission rate. Third, the time segment of the release periods from 15–16 March was set to every hour to several hours to resolve drastic temporal changes in the release rate. Our results show that the combination of local-scale monitoring and detailed numerical analysis using atmospheric dispersion models with sophisticated deposition schemes is the most important factors required to estimate the release

rates associated with the time-varying events in the reactors (e.g., hydrogen explosion, venting, and pressure drop).

For the periods when the plume flowed over the land from the night on 14 March to the morning 15 March, and from 20–21 March, the release rates of the new source term were on the same order of those estimated by previous regional simulation studies (Hirao et al., 2013; Saunier et al., 2013) as well as Terada et al. (2012) (Figs. 22 and 23). In other periods, Saunier et al. (2013) frequently shows higher release rates with uncertainties when the plume flowed toward the ocean. Winiarek et al. (2014) acknowledged that they also overestimated the release rate on 20, 22–23, 25, 27, and 30 March (Fig. 22b).

Interestingly, when the plume flowed toward the Pacific Ocean, our new source term for ^{137}Cs often agreed well with that of Stohl et al. (2012), despite using the different estimation method (Fig. 22). The former used ^{134}Cs sea surface concentration data, while the latter was mainly based on daily mean air concentrations of ^{137}Cs sampled throughout the world. This indicates that the estimated values in this study were also indirectly confirmed as being reasonable.

Table 8 shows the total release amounts of ^{131}I and ^{137}Cs to the atmosphere from FNPS1. For both radionuclides, the total amounts estimated by coupling the atmospheric and oceanic simulations are clearly larger (approximately 151 and 14.5 PBq for ^{131}I and ^{137}Cs, respectively) than those of Terada et al. (2012). From the comparison between the two calculations in this study using source terms estimated from land data only and from both land and sea data (Table 8), these increases were mainly due to an increase of the release rate when the plume flowed over the ocean resulting from the optimization of release rates using additional data over the land and the ocean. However, the estimated release amount of ^{137}Cs to the atmosphere was still lower than those of several prior studies (Stohl et al., 2012; Saunier et al., 2013; Winiarek et al., 2014).

Figure 22

Figure 23

Table 8

5 Conclusions

The detailed source terms of total ^{131}I and ^{137}Cs were estimated using a reverse estimation method which coupled environmental monitoring data with the simulation of an atmospheric dispersion model (WSPEEDI-II) and an oceanic dispersion model (SEA-GEARN-FDM). To improve the accuracy of the estimate, we enhanced the deposition scheme of WSPEEDI-II to calculate dry deposition of gaseous and particulate substances, and used additional air dose rate data at automated monitoring posts, dust sampling and airborne survey data, which were not available in the previous work (Terada et al., 2012).

The major differences in the estimated source term in this work from our previous work are as follows: (1) Afternoon of 12 March: The release amount from the wet venting of Unit 1 between 14:00 and 15:00 was newly estimated from the air dose rates at the automated monitoring post near FNPS1. The release amount was approximately half of that from the hydrogen explosion of Unit 1 at 15:36, which was also re-estimated using the data at the automated monitoring post. (2) Night of 14 March to early morning of 15 March: The major release from Unit 2 could be separated into three time segments starting from 21:00, 23:00, and 01:00, although the previous study estimated one release rate for this entire period. The results suggest a relationship between the operations of the Safety Relief Valve (SRV) of Unit 2 and discharges to the atmosphere. (3) Morning of 15 March to noon of 16 March: The major releases were estimated during three periods from 07:00 to 11:00, and from 18:00 on 15 March to 1:00 on 16 March, and from 9:00 to 11:00 on 16 March using the air dose rate at automated monitoring posts near the plant. The release rates during the first two periods were similar to those estimated by our previous work, while the third major release was estimated for the first time in this study. However, the second major release started 4 hours later and continued for 3 hours longer than determined in the previous work. Furthermore, it was revealed that this release was iodine-rich compared with other releases, which was supported by the spatial patterns of the airborne survey of ^{131}I and ^{137}Cs depositions and the dust sampling data at JAEA-Tokai. The plumes of the first and second releases created the highest dose rate zone to the northwest and west of FNPS1 by wet deposition with complicated interactions between rainfall, plume movements, and temporal variety in the release rates.

The total amounts of released ^{131}I and ^{137}Cs estimated in this work were 151 and 14.5 PBq, respectively, which were clearly larger than those of the previous work for both radionuclides. The major reason for this increase was that when the plume flowed toward the Pacific Ocean

we directly computed a significantly larger release amount, while previously it was simply estimated by a temporal interpolation between release rates computed from land based measurements.

The new source term estimated in this study was first validated by comparing calculation results of the modified WSPEEDI-II with the data of cumulative surface deposition of ^{137}Cs and ^{131}I and air dose rates over local- and regional-scales. The spatial patterns of cumulative surface deposition were reproduced well. The simulation accuracies including both ^{137}Cs and ^{131}I were within a factor of 5 for 76–89% of data points for cumulative surface deposition and air dose rates. Furthermore, the new source term was also tested with three atmospheric dispersion models (MLDP0, HYSPLIT, and NAME) for regional and global simulations. All models using the new source term and the same meteorological input data generally reproduced the time series of air concentrations at JAEA-Tokai and surface deposition of ^{137}Cs over East Japan. The global calculations using HYSPLIT showed a good agreement with the time of the first arrival of the plume by comparing the model results with daily mean air concentration data at various monitoring sites over North America, Hawaii, Alaska, Ireland, and Canada.

These validation results indicated the applicability of the new source term for atmospheric dispersion studies of the FNPS1 accident. However, our estimation results still have uncertainties due to the following assumptions and model capabilities:

1) When the monitoring data observed close to the FNPS1 were used for our source term estimation, the height (or size of volume) and the time interval of releases determined from the limited information of the reactors should cause the errors.

2) The composition ratios of radionuclides determined from the observational data are highly scattered (Fig. 4c). The ratio of gaseous and particulate iodine was determined from the data from only one point (JAEA-Tokai). Furthermore, the ratio of I_2 and CH_3I in gaseous iodine is given by literature due to lack of data. The former has large uncertainties when our source term was estimated based on the ground-shine, while the latter can cause the errors in estimated results affected by wet deposition (Fig. S5b).

3) There are also uncertainties caused by the estimation method. For the reverse estimation method, the careful comparison between observations and calculations is particularly needed to reduce the errors,

It is difficult to shrink the above uncertainties unless new information from such as severe accident analysis and observation data is available. Further analyses of modeled meteorological fields such as precipitation and the impact of deposition processes of dry, wet, and fogwater (partially done in Supplement) are also required in future studies.

Appendix A: Modifications of deposition scheme in WSPEEDI-II

The processes in the following subsections are incorporated into WSPEEDI-II to improve the accuracy of the source term estimation and the atmospheric dispersion simulation.

Dry deposition of gases

Dry deposition flux of gases and particles is normally represented by the deposition velocity, V_d (m s^{-1}), and the concentration, c (Bq m^{-3}) according to the inferential technique (Hicks et al., 1987):

$$F = cV_d, \tag{A1}$$

where the downward flux is positive for F. As described in chapter 1, WSPEEDI-II used the typical constant values for V_d over short vegetation, the same as many of the other dispersion models (Table 1). However, V_d of gases and particles depends on many factors such as meteorological variables (wind speed and atmospheric stability), physic-chemical forms of substances, and land surface characters (Katata et al., 2011). To improve the accuracy of dry deposition, the more sophisticated resistance model of Zhang et al. (2003) for gaseous radioactive iodine (I_2 and CH_3I) is incorporated into WSPEEDI-II so that the model can consider the influences of these factors in its dry deposition calculations.

The original model of Zhang et al. (2003) calculates deposition velocity of gases (V_{dg}) based on the big-leaf resistance modeling approach for various chemical species. Deposition velocity is parameterized by an analogy to electrical flow through a series of transfer resistances. The model of Zhang et al. (2003) considers transfer resistances of the aerodynamic, quasi-laminar sublayer, and overall canopy resistance. The canopy resistance is separated into two parallel paths; one is the stomatal resistance with its associated mesophyll resistance, and the other is non-stomatal resistance. The non-stomatal resistance is further decomposed into resistance to soil uptake, which includes the in-canopy aerodynamic resistance and the subsequent soil resistance, as well as resistance to cuticle uptake.

According to the scheme, the non-stomatal resistance for gas species i, r_{nsi}, is parameterized by combining those for O_3 and SO_2 with the scaling factors of α_i and β_i:

$$r_{nsi}^{-1} = \alpha_i / r_{ns\mathrm{SO}_2}^{-1} . + \beta_i / r_{ns\mathrm{O}_3}^{-1}, \tag{A2}$$

where α_i and β_i represent the solubility and half-redox reactivity for species i, respectively. We rely on the equation to calculate dry deposition of gaseous ^{131}I by determining appropriate

values for α_i and β_i for the non-stomatal resistance in the following way. The behavior of ^{131}I in atmosphere is complicated because it is either bound to particles (aerosols) or in gaseous form. Unfortunately there is no available data of chemical analysis of gaseous ^{131}I during FNPS1 accident and therefore, we focus on two species of elemental (I_2) and organic forms (CH_3I) which have been known to be dominant in the past nuclear accidents (Baklanov and Sørensen, 2001). The former gas is more reactive than the latter probably due to larger reactivity and solubility. The observational results summarized in Sehmel (1980) also suggest that deposition velocity for I_2 (V_{dg}=0.02–7.2 cm s^{-1}) in the same range of SO_2 (V_{dg}=0.04–7.5 cm s^{-1}) was more than ten times of that for CH_3I (V_{dg}=0.0001–0.01 cm s^{-1}). By considering this fact, we set the values of (α_i,β_i)=(1,0) and (0.01,0) for I_2 and CH_3I, respectively. The ratio of gaseous CH_3I to ^{131}I gas was assumed to be constant of 0.6 throughout the simulation period (US NRC, 2012) due to lack of field data.

Dry deposition of particles

With regard to the calculation of the dry deposition for particles, the modified parameterization of Zhang et al. (2001) is implemented for V_d for particle (V_{dp}) in Eq. (A1) as Kajino et al. (2012). The original parameterization calculates deposition velocity of particles as a reciprocal of total transfer resistance in series of aerodynamic and surface resistances for each particle size bin. From this, the following modifications are made based on more recent studies (Katata et al., 2008, 2011; Petroff and Zhang, 2010): (1) On the basis of the fact that forests can collect a large amount of sub-micron particles (Gallagher et al., 1997; Matsuda et al., 2010) caused by high turbulence over the canopy (e.g., Petroff et al., 2009), hygroscopic growth of particles under humid conditions (Katata et al., 2013), and other collection mechanisms, the empirical constant ε_0, which is inversely proportional to the surface resistance (Zhang et al., 2001), was set to 5 and 1 for the forest and short vegetation categories, respectively. (2) For the collection efficiency by leaves due to inertial impaction, we used the modified function of Peters and Eiden (1992). (3) Collection efficiencies for vegetative surfaces due to interception and Brownian diffusion were modeled based on Kirsch and Fuchs (1968) and Fuchs (1964), respectively. (4) For the land use categories of desert, tundra, ice cap, glacier, inland water, and ocean, we adopted the surface resistance for non-vegetated surfaces proposed by Petroff and Zhang (2010).

After these modifications, the dry deposition velocity calculated by the modified model better agreed with the observational data than did the original model of Zhang et al. (2001). For example, the size-segregated V_d for forest is 0.1–1 cm s^{-1} in the range from 0.1–1 μm diameter and corresponded to the observations. For ground and water surfaces, a good agreement was found between the modified model calculations and the observations from the literature, as shown in Petroff and Zhang (2010) (not shown in the figure). For calculation of V_{dp}, a single log-normal size distribution is assumed for all radioactive particles. The mean mass equivalent particle diameters are set to 0.5 and 1.5 μm for ^{131}I and other radionuclides, respectively, based on the observational results at JAEA-Tokai from 17 March to 1 April (Miyamoto et al., 2014) with a geometric standard deviation of 1.6 μm (Kaneyasu et al., 2012).

Figure A1 illustrates the dry deposition velocity of ^{131}I, gaseous I_2 and CH_3I, and particulate iodine and ^{137}Cs (expecting the chemical form of CsI) for grassland and forest against horizontal wind speed for a typical sunny period during the accident. Generally, the deposition velocity of particles is larger in forest than on short vegetation as explained above, while deposition velocities of gases over two vegetation types do not have a large difference because stomata resistance is dominant rather than aerodynamic resistance. Atmospheric stability significantly decreases the nighttime V_d under low wind speed condition < 5 m s^{-1} (Fig. A1b). Consequently, the modeled dry deposition velocity of I_2, CH_3I, particulate iodine, and other particles can vary in the range of 0.001–0.5 cm s^{-1}, 0.0004–0.001 cm s^{-1}, 0.005–0.1 cm s^{-1}, and 0.02–0.3 cm s^{-1} over short vegetation. Deposition velocity of ^{131}I depends on the chemical composition, and has values from 0.003–0.2 cm s^{-1} when for example I_2: CH_3I: particulate iodine=2:3:5 based on the measurement of gaseous and particulate iodine concentrations at JAEA-Tokai on 15 March 2011. It should be noted that the original WSPEEDI-II used constant values of V_d of 0.3 and 0.1 cm s^{-1} for ^{131}I and ^{137}Cs, respectively, which are similar to daytime values calculated by the modified scheme.

During the FNPS1 accident, a few studies have reported the V_d for ^{131}I and ^{137}Cs calculated by the data of deposition flux and air concentration measured by bulk samplers and combined samplers of the dust filter and charcoal cartridge, respectively. Amano et al. (2012) showed that daily mean values of V_d were from 0.1–0.2 cm s^{-1} and 0.2–0.3 cm s^{-1} for ^{131}I and ^{137}Cs, respectively, at Chiba Prefecture from 14–17 March. Takeyasu and Sumiya (2014) used the daily fallout data sampled at JAEA-Tokai in Ibaraki Prefecture, and estimated the similar

values of V_d of both radionuclides as 0.26 cm s^{-1} and 0.43 cm s^{-1} in 15–16 March, respectively. Those results indicate that the modified dry deposition scheme is reasonable.

The in-cloud scavenging is activated in a model grid cell, where cloud water mixing ratio is higher than 10^{-6} (kg kg^{-1}) and the surface precipitation intensity is larger than zero.

Figure A1

In-cloud scavenging

Wet deposition has been also treated in WSPEEDI-II by a simple exponential function between scavenging coefficient (Λ) and precipitation intensity (P_r) without separation of chemical forms as in some other dispersion models (Table 1). We modified the scheme to be more mechanistic based on the in-cloud scavenging parameterization of Giorgi and Chameides (1986) for highly hygroscopic aerosols and soluble gases. Furthermore, the effects of gas solubility, aerosol hygroscopicity, and mixed phase cloud microphysics processes are also considered to the scheme. The new equation for scavenging coefficient due to nucleation (in-cloud) scavenging for non-convective clouds Λ_{in}, which considers the chemical forms of radionuclides, height dependency, aerosol activation, and ice phase, is expressed as:

$$\Lambda_{in}(z) = \frac{F_{in}}{\Delta t}\left[1 - \exp\left(-b_{in}\Delta t\right)\right] f_{ccn}(z) f_{ice}(z) f_{qt}(z), \quad \text{(A3)}$$

$$F_{in} = \frac{F_0}{1 + b_0 \tau_{in}}, \quad \text{(A4)}$$

$$b_{in} = \frac{b_0 + \tau_{in}^{-1}}{F_0}, \quad \text{(A5)}$$

where z is the height, f_{qt} is the fraction of total (solid + liquid) water mixing ratio (q_t) at each height to q_t accumulated throughout the cloud layer, τ_{in} is the lifetime of clouds (not indicating lifetime of a cloud or a cloud system but time for evolution of cloud droplets to settling hydrometeors and precipitation to ground surface), and F_0 and b_0 are the parameters given as 0.8 and $F_0 \cdot 10^{-4}$, respectively (Giorgi and Chameides, 1986). $F_{in}\left[1 - \exp\left(-b_{in}\Delta t\right)\right]$ indicates a fraction of hydrometeors in atmosphere reaching to ground surface within a time

step Δt, whereas $f_{ccn}(z)f_{ice}(z)f_{qt}(z)$ indicates a fraction of aerosols transferring to the hydrometeors in the time step. f_{ccn} and f_{ice} in Eq. (A3) are the fraction of the CCN activated aerosols forming the cloud droplets and the ratio of evolution rate of mixed phase cloud process relative to warm cloud processes, respectively, which are described later. It should be noted that $f_{ccn} = 1$ for gaseous iodine.

The scavenged time for gases and aerosols in the accumulation mode, τ_{in}, represents the amount of time required to remove aerosols or gases dissolved into all of the water from the cloud layer at the specified water equivalent precipitation rate, P_r (Byun and Schere, 2006), and is given

$$\tau_{in} = \frac{\overline{W_T}}{\rho_w P_r}(1+\gamma_{in}), \quad \text{(A6)}$$

$$\gamma_{in} = \begin{cases} 0 & \text{(particles)} \\ \dfrac{\rho_w}{H_i^* \overline{W_L} RT} & \text{(gases)} \end{cases}, \quad \text{(A7)}$$

where $\overline{W_T}$ is the vertically averaged total (i.e., solid + liquid) water content, ρ_w is the density of liquid water, $\overline{W_L}$ is the vertically averaged liquid water content (cloud + rain), R is the universal gas constant, T is the in-cloud air temperature, and H^*_i is the effective Henry's constant for gas species i. For gases, only dissolution to liquid hydrometeors is considered and deposition to solid hydrometeors is not considered. H_i^* is calculated for gaseous ^{131}I using input data of I^- concentration in rainwater of 3×10^{-9} mol l^{-1} (Gilfedder et al., 2008) and a typical value of rainwater pH=5 observed in Eastern Japan (Ministry of the Environment of Japan, 2010), resulting in H_i^* of approximately 55 and 0.23 for I_2 and CH_3I, respectively.

Cloud condensation nuclei (CCN) activation

For calculating f_{ccn}, the CCN activation and subsequent cloud microphysical processes were parameterized using Abdul-Razzak and Ghan (2000) and Lin et al. (1983). When the Abdul-Razzak and Ghan (2000) parameterization predicts that CCN activation occurs in a grid cell, the portions of the mass (calculated based on the predicted critical diameters and prescribed log-normal size distribution parameters of radioactive aerosols) were transferred to the grid-scale cloud droplets (f_{ccn}). In the above CCN activation scheme, the following size distribution

parameters are adopted. Number equivalent geometric mean dry diameter was set to 100 nm with geometric standard deviation of 1.6 (Adachi et al., 2013). The aerosol hygroscopicity κ=0.4 was assumed based on an internal mixture of sulfate and organics (Petters and Kreidensweis, 2007), which is consistent with the activity (mass) equivalent wet particle diameter obtained by Kaneyasu et al. (2012) under the typical meteorological conditions in the season in Japan. Figure A2a shows the sensitivity of CCN activation fraction, f_{ccn}, to vertical wind velocity. As shown in the figure, the value of f_{ccn} rapidly increases with an increase of vertical wind speed, and ambient aerosols become almost completely activated with vertical wind speed of > 0.1 m s^{-1}.

Figure A2

Mixed phase cloud microphysical processes

Lin et al. (1983) developed a grid-scale explicit cloud microphysics model in which interactions between cloud droplets and other hydrometers, such as rain, snow and graupel droplets, are formulated. The autoconversion rate (cloud→rain) and the accretion rate of cloud droplets by rain, snow, and graupel (cloud→rain, cloud→snow, cloud→graupel), predicted by Lin et al. (1983), were used to calculate the transfer of the aerosol moments and mass in the cloud droplets to the other hydrometers. To include the difference in the scavenging coefficient between liquid (rain) and ice phases (snow, ice crystal, and graupel), f_{ice} in Eq. (A3) is modeled based on the accretion rates for both phases using the cloud microphysics model of Lin et al. (1983) as follows. First, the accretion rate from cloud to the mixture of rain, snow, and graupel is calculated at each atmospheric layer. Then, the accretion rate of cloud droplets by rain by assuming all snow and graupel water are rain water. Finally, f_{ice} is determined by dividing the former accretion ratio for mixed with rain, snow, and graupel by the latter for rain, which is considered to represent the evolution rates for ice phase hydrometeors. During the FNPS1 accident, this modeling approach using f_{ice} increased the snowfall Λ_{in} up to 1.4 times of the rainfall Λ_{in} in the model domain (Figs. S7c and e) due to the effects of riming under the supercooling environment and smaller number concentration and density of ice crystals. This is consistent to the experimental (Wolf and Dana, 1969; Graedel and Franey, 1975; Sparmacher et al., 1993; Kyrö et al., 2009; Paramonov et al., 2011)

and modeling works of snow scavenging of aerosols with 1 μm in mass-equivalent diameter (Stier et al., 2005; Croft et al., 2009; Zhang et al., 2013). However, some modeling studies reported less scavenging rate of snow crystals (Maryon and Ryall, 1996; Hongisto, 1998). This difference may be caused by a large variety in the collection efficiencies of cloud droplets by snow crystals (Sauter and Wang, 1989; Mircea and Stefan, 1998) depending on complex physical background such as the size and shape of ice crystals and the ambient humidity (Miller and Wang, 1991; Feng, 2009; Wang et al., 2010).

Subgrid scale scavenging is not considered in the study because the horizontal grid resolution is fine enough for regional scale analysis (< 3 km) and, in addition, the subgrid scale convection should not be strong during the cold season.

Below-cloud scavenging

The below-cloud scavenging of aerosols by raindrops and ice crystals (aerosol-hydrometeor coagulation) is very small when compared with the nucleation scavenging rate for low and moderate rainfall rates of 0.1–10 mm h^{-1} (Andronache, 2003; Henzing et al., 2006; Zhang et al., 2013), Oshima et al. (2013) reported that even neglecting below-cloud scavenging resulted better performance in a regional scale aerosol transport simulation. However, even though the scavenging coefficient is small, below-cloud scavenging may be dominant to in-cloud scavenging at locations where few aerosols exists above the cloud base, such as areas close to the emission source.

Similarly to the in-cloud scavenging, the below-cloud scavenging of aerosols and gases are formulated as follows:

$$\Lambda_{bl}(z) = \frac{\left[1-\exp\left(-\Delta t/\tau_{bl}\right)\right]}{\Delta t} f_{wash}(z) f_{qs}(z), \qquad \text{(A8)}$$

where $f_{wash}(z)$ is a fraction of aerosols scavenged by settling hydrometeors in atmosphere within a time step Δt described as $1-\exp(-\lambda\Delta t)$ where λ is a sum of below-cloud scavenging coefficients of aerosols by rain, snow, and graupel particles. The values of Slinn et al. (1983) with enhancement due to thermophoresis, diffusiophoresis, and electrostatic forces (Andronache, 2004; 2006) are used for the scavenging coefficient of aerosols by rain droplets, while the values of Murakami et al. (1985) are used for that by snow and graupel particles. f_{qs} is the fraction of settling hydrometeors (rain, snow, and graupel) mixing ratio (q_s) at each

height to q_s accumulated throughout the cloud layer. Number equivalent geometric mean diameter of aerosols is set as 500 nm here considering hygroscopic growth under rainfall condition. The term $\left[1-\exp\left(-\Delta t/\tau_{bl}\right)\right]$ indicates a fraction of the relevant hydrometeors in atmosphere reaching to ground surface within a time step Δt, whereas $f_{wash}(z)f_{qs}(z)$ indicates a fraction of aerosols transferring to the hydrometeors within the time step. τ_{bl} is defined as

$$\tau_{bl} = \frac{\overline{W_S}}{\rho_w P_r}\left(1+\gamma_{bl}\right), \tag{A9}$$

$$\gamma_{bl} = \begin{cases} 0 & \text{(particles)} \\ \dfrac{\rho_w}{H_i^* \overline{W_r} RT} & \text{(gases)} \end{cases} \tag{A10}$$

where $\overline{W_S}$ is the vertically averaged settling hydrometeors water content and γ_{bl} is similar to that of Eq. (A7) but with $\overline{W_r}$, the vertically averaged rain water content. It should be noted that f_{wash} = 1 for gaseous iodine. The below-cloud scavenging is activated in a model grid cell, when the settling hydrometeor mixing ratio is higher than 10^{-9} (kg kg^{-1}) and the surface precipitation intensity is larger than zero.

Modeled scavenging coefficient

The modeled scavenging coefficient (Λ_{in}) by the modified wet deposition scheme for particle and gas is depicted in Fig. A2b. It is shown that Λ for particles decreases with an increase of total water content ($\overline{W_T}$) with constant precipitation rate (P_r) according to Eqs. (A3)–(A5) because Λ is a function of a reciprocal of τ represented as Eqs. (A6) and (A9). This means that less scavenged water is present in the atmosphere when $\overline{W_T}$ is small. For I_2 and CH_3I gases, γ becomes large compared with that of a particle (Eqs. A7 and A10) because it takes a longer time for the cloud droplets to dissolve less soluble gases. This increases the removal time for clouds (Eqs. A6 and A9), resulting in a lower scavenging coefficient. Figure A2c shows the precipitation intensity dependence of f_{wash} for aerosols in Eq. (A8). As seen in Fig. A2c, f_{wash} increases as the precipitation increases but the values are up to 0.1, 1, and 10% for rain, snow, and graupel, respectively, even at the very high precipitation intensity (10 mm h^{-1}). In the presence of same amounts of radionuclides, hydrometeors in the air, and precipitation

intensity, Λ_{bl} is almost equivalent to Λ_{in} as shown in Fig. A2b multiplied by f_{wash}. Therefore, the contribution of Λ_{bl} to total scavenging coefficient Λ ($\Lambda_{in} + \Lambda_{bl}$) for rain, snow, and graupel are approximately 0.01–0.1, 0.1–1, and 1–10 %, respectively. In the current simulation, since most of the precipitation was due to rain and snow in the contaminated areas, Λ_{bl} was smaller. The contribution of below-cloud scavenging to the total wet deposition over the whole regional as well as local domains was up to 1%. The original WSPEEDI-II has $\Lambda = 10^{-5}$–10^{-4} s^{-1} empirically determined from field measurement data of Λ by Brenk and Vogt (1981). This value is consistent with the calculation result of the modified scheme of Eq. (A3) when the cloud liquid water content is high. For low cloud water content (< 1 g m^{-3}), Λ becomes large up to 10^{-1} s^{-1} in the new scheme. In the FNPS1 accident, for example, calculated values of Λ in the areas of Naka-Dori and Tochigi and Gunma Prefectures in the WSPEEDI simulation were ranged from 10^{-4}–10^{-3} s^{-1} when the plume passed through there in the afternoon on 15 March (Fig. S6). This result is reasonable when compared with many observational studies for light and moderate rain events in various areas including Japan (Jylhä, 1991; Okita et al., 1996; Minoura and Iwasaka, 1997; Laakso et al., 2003; Andronache, 2004; Zhang et al., 2013). A few studies also reported very high values of $\Lambda > 10^{-3}$ s^{-1} for cosmogenic radionuclides (Davis, 1972) and of Λ=0.2 s^{-1} for cloud droplets in 5–60 μm diameter range (Levine and Schwartz, 1982).

The Λ for particle is two orders of higher magnitude than that of I_2 gas due to the effect of gas solubility modeled in Eqs. (A7) and (A10). In the same manner, the Λ for CH_3I gas has very small values in the range of 10^{-10}–10^{-8} s^{-1} due to its very low Henry's constant (Fig. A2b). Such tendency as lower Λ for gas than that for particle is supported by the observational studies (Brenk and Vogt, 1981).

Fogwater deposition

Fogwater deposition is the phenomenon that radionuclides in liquid water droplets of fog or low-cloud are transported downward by turbulence above the ground, and eventually these droplets are intercepted by the plant canopies (Lovett, 1984). Although the potential effect of this process has been suggested in prior work (Baklanov and Sørensen, 2001), modeling of fogwater deposition is not done in any of the existing dispersion models (Table 1). This study introduces a simple and accurate Fog Deposition EStimation (FogDES) scheme for

meteorological models (Katata et al., 2010; Katata, 2014). In general, fogwater deposition can be also calculated using Eq. (A1) with the concentration of radionuclides in cloud liquid water in the lowest atmospheric layer. To simplify, radionuclides are assumed to be completely absorbed by fogwater. Only the parameter of V_d is required to calculate the fogwater deposition flux. In FogDES scheme, V_d for fogwater (V_{df}) can be parameterized as a linear function of the horizontal wind speed and vegetation parameters:

$$V_{df} = R_{\mathrm{LUC}} A_c U \,, \tag{A11}$$

$$A_c = \begin{cases} 0.0164(\mathrm{LAI}/h)^{-0.5} \\ 0.0095\mathrm{LAI}^3 - 0.05\mathrm{LAI}^2 + 0.0916\mathrm{LAI} + 0.0082 \end{cases}, \tag{A12}$$

where LAI is the leaf area index, h is the canopy height, R_{LUC} is the ratio of V_{df} for each landuse category (LUC) of MM5 to that for coniferous forest (i.e., R_{LUC} = 1 for coniferous forest). A_c value was set to be constant as 0.0248 determined at dense mountainous forest in Germany (Katata et al., 2008) due to lack of accurate data of vegetation parameters (LAI and h) in the study area. By considering relatively small V_{df} for short vegetation compared with tall vegetation (e.g., Gallagher et al., 1988), the value of 1, 0.2, and 0.1 were applied to R_{LUC} for forest, short vegetation (such as crop- and grassland), and smooth surface (such as water bodies and bare soil).

The deposition velocity due to fogwater is plotted against wind speed in Fig. A1. The calculations are in the range of observation data ranging from 2–8 cm s^{-1} and 1–100 cm s^{-1} over short vegetation (e.g., Gallagher et al., 1988; Thalmann et al.., 2002) and dense closed forest (e.g., Dasch, 1988; Klemm and Wrzesinsky, 2007; Eugster et al., 2006) as reviewed in Katata (2014). Importantly, the figure also shows relatively large impacts of fogwater deposition to total deposition compared with dry deposition because the fog droplets are larger than submicron aerosols and have a higher impaction efficiency to plant leaves.

Acknowledgements

The authors express their gratitude to Drs. Fumiya Tanabe and Yu Maruyama for their helpful comments and suggestions. Dr. Kevin Foster, Lawrence Livermore National Laboratory, Livermore (LLNL) of the USA, provided the digital data of air dose rate by US-DOE airborne monitoring. The source terms of Hirao et al. (2013) and Winiarek et al. (2014) were provided by Dr. Shigekazu Hirao, Nagoya University in Japan and Mr. Victor Winiarek, Centre d'Enseignement et de Recherche en Environnement Atmosphérique (CEREA) in France, respectively. This study was partly supported by a Grant-in-Aid for Scientific Research, No. 21120512, provided by the Japan Society for the Promotion of Science (JSPS).

References

Abdul-Razzak, H., and Ghan, S.J.: A parameterization of aerosol activation. 2. Multiple aerosol types, J. Geophys. Res., 105, 6837-6844, 2000.

Achim, P., Monfort, M., Le Petit, G., Gross, P., Douysset, G., Taffary, T., Blanchard, X., and Moulin, C.: Analysis of Radionuclide Releases from the Fukushima Dai-ichi Nuclear Power Plant Accident Part II, Pure Appl. Geophys., 171, 645-667, 2014.

Adachi, K., Kajino, M., Zaizen, Y., and Igarashi, Y.: Emission of spherical cesium-bearing particles from an early stage of the Fukushima nuclear accident, Sci. Rep., 3, 2554, 2013.

Amano, H., Akiyama, M., Chunlei, B., Kawamura, T., Kishimoto, T., Kuroda, T., Muroi, T., Odaira, T., Ohta, Y., Takeda, K., Watanabe, Y., and Morimoto, T.: Radiation measurements in the Chiba Metropolitan Area and radiological aspects of fallout from the Fukushima Dai-ichi Nuclear Power Plants accident, J. Environ. Radioact., 111, 42-52, 2012.

Andronache, C.: Estimated variability of below-cloud aerosol removal by rainfall for observed aerosol size distributions, Atmos. Chem. Phys., 3, 131-143, 2003.

Andronache, C.: Estimates of sulfate aerosol wet scavenging coefficient for locations in the Eastern United States, Atmos. Environ., 38, 795-804, 2004.

Aoyama M., Tsumune D., and Hamajima Y.: Distribution of ^{137}Cs and ^{134}Cs in the North Pacific Ocean: impacts of the TEPCO Fukushima-Daiichi NPP accident, J. Radioanal. Nucl.

Ch., 296, 535-539, 2012.

Baklanov, A., and Sørensen, J.H.: Parameterisation of radionuclide deposition in atmospheric long-range transport modelling, Phys. Chem. Earth, 26, 787-799, 2001.

Brenk, H.D., and Vogt, K.J., The calculation of wet deposition from radioactive plumes, Nucl. Safety, 22, 362-371, 1981.

Byun, D., and Schere, K. L.: Review of the governing equations, computational algorithms, and other components of the models-3 Community Multiscale Air Quality (CMAQ) modeling system, Appl. Mech. Rev., 59, 1-6, 2006.

Chino, M., Nakayama, H., Nagai, H., Terada, H., Katata, G., and Yamazawa, H.: Preliminary estimation of release amounts of ^{131}I and ^{137}Cs accidentally discharged from the Fukushima Daiichi nuclear power plant into atmosphere, J. Nucl. Sci. Technol., 48, 1129-1134, 2011.

Christoudias, T., and Lelieveld, J.: Modelling the global atmospheric transport and deposition of radionuclides from the Fukushima Dai-ichi nuclear accident, Atmos. Chem. Phys., 13, 1425-1438, 2013.

CTBTO (Comprehensive Nuclear-Test-Ban Treaty Organization, Preparatory Commission): Fukushima-related Measurements by CTBTO, http://www.ctbto.org/press-centre/highlights/2011/fukushima-related-measurements-by-the-ctbto, 2011 (last access: 25 12 November 2014).

Croft, B., ; Lohmann, U., Martin, R. V., Stier, P., Wurzler, S., Feichter, J., Posselt, R., and Ferrachat, S.: Aerosol size-dependent below-cloud scavenging by rain and snow in the ECHAM5-HAM, Atmos. Chem. Phys., 14, 4653-4675, 2009

D'Amours, R., Malo, A., Servranckx, R., Bensimon, D., Trudel, S. and Gauthier, J.-P.: Application of the atmospheric Lagrangian particle dispersion model MLDP0 to the 2008 eruptions of Okmok and Kasatochi volcanoes, J. Geophys. Res., 115, D00L11, 2010.

Dasch, M.J.: Hydrological and chemical inputs to fir trees from rain and clouds during a 1-month study at Clingmans Peak, NC, Atmos. Environ., 22, 2255-2262, 1988.

Davis, W.E.: A model for in-cloud scavenging of cosmogenic radionuclides, J. Geophys. Res., 77, 2159-2165, 1972.

Draxler, R.R.: The use of global and mesoscale meteorological model data to predict the transport and dispersion of tracer plumes over Washington, D.C., Wea. Forecasting, 21, 383-394, 2006.

Draxler, R.R., and Rolph, G.D.: Evaluation of the transfer coefficient matrix (TCM) approach to model the atmospheric radionuclide air concentrations from Fukushima, J. Geophys. Res., 117, D05107, 2012.

Draxler, R., Arnold, D., Chino, M., Galmarini, S., Hort, M., Jones, A., Leadbetter, S., Malo, A., Maurer, C., Rolph, G., Saito, K., Servranckx, R., Shimbori, T., Solazzo, E., and Wotawa, G.: World Meteorological Organization's model simulations of the radionuclide dispersion and deposition from the Fukushima Daiichi Nuclear Power Plant accident, J. Environ. Radioact., 2014 (in press). DOI: 10.1016/j.jenvrad.2013.09.014

Dvorzhak, A., Puras, C., Montero, M.: Spanish Experience on Modeling of Environmental Radioactive Contamination Due to Fukushima Daiichi NPP Accident Using JRODOS, Environ. Sci. Technol., 46, 11887-11895, 2012.

Eugster, W., Burkard, R., Holwerda, F., Scatena, F.N., and Bruijnzeel, L. A.: Characteristics of fog and fogwater fluxes in a Puerto Rican elfin cloud forest, Agri. Forest Meteorol., 139, 288-306, 2006.

Evangeliou, N., Balkanski, Y., Cozic, A., Moller, A.P.: Global Transport and Deposition of Cs-137 Following the Fukushima Nuclear Power Plant Accident in Japan: Emphasis on Europe and Asia Using High-Resolution Model Versions and Radiological Impact Assessment of the Human Population and the Environment Using Interactive Tools, Environ. Sci. Technol., 47, 5803-5812, 2013.

Feng, J.: A size-resolved model for below-cloud scavenging of aerosols by snowfall, J. Geophys. Res., 114, D08203, 2009.

Fuchs, N. A.: The Mechanics of Aerosols, Pergamon Press, Oxford, 1964.

Fukushima Prefecture: http://www.pref.fukushima.lg.jp/sec_file/monitoring/m-3/20-50km0312-0331.pdf, 2011a (in Japanese, last access: 12 November 2014).

Fukushima Prefecture: http://www.pref.fukushima.lg.jp/sec_file/monitoring/m-1/7houbu0311-0331.pdf, 2011b (in Japanese, last access: 12 November 2014).

Fukushima Prefecture: Results of air dose rate measurement on March 2011 (data retrieved from monitoring posts in Fukushima Prefecture), http://www.atom-moc.pref.fukushima.jp/monitoring/monitoring201103/201103_mpdata.html, 2012 (in Japanese, last access: 12 November 2014).

Furuno, A., Terada, H., Chino, M., and Yamazawa, H.: Experimental verification for real-time environmental emergency response system: WSPEEDI by European tracer experiment. Atmos. Environ., 38, 6989-6998, 2004.

Furuta, S., Sumiya, S. Watanabe, H. Nakano, M., Imaizumi, K., Takeyasu, M., Nakada, A., Fujita, H., Mizutani, T., Morisawa, M., Kokubun, Y., Kono, T., Nagaoka, M., Yokoyama, H., Hokama, T., Isozaki, T., Nemoto, M., Hiyama, Y., Onuma, T., Kato, C., and Kurachi, T.: Results of the environmental radiation monitoring following the accident at the Fukushima Daiichi Nuclear Power Plant; Interim report (Ambient radiation dose rate, radioactivity concentration in the air and radioactivity concentration in the fallout), JAEA-Review 2011-035, Japan Atomic Energy Agency, 2011 (in Japanese with English abstract).

Gallagher, M.W., Choularton, T.W., Morse, A.P., and Fowler, D.: Measurements of the size dependence of cloud droplet deposition at a hill site, Q. J. Roy. Meteorol. Soc., 114, 1291-1303, 1988.

Gallagher, M.W., Beswick, K.M., Choularton, T.W., Duyzer, J., Westrate, H., and Hummelshøj, P.: Measurements of aerosol fluxes to speulder forest using a micrometeorological technique, Atmos. Environ., 31, 359-373, 1997

Gilfedder, B.S., Lai, S.C., Petri, M., Biester, H., Hoffmann, T.: Iodine speciation in rain, snow and aerosols, Atmos. Chem. Phys., 8, 6069-6084, 2008.

Giorgi, F., and Chameides, W. L.: Rainout lifetimes of highly soluble aerosols and gases inferred from simulations with a general circulation model, J. Geophys. Res., 91, 14367-14376, 1986.

Graedel, T. E., and Franey, J. P.: Field measurements of submicron aerosol washout by snow, Geophys. Res. Lett., 2, 325-328, 1975.

Grell, G.A., Dudhia, J., and Stauffer, D.R.: A Description of the Fifth-generation Penn State/NCAR Mesoscale Model (MM5), NCAR Tech. Note NCAR/TN-3921STR, 122 pp, 1994.

Haba, H., Kaneya, J., Mukai, H., Kambara, T., Kase, M.: One-year monitoring of airborne radionuclides in Wako, Japan, after the Fukushima Dai-ichi nuclear power plant accident in 2011, Geochem. J., 46, 271-278, 2012.

HCRM (Health Canada's Radiation Monitoring): Health Canada's Radiation Monitoring (HCRM) Data and the Nuclear Emergency in Japan, the CTBTO data for Canadian stations. http://www.hc-sc.gc.ca/hc-ps/ed-ud/respond/nuclea/data-donnees-eng.php, 2011 (last access: 12 November 2014).

Henzing, J. S., Olvie, D. J. L., and van Velthoven, P. F. J.: A parameterization of size resolved below cloud scavenging of aerosols by rain, Atmos. Chem. Phys., 6, 3363-3375, 2006.

Hertel, O., Christensen, J., Runge, E. H., Asman, W. A. H., Berkowicz, R., Hovmand, M. F., Hov, Ø.: Development and testing of a new variable scale air pollution model—ACDEP, Atmos. Environ., 29, 1267-1290, 1995.

Hicks, B.B., Baldocchi, D. D., Meyers, T. P., Hosker, R. P., and Matt, D. R.: A preliminary multiple resistance routine for deriving dry deposition velocities from measured quantities, Water Air Soil Pollut., 36, 311-330, 1987.

Hirao, S., Yamazawa, H.; Nagae, T.: Estimation of release rate of iodine-131 and cesium-137 from the Fukushima Daiichi nuclear power plant, J. Nucl. Sci. Technol., 50, 139-147, 2013.

Honda M.C., Aono T., Aoyama M., Hamajima Y., Kawakami H., Kitamura M., Masumoto Y., Miyazawa Y., Takigawa M., and Saino T.: Dispersion of artificial caesium-134 and -137 in the western North Pacific one month after the Fukushima accident. Geochem. J., 46, E1-E9, 2012.

Hongisto, M.: HILATAR, a regional scale grid model for the transport of sulphur and nitrogen compounds. Description of the model and simulation results for the year 1993. Finnish Meteorological Institute, Helsinki, No 21, 1998.

Ibaraki Prefecture: http://www.pref.ibaraki.jp/20110311eq/radiation.html, 2011 (in Japanese, last access: 12 November 2014).

Jacobson, M.Z.: Fundamentals of Atmospheric Modeling, Cambridge University Press, Cambridge, 828 pp., 2005.

Jones, A.R., Thomson, D.J., Hort, M.C. and Devenish, B.: The U.K. Met Office's next-generation atmospheric dispersion model, NAME III, In: Borrego, C., Norman, A.L. (Eds.), Air Pollution and Its Applications XVII, Proceedings of the 27th NATO/CCMS International Technical Meeting on Air Pollution Modelling and Its Application. Springer, pp. 580, 2007.

Jylhä, K.: Empirical scavenging coefficients of radioactive substances released from chernobyl, Atmos. Environ., 25, 263-270, 1991.

Kajino, M., Inomata, Y., Sato, K., Ueda, H., Han, Z., An, J., Katata, G., Deushi, M., Maki, T., Oshima, N., Kurokawa, J., Ohara, T., Takami, A., and Hatakeyama, S.: Development of the RAQM2 aerosol chemical transport model and predictions of the Northeast Asian aerosol mass, size, chemistry, and mixing type. Atmos. Chem. Phys., 12, 11833-11856, 2012.

Kaneyasu, N., Ohashi, H., Suzuki, F., Okuda, T., and Ikemori, F.: Sulfate aerosol as a potential transport medium of radiocesium from the Fukushima nuclear accident, Environ. Sci. Technol., 46, 5720-5726, 2012.

Katata, G.: Fogwater deposition modeling for terrestrial ecosystems: A review of developments and measurements. J. Geophys. Res., 119, 8137-8159, 2014.

Katata, G., Kajino, M., Hiraki, T., Aikawa, M., Kobayashi, T., and Nagai, H.: A method for simple and accurate estimation of fog deposition in a mountain forest using a meteorological model. J. Geophys. Res., 116, D20102, 2011.

Katata G., Nagai H., Wrzesinsky T., Klemm O., Eugster W., and Burkard R.: Development of a land surface model including cloud water deposition on vegetation. J. Appl. Meteorol. Climatol., 47, 2129-2146, 2008.

Katata G., Nagai H., Zhang L., Held A., Serça D., and Klemm O.: Development of an atmosphere-soil-vegetation model for investigation of radioactive materials transport in the terrestrial biosphere, Prog. Nucl. Sci. Technol., 2, 530-537, 2011.

Katata, G., Terada, H., Nagai, H., and Chino, M.: Numerical reconstruction of high dose rate zones due to the Fukushima Daiichi Nuclear Power Plant accident, J. Environ. Radioact., 111, 2-12, 2012a.

Katata, G., Ota, M., Terada, H., Chino, M., and Nagai, H.: Atmospheric discharge and dispersion of radionuclides during the Fukushima Dai-ichi Nuclear Power Plant accident. Part I: Source term estimation and local-scale atmospheric dispersion in early phase of the accident. J. Environ. Radioact., 109, 103-113, 2012b.

Katata, G., Kajino, M., Matsuda, K., Takahashi, A., and Nakaya, K.: A numerical study of the effects of aerosol hygroscopic properties to dry deposition on a broad-leaved forest, Atmos. Environ., 97, 501-510, 2014.

Kawamura, H., Kobayashi, T., Furuno, A., Usui, N., Kamachi, M.: Numerical simulation on the long-term variation of radioactive cesium concentration in the North Pacific due to the Fukushima disaster, J. Environ. Radioact., 136, 64-75, 2014.

KEK (High Energy Accelerator Research Organization): http://legacy.kek.jp/quake/radmonitor/index-e.html, 2011 (last access: 12 November 2014).

Kerkweg, A., Buchholz, J., Ganzeveld, L., Pozzer, A., Tost, H., Jockel, P.: Technical note: An implementation of the dry removal processes DRY DEPosition and SEDImentation in the modular earth submodel system (MESSy), Atmos. Chem. Phys., 6, 4617-4632, 2006.

Kirsch, A. A. and Fuchs, N. A.: Studies on fibrous aerosol filters. III. Diffusional deposition of aerosols in fibrous filters, Ann. Occup. Hyg., 11, 299-304, 1968.

Klemm, O., and Wrzesinsky, T.: Fog deposition fluxes of water and ions to a mountainous site in Central Europe, Tellus, 59B, 705-714, 2007.

Kobayashi, T., Otosaka, S., Togawa, O., and Hayashi, K.: Development of a non-conservative radionuclides dispersion model in the ocean and its application to surface cesium-137 dispersion in the Irish Sea, J. Nucl. Sci. Technol., 44, 238-247, 2007.

Kobayashi, T., Nagai, H., Chino, M., and Kawamura, H.: Source term estimation of atmospheric release due to the Fukushima Dai-ichi Nuclear Power Plant accident by atmospheric and oceanic dispersion simulations, J. Nucl. Sci. Technol., 50 255-264, 2013.

Korsakissok, I., Mathieu, A., and Didier, D.: Atmospheric dispersion and ground deposition induced by the Fukushima Nuclear Power Plant accident: A local-scale simulation and sensitivity study, Atmos. Environ., 70, 267-279, 2013.

Kyrö, E. M.., Grönholm, T., Vuollekoski, H., Virkkula, A., Kulmala, M., and Laakso, L.: Snow scavenging of ultrafine particles: Field measurements and parameterization, Borel Environ. Res., 14, 527-538, 2009.

Laakso, L., Grönholm, T., Rannik, U., Kosmale, M., Fiedler, V., Vehkamäki, H., and Kulmala, M.: Ultrafine particle scavenging coefficients calculated from 6 years field measurements, Atmos. Environ., 37, 3605-3613, 2003.

Leadbetter, S., Hort, M., Jones, A., Webster, H., and Draxler, R.: Sensitivity of the modeled deposition of Caesium-137 from the Fukushima Dai-ichi nuclear power plant to the wet deposition parameterization in NAME, 2014 (in press). DOI: 10.1016/j.jenvrad.2014.03.018

Levine, S. Z., and Schwartz, S. E.: In-cloud and below-cloud scavenging of Nitric acid vapor, Atmos. Environ., 16, 1725-1734, 1982.

Lin, Y.-L., Richard, D. F., and Harold, D. O.: Bulk parameterization of the snow field in a cloud model, J. Clim. Appl. Meteorol., 22, 1065-1092, 1983.

Lovett, G. M.: Rates and mechanisms of cloud water deposition to a subalpine balsam fir forest, Atmos. Environ., 18, 361-371, 1984.

Masson, O., Baeza, A., Bieringer, J., Brudecki, K., Bucci, S., Cappai, M., Carvalho, F. P., Connan, O., Cosma, C., Dalheimer, A., D. Didier, G. Depuydt, L.E. De Geer, A. De Vismes, L. Gini, F. Groppi, K. Gudnason, R. Gurriaran, D. Hainz, Halldorsson, O., D. Hammond, O. Hanley, K. Holey, Zs. Homoki, A. Ioannidou, K. Isajenko, M. Jankovic, C. Katzlberger, M. Kettunen, R. Kierepko, R. Kontro, P.J.M. Kwakman, M. Lecomte, L. Leon Vintro, A.-P. Leppänen, B. Lind, G. Lujaniene, P. Mc Ginnity, C. Mc Mahon, H. Mala, S. Manenti, M. Manolopoulou, A. Mattila, A. Mauring, J.W. Mietelski, B. Moller, S.P. Nielsen, J. Nikolic, R.M.W. Overwater, S. E. Palsson, C. Papastefanou, I. Penev, M.K. Pham, P.P. Povinec, H. Ramebäck, M.C. Reis, W. Ringer, A. Rodriguez, P. Rulik, P.R.J. Saey, V. Samsonov, C. Schlosser, G. Sgorbati, B. V. Silobritiene, C. Söderström, R. Sogni, L. Solier, M. Sonck, G. Steinhauser, T. Steinkopff, P. Steinmann, S. Stoulos, I. Sykora, D. Todorovic, N. Tooloutalaie, L. Tositti, J. Tschiersch, A. Ugron, E. Vagena, A. Vargas, H. Wershofen, and Zhukova, O.: Tracking of airborne radionuclides from the damaged Fukushima Dai-Ichi nuclear reactors by European Networks, Environ. Sci. Technol., 45, 7670-7677, 2011.

Masuda, S., Awaji, T., Sugiura, N., Toyoda, T., Ishikawa, Y., and Horiuchi, K.: Interannual variability of temperature inversions in the subarctic North Pacific, Geophys. Res. Lett., 33, L24610, 2006.

Matsuda, K., Fujimura, Y., Hayashi, K., Takahashi, A., and Nakaya, K.: Deposition velocity of PM2.5 sulfate in the summer above a deciduous forest in central Japan. Atmos. Environ. 44, 4582-4587, 2010.

Maryon, R. H., and Ryall, D. B.: Developments to the UK nuclear accident response model (NAME). Department of Environment, UK Met. Office. DoE Report # DOE/RAS/96.011, 1996.

Mathieu, A., Korsakissok, I., Quélo, D., Groëll, J., Tombette, M., Didier, D., Quentric, E., Saunier, O., Benoit, J.-P., and Isnard, O.: Atmospheric dispersion and deposition of

radionuclides from the Fukushima Daiichi nuclear power plant accident, Elements, 8, 195-200, 2012.

METI (Ministry of Economy, Trade and Industry): http://www.meti.go.jp/press/2011/06/20110603019/20110603019.html, 2011 (in Japanese, last access: 12 November 2014).

Miller, C. T., Poirier Mcneill, M. M., and Mayer, A. S.: Dissolution of trapped nonaqueous phase liquids: mass transfer characteristics, Water Resour. Res., 26, 2783-2796, 1990.

Miller, N. L., and Wang, P. K.: Theoretical determination of the efficiency of aerosol particle collection by falling columnar ice crystals, J. Atmos. Sci., 46, 1656-1663, 1989.

Ministry of the Environment of Japan: Comprehensive summary report on acid deposition monitoring survey Phase 4, http://db.cger.nies.go.jp/dataset/acidrain/ja/04/index.html, 2010 (in Japanese, last access: 12 November 2014)

Minoura, H., and Iwasaka, Y.: Ion concentration changes observed in drizzling rains, Atmos. Res., 45, 165-182, 2006.

Mircea, M., and Stefan, S.: A theoretical study of the microphysical parameterization of the scavenging coefficient as a function of precipitation type and rate, Atmos. Environ., 32, 2931-2938, 1998.

Miyamoto, Y., Yasuda, K., and Magara, M.: Size distribution of radioactive particles collected at Tokai, Japan 6 days after the nuclear accident, J. Environ. Radioact., 132, 1-7, 2014.

Morino, Y., Ohara, T., and Nishizawa, M.: Atmospheric behavior, deposition, and budget of radioactive materials from the Fukushima Daiichi nuclear power plant in March 2011, Geophys. Res. Lett., 38, L00G11, 2011.

Morino, Y., Ohara, T., Watanabe, M., Hayashi, S., and Nishizawa, M.: Episode analysis of deposition of radiocesium from the Fukushima Daiichi nuclear power plant accident, Environ. Sci. Technol., 47, 2314-2322, 2013.

Morrison, H., Curry, J. A., and Khvorostyanov, V. I.: A new double-moment microphysics parameterization for application in cloud and climate models. Part I: Description, J. Atmos. Sci., 62,1665-1677, 2005.

NOAA (National Oceanic and Atmospheric Administration): National Oceanic and Atmospheric Administration, Air Resources Laboratory, Fukushima Daiichi Nuclear Power Plant Transfer Coefficient Matrix, http://ready.arl.noaa.gov/READY_fdnpp.php, 2012 (last access: 12 November 2014).

NOAA: World Meteorological Organization (WMO) Atmospheric Dispersion Model Simulations of Fukushima Daiichi Accident. U.S. National Oceanic and Atmospheric Administration, http://ready.arl.noaa.gov/READY_fdnppwmo.php, 2014 (last access: 12 November 2014).

NISA: nuclear species analysis by gamma-ray detection at Fukushima Daini Nuclear Power Station (16 March 2011), http://www.nsr.go.jp/archive/nisa/disclosure/kaijiseikyu/files/20-1.pdf, 2011 (in Japanese, last access: 12 November 2014).

Nishihara, K., Iwamoto, H., and Suyama, K.: Estimation of fuel compositions in Fukushima-Daiichi nuclear power plant, JAEA-Data/Code 2012-018, Japan Atomic Energy Agency, 2012 (in Japanese with English abstract).

NRA (Nuclear Regulation Authority), Readings of Seawater and Dust Monitoring in Sea Area by MEXT (March 2011), http://radioactivity.nsr.go.jp/en/list/259/list-201103.html, 2011 (last access: 12 November 2014)

NRA: Results of the (i) Fifth Airborne Monitoring Survey and (ii) Airborne Monitoring Survey Outside 80km from the Fukushima Dai-ichi NPP, http://radioactivity.nsr.go.jp/en/contents/6000/5790/24/203_0928_14e.pdf, 2012a (last accress: 12 November 2014)

NRA: Readings of dust sampling (All Results for May 2011), http://radioactivity.nsr.go.jp/en/contents/4000/3156/24/dust%20sampling_All%20Results%20for%20May%202011.pdf, 2012b (last access: 12 November 2014).

Ohfuchi, W., Nakamura, H., Yoshioka, M. K., Enomoto, T., Takaya, K., Peng, X., Yamane, S., Nishimura, T., Kurihara, Y., and Ninomiya, K.: 10-km mesh meso-scale resolving simulations of the global atmosphere on the Earth Simulator: Preliminary outcomes of AFES (AGCM for the Earth Simulator), J. Earth Simul., 1, 8-34, 2004.

Ohkura, T., Oishi, T., Taki, M., Shibanuma, Y., Kikuchi, M., Akino, H., Kikuta, Y., Kawasaki, M., Saegusa, J., Tsutsumi, M., Ogose, H., Tamura, S., and Sawahata, T.: Emergency monitoring of environmental radiation and atmospheric radionuclides at Nuclear

Science Research Institute, JAEA following the accident of Fukushima Daiichi nuclear power plant, JAEA-Data/Code 2012-010, Japan Atomic Energy Agency, 2012 (in Japanese with English abstract).

Okita, T., Hara, H., and Fukuzaki, N.: Measurements of atmospheric SO_2 and SO_4^{2-}, and determination of the wet scavenging coefficient of sulfate aerosols for the winter monsoon season over the sea of Japan, Atmos. Environ., 30, 3733-3739, 1996.

Oshima, N., Koike, M., Kondo, Y., Nakamura, H., Moteki, N., Matsui, H., Takegawa, N., and Kita, K.: Vertical transport mechanisms of black carbon over East Asia in spring during the A-FORCE aircraft campaign, J. Geophys. Res., 118, 13175-13198, 2013.

Paramonov, M., Grönholm, T., and Virkkula, A.: Below-cloud scavenging of aerosol particles by snow at an urban site in Finland, Boreal Environ. Res.., 16, 304-320, 2011.

Peters, K., and Eiden, R.: Modelling the dry deposition velocity of aerosol particles to a spruce forest, Atmos. Environ., 26A, 2555-2564, 1992.

Petroff, A. and Zhang, L.: Development and validation of a size-resolved particle dry deposition scheme for application in aerosol transport models, Geosci. Model Dev., 3, 753-769, 2010.

Petroff, A., Zhang, L., Pryor, S.C., and Belot, Y.: An extended dry deposition model for aerosols onto broadleaf canopies, J. Aerosol Sci., 40, 218-240, 2009.

Petters, M. D., and Kreidenweis, S. M.: A single parameter representation of hygroscopic growth and cloud condensation nucleus activity, Atmos. Chem. Phys., 7, 1961-1971, 2007.

Prime Minister of Japan and His Cabinet: Report of Japanese Government to the IAEA Ministerial Conference on Nuclear Safety–The Accident at TEPCO's Fukushima Nuclear Power Stations–, http://japan.kantei.go.jp/kan/topics/201106/iaea_houkokusho_e.html, 2011 (last access: 12 November 2014).

RADNET: United States Environmental Protection Agency's Radiation monitoring Network (RADNET) sampling data for the Japanese Nuclear Emergency, http://www.epa.gov/japan2011/rert/radnet-sampling-data.html, 2011 (last access: 12 November 2014).

Reisner, J., Rasmussen, R. M., and Bruintjes, R. T.: Explicit forecasting of supercooled liquid water in winter storms using the MM5 mesoscale model, Q. J. Roy. Meteorol. Soc., 124, 1071-1107, 1998.

Sanada, N., and Torii, T.: Aerial radiation monitoring around the Fukushima Dai-ichi Nuclear Power Plant using an unmanned helicopter, J. Environ. Radioact., 2014 (in press). doi: 10.1016/j.jenvrad.2014.06.027.

Saunier, O., Mathieu, A., Didier, D., Tombette, M., Quélo, D., Winiarek, V., and Bocquet, M.: An inverse modeling method to assess the source term of the Fukushima Nuclear Power Plant accident using gamma dose rate observations, Atmos. Chem. Phys. 13, 11403-11421, 2013.

Sauter, D.P., and Wang, P.K.: An experimental study of the scavenging of aerosol particles by natural snow crystals, J. Atmos. Sci., 46, 1650-1655, 1989.

Sehmel, G.A.: Particle and gas dry deposition: A review, Atmos. Environ., 14, 983-1011, 1980.

Smagorinsky, J.: General circulation experiments with the primitive equations, Mon. Wea. Rev., 91, 99-164, 1963.

Sparmacher, H., Fulber, K., and Bonka, H.: Below-cloud scavenging of aerosol particles: particle-bound radionuclides – experimental, Atmos. Environ., 27, 605-618, 1993.

Srinivas, C.V., Venkatesan, R., Baskaran, R., Rajagopal, V., and Venkatraman, B.: Regional scale atmospheric dispersion simulation of accidental releases of radionuclides from Fukushima Dai-ichi reactor, Atmos. Environ., 61, 66-84, 2012.

Stier, P., Feichter, J., Kinne, S., Kloster, S., Vignati, E., Wilson, J., Ganzeveld, L., Tegen, I., Werner, M., Balkanski, Y., Schulz, M., Boucher, O., Minikin, A., and Petzold, A.: The aerosol-climate model ECHAM5-HAM, Atmos. Chem. Phys., 5, 1125-1156, 2005.

Stohl, A., Seibert, P., Wotawa, G., Arnold, D., Burkhart, J.F., Eckhardt, S., Tapia, C., Vargas, A., and Yasunari, T.J.: Xenon-133 and caesium-137 releases into the atmosphere from the Fukushima Dai-ichi nuclear power plant: determination of the source term, atmospheric dispersion, and deposition, Atmos. Chem. Phys., 12, 2313–2343, 2012.

Sugiyama, G., Nasstrom, J., Pobanz, B., Foster, K., Simpson, M., Vogt, P., Aluzzi, F., and Homann, S.: Atmospheric sispersion modeling: challenges of the Fukushima Daiichi response, Health Phys., 102, 493-508, 2012.

Sugiura, N., Awaji, T., Masuda, S., Mochizuki, T., Toyoda, T., Miyama, T., Igarashi, H., and Ishikawa, Y.: Development of a four-dimensional variational coupled data assimilation system for enhanced analysis and prediction of seasonal to interannual climate variations, J. Geophys. Res., C10017, 2008.

Takemura, T., Nakamura, H., Takigawa, M., Kondo, H., Satomura, T., Miyasaka, T., and Nakajima, T.: A numerical simulation of global transport of atmospheric particles emitted from the Fukushima Daiichi nuclear power plant, Sola, 7, 101-104, 2011.

Takeyasu, M., and Sumiya, S.: Estimation of dry deposition velocities of radionuclides released by the accident at the Fukushima Dai-ichi Nuclear Power Plant, Prog. Nucl. Sci. Technol., 4, 64-67, 2014.

Tanabe, F.: A scenario of large amount of radioactive materials discharge to the air from the Unit 2 reactor in the Fukushima Daiichi NPP accident, J. Nucl. Sci. Technol., 49, 360-365, 2012.

Ten Hoeve, J.E., and Jacobson, M.Z.: Worldwide health effects of the Fukushima Daiichi nuclear accident, Energy Environ. Sci., 5, 8743-8757, 2012.

TEPCO (Tokyo Electric Power Company): Press Releases, http://www.tepco.co.jp/en/press/corp-com/release/index-e.html, 2011a (last access: 12 November 2014)

TEPCO: Radiation dose measured in the Fukushima Daini Nuclear Power Station 2011 Archives. http://www.tepco.co.jp/en/nu/fukushima-np/f2/index-e.html, 2011b (last access: 12 November 2014).

TEPCO: Radiation dose measured in the Fukushima Daini Nuclear Power Station 2011 Archives. http://www.tepco.co.jp/en/nu/fukushima-np/f2/data/2011/index-e.html, 2011c (last access: 12 November 2014).

TEPCO: Release of the Fukushima Nuclear Accidents Investigation Report, http://www.tepco.co.jp/en/press/corp-com/release/2012/1205638_1870.html, 2012 (last access: 12 November 2014).

Terada, H., and Chino, M.: Improvement of Worldwide Version of System for Prediction of Environmental Emergency Dose Information (WSPEEDI), (II) Evaluation of numerical models by 137Cs deposition due to the Chernobyl nuclear accident. J. Nucl. Sci. Technol., 42, 651-660, 2005.

Terada, H., and Chino, M.: Development of an atmospheric dispersion model for accidental discharge of radionuclides with the function of simultaneous prediction for multiple domains and its evaluation by application to the Chernobyl nuclear accident. J. Nucl. Sci. Technol., 45, 920-931, 2008.

Terada, H., Furuno, A., and Chino, M.: Improvement of Worldwide Version of System for Prediction of Environmental Emergency Dose Information (WSPEEDI), (I) New combination of models, atmospheric dynamic model MM5 and particle random walk model GEARN-new. J. Nucl. Sci. Technol., 41, 632-640, 2004.

Terada, H., Katata, G., Chino, M., and Nagai, H.: Atmospheric discharge and dispersion of radionuclides during the Fukushima Dai-ichi Nuclear Power Plant accident. Part II: Verification of the source term and analysis of regional-scale atmospheric dispersion. J. Environ. Radioact., 112, 141-154, 2012.

Thalmann, E., Burkard, R., Wrzesinsky, T., Eugster, W., and Klemm, O.: Ion fluxes from fog and rain to an agricultural and a forest ecosystem in Europe, Atmos. Res., 64, 147-158, 2002.

Tochigi Prefecture: http://www.pref.tochigi.lg.jp/kinkyu/documents/20110312-18.pdf, 2011 (in Japanese, last access: 12 November 2014).

Tohoku Electric Power: http://www.tohoku-epco.co.jp/news/atom/topics/1183332_1984.html, 2011 (in Japanese, last access: 12 November 2014).

Tokyo Metropolitan Government: Measurement of nuclear fission products of dust particles in the air in Tokyo, http://www.sangyo-rodo.metro.tokyo.jp/whats-new/measurement-kako.html, 2011 (last access: 12 November 2014).

Torii, T., Sugita, T., Okada, C.E., Reed, M.S., Blumenthal, D.J.: Enhanced analysis methods to derive the spatial distribution of I-131 deposition on the ground by airborne surveys at an early stage after the Fukushima Daiichi nuclear power plant accident, Health Phys., 105, 192-200, 2013.

Tost, H., Jöckel, P., Kerkweg, A., Sander, R., and Lelieveld, J.: Technical note: A new comprehensive SCAVenging submodel for global atmospheric chemistry modeling, Atmos. Chem. Phys., 6, 565-574, 2006.

Tsuruta, H., Takigawa, M., and Nakajima, M., Summary of atmospheric measurements and transport pathways of radioactive materials released by the Fukushima Daiichi Nuclear Power Plant accident. In: Kurihara, O. et al. (Eds.), Proceedings on the 1st NIRS Symposium on Reconstruction of Early Internal Dose in the TEPCO Fukushima Daiichi Nuclear Power Station Accident. National Institute of Radiological Sciences, 101-111, 2012.

Uematsu, M., Merrill, J.T., Patterson, T.L., Duce, R.A., and Prospero, J.M.: Aerosol residence times and iodine gas/particle conversion over the North Pacific as determined from Chernobyl radioactivity, Geochem. J., 22, 157-163, 1988.

UNSCEAR (United Nations Scientific Committee on the Effects of Atomic Radiation): UNSCEAR 2013 Report: Sources, effects and risks of ionizing radiation, Volume I, http://www.unscear.org/docs/reports/2013/13-85418_Report_2013_Annex_A.pdf, 2014 (last access: 12 November 2014).

US DOE (Department of Energy): Response to 2011 Fukushima Incident- Data and Documentation, http://energy.gov/downloads/us-doennsa-response-2011-fukushima-incident-data-and-documentation, 2011 (last access: 12 November 2014).

US DOE/NNSA (National Nuclear Security Administration): Response to 2011 Fukushima incident—raw aerial data and extracted ground exposure rates and cesium deposition, https://explore.data.gov, 2011 (last access: 12 November 2014).

US NDC (United States National Data Center): United States National Data Center, International Monitoring System Data for the CTBTO network, http://www.usandc.gov/radionuclide.html, 2011 (last access: 12 November 2014).

US NRC (Nuclear Regulatory Commission): RASCAL 4: Description of Models and Methods, NUREG-1940, Richland, WA, 2012.

Wang, X., Zhang, L., and Moran, M.D.: Uncertainty assessment of current size-resolved parameterizations for below-cloud particle scavenging by rain, Atmos. Chem. Phys., 10, 5685-5705, 2010.

Wesely, M.L.: Parameterization of surface resistances to gaseous dry deposition in regional-scale numerical models, Atmos. Environ., 23, 1293-1304, 1989.

Wesely, M. L., and Hicks, B. B.: Some factors that affect the deposition rates of sulfur dioxide and similar gases on vegetation, J. Air Pollut. Control Assoc., 27, 1110-1116, 1977.

Winiarek, V., Bocquet, M., Duhanyan, N., Roustan, Y., Saunier, O., and Mathieu, A.: Estimation of the caesium-137 source term from the Fukushima Daiichi nuclear power plant using a consistent joint assimilation of air concentration and deposition observations, Atmos. Environ., 82, 268-279, 2014.

WMO (World Meteorological Organization): Evaluation of Meteorological Analyses for the Radionuclide Dispersion and Deposition from the Fukushima Daiichi Nuclear Power Plant Accident, 1120, 64 pp, https://www.wmo.int/e-catalog/detail_en.php?PUB_ID=669&SORT=N&q=, 2014 (last access: 12 November 2014).

Wolf, M.A. and Dana, M.T.: Experimental studies on precipitation scavenging, USAEC Report BNWL-105, Battelle Pacific Northwest Laboratory, Richland, Wash., 18-25, 1969.

Yasunari, T. J., Stohl, A., Hayano, R. S., Burkhart, J. F., Eckhardt, S., and Yasunari, T.: Cesium-137 deposition and contamination of Japanese soils due to the Fukushima nuclear accident, 2011.

Zhang, L., Gong, S., Padro, J., and Barrie, L.: A size-segregated particle dry deposition scheme for an atmospheric aerosol module, Atmos. Environ., 35, 549-560, 2001.

Zhang, L., Brook, J. R., and Vet, R.: A revised parameterization for gaseous dry deposition in air-quality models, Atmos. Chem. Phys., 3, 2067-2082, 2003.

Zhang, L., Wang, X., Moran, M. D., and Feng, J.: Review and uncertainty assessment of size-resolved scavenging coefficient formulations for below-cloud snow scavenging of atmospheric aerosols, Atmos. Chem. Phys., 13, 10005-10025, 2013.

Table 1. The simulation settings of deposition scheme in atmospheric dispersion models applied to the FNPS1 accident; CCN: cloud condensation nuclei, d_m: geometric mass particle diameter, d_n: geometric number particle diameter, U: wind speed, RH: relative humidity, Pr: Precipitation, CLW: cloud liquid water content, T: air temperature, H: (effective) Henry's constant, z: height, dz_c: cloud height, dz_p: depth of the pollutant layer. The reverse and inverse estimation methods are defined in UNSCEAR (2014).

Model name	Dispersion	Radionuclides	Chemical form	Particle size distribution	Dry deposition	Wet deposition	Fog deposition	Snow scavenging	CCN activation	Source term estimation	Model application papers to the FNPS1 accident
GEARN	Lagrangian	^{131}I, ^{132}Te (^{132}I), ^{134,137}Cs	Bulk	No	Constant	Pr	No	No	No	Reverse method	Chino et al. (2011), Katata et al. (2012a, b), Terada et al. (2012), Kobayashi et al. (2013)
CMAQ	Eulerian	^{131}I, ^{137}Cs	Gas/submicron particle	Log-normal (Kaneyasu et al., 2012)	Resistance (Zhang et al., 2001)	Pr, CLW, H, dz_c	No	No	Complete activation	No	Morino et al. (2011), (2013)
SPRINTERS	Eulerian	Not specified	Coarse particle	Log-normal (d_m=10 μm)	Constant	CLW, Pr	No	No	30–60% activation	No	Takemura et al. (2011)
FLEXPART	Lagrangian	^{133}Xe, ^{137}Cs	Gas/submicron particl	Log-normal (d_m =0.4 μm)	Resistance (Wesely and Hicks,	RH, Pr, H, z (Herte	No	No	Complete activation	Inverse method	Yasunari et al. (2011), Stohl et al. (2012), Srinvas et al. (2012), Sugiyama et al. (2012),

			e		1977)	l et al., 1995)					Draxler et al. (2014), Achim et al. (2014)
HYSPLIT	Lagrangian	^{131}I, ^{137}Cs	Gas/particle	No	Constant	RH, Pr, H, dz_p	No	No	No	No[1]	Draxler and Rolph (2012), Srinvas et al. (2012), Draxler et al. (2014)
RASCAL v3	Gauss plume	^{131}I, ^{137}Cs	I_2 or HI, CH_3I, CsI	1 µm	Constant	Pr	No	Yes	No	No	Dvorzhak et al. (2012)
ldX, Polair3D//pX	Eulerian/puff	73 species	Bulk	No	Constant	Pr	No	No	No	Inverse method	Mathieu et al. (2012), Korsakissok et al. (2013), Saunier et al. (2013), Winiarek et al. (2012, 2014)
LODI	Lagrangian	^{131}I, ^{132}Te (^{132}I), $^{134,137}Cs$	Gas/particle	Log-normal	Resistance	Pr	No	No	No	No	Sugiyama et al. (2012)
GATOR-GCMOM	Lagrangian	^{131}I, ^{137}Cs	Gas/particle	Log-normal (d_n = 0.06 µm)	Resistance (Wesely, 1989)	Jacobson (2005)	No	No	Jacobson (2005)	Inverse method	Ten Hoeve and Jacobson (2012)
EMAC	Lagrangian	^{131}I, ^{137}Cs	Gas/particle	Log-normal	Resistance	Pr, CLW,	No	No	No	No	Christoudias and Lelieveld (2013)

[1] These models are available for inverse estimation for source attribution, while this option was not exercised for FNPS1 accident.

					(Kerkweg et al., 2006)	dz_c, U (Tost et al., 2006)					
LPRM	Lagrangian	^{131}I, ^{137}Cs	Bulk	No	Constant	Pr	No	No	No	Inverse method	Hirao et al. (2013)
MLDP0	Lagrangian	^{131}I, ^{137}Cs	Gas/particle	No	Constant	Cloud fraction	No	No	No	No	Draxler et al. (2014)
RATM	Lagrangian	^{131}I, ^{137}Cs	Gas/particle	No	Constant	RH, Pr, H, z<1500m (Hertel et al., 1995)	No	No	90% activation	No	Draxler et al. (2014)
NAME	Lagrangian	^{131}I, ^{137}Cs	Gas/particle	No	Resistance	Pr, CLW, dz_c	No	Yes	No	No1	Leadbetter et al. (2014), Draxler et al. (2014)
Modified GEARN	Lagrangian	^{131}I, ^{132}Te (^{132}I), $^{134,137}Cs$	I_2, CH_3I, CsI	Log-normal (Miyamoto et al., 2014)	Resistance (Kajino et al., 2012)	Pr, CLW, H, dz_c (Giorgi and Chameides, 1986)	CLW, U (Katata, 2014)	Yes	Abdul-Razzak and Ghan (2000)	Reverse method	This study

1

2

Table 2. Dust sampling data used for the source term estimation. The locations of monitoring data are illustrated in Fig. 2. The concentration calculations for source term estimation were carried out under the assumption of unit release rate (1Bq h^{-1}).

Data No.	Location code in Fig. 2	Sampling location	Sampling date and time (Japan Standard Time)	Total ^{131}I Concentration (Bq m^{-3})		^{137}Cs Concentration (Bq m^{-3})	
				Observed	Calculated	Observed	Calculated
1	a	JAEA-Tokai	3/15 01:25-3/15 01:45	240	–[a]	16	–[a]
2		(Ohkura et	3/15 04:25-3/15 04:45	1260	–[a]	160	–[a]
3		al., 2012)	3/15 06:55-3/15 08:15	920–2600	8.0×10^{-13}-2.8×10^{-12}	110–310	6.4×10^{-13}-2.7×10^{-12}
4			3/20 11:35-3/20 11:55	140	4.4×10^{-12}	26	4.7×10^{-12}
5			3/21 03:45-3/21 07:05	1916	1.0×10^{-11}	438	1.1×10^{-11}
6	b	MEXT21	3/20 14:13-3/20 14:33	4800	1.6×10^{-11}	1000	1.5×10^{-11}
7	c	MEXT31	3/20 14:15-3/20 14:35	1000	1.1×10^{-11}	180	1.1×10^{-11}
8	d	MEXT41	3/20 11:37-3/20 11:49	970	2.2×10^{-11}	–	–
9	e	MEXT44	3/21 10:50-3/21 11:08	1420	3.4×10^{-11}	–	–
10	f	MEXT71	3/21 13:00-3/21 13:40	5600	9.4×10^{-11}	36	8.8×10^{-11}
11			3/22 14:55-3/22 16:30	570–1100	4.8×10^{-12}–1.1×10^{-11}	7.7–11	4.8×10^{-12}–1.1×10^{-11}
12			3/23 13:15-3/23 15:59	110–530	7.4×10^{-13}–2.0×10^{-12}	2.1–6.6	7.3×10^{-13}–2.0×10^{-12}
13			3/24 10:06-3/24 12:26	5.9–12	2.2×10^{-13}–2.4×10^{-12}	0.7–1.1	2.2×10^{-13}–2.4×10^{-12}
14			3/25 11:51-3/25 16:42	10–43	3.4×10^{-13}–1.0×10^{-12}	0.7–2.3	3.5×10^{-13}–1.0×10^{-12}
15			3/31 12:22-3/31 15:44	13–24	1.6×10^{-12}–9.2×10^{-12}	1.0–4.5	1.6×10^{-12}–9.3×10^{-12}
16	g	MEXT46	3/20 14:45-3/20 14:55	4100	1.3×10^{-11}	–	–
17			3/25 15:02-3/25 15:22	290–555	2.1×10^{-13}–1.9×10^{-11}	7.7–14	2.0×10^{-13}–8.7×10^{-12}
18			3/30 14:11-3/30 14:32	89	1.0×10^{-12} [a]	91	1.0×10^{-12} [a]
19	h	DOE	3/22 06:00-3/22 07:00	360–2960	1.4×10^{-12}–1.3×10^{-11}	2-19	9.4×10^{-13}–8.3×10^{-12}
20	i	MEXT80	3/24 14:55-3/24 15:15	193	7.3×10^{-12}	2.9	7.0×10^{-12}
21			3/29 11:17-3/29 15:00	29–75	5.4×10^{-12}–1.1×10^{-11}	23–46	5.3×10^{-12}–1.1×10^{-11}
22	j	MEXTsea8	3/27 11:45-	20	9.8×10^{-13}	0.88	1.0×10^{-12}

[a] Expert judgment (subsection 2.1.1)

23	k	FNPS2	3/30 09:27-3/30 09:35	1490	1.7×10^{-10}	820	1.6×10^{-10}
24	l	MEXT61	3/30 14:15-3/30 14:35	28	1.1×10^{-12}	20	1.3×10^{-12}
25			4/1 12:00-4/1 12:20	1.78	1.1×10^{-11}	1.69	1.1×10^{-11}

1

2

Table 3. Air dose rate monitoring data used for the source term estimation. The locations of monitoring site are illustrated in Fig. 2. The air dose rate calculations for source term estimation were carried out under the assumption of unit release rate (1Bq h^{-1}).

Data No.	Name of monitoring location	Monitoring date and time (Japan Standard Time)	Ground-shine (μGy h^{-1}) Observed	Calculated
1	Kamihatori MP	3/14 00:00	37	1.3×10^{-14}
2	Shinzan MP	3/14 00:00	250	1.7×10^{-14}
3	Nasu MP	3/17 00:00	0.6	2.5×10^{-15}
4	Koriyama MP	3/17 00:00	2.8	3.3×10^{-15}
5	Kawauchi MP	3/17 00:00	1.6	1.3×10^{-15}
	Ohno MP	3/17 00:00	3.4[a]	5.2×10^{-15}
	Yamada MP	3/17 00:00	10.1[a]	8.0×10^{-15}
6	Iitate MP	3/17 00:00	6.9[a]	1.9×10^{-14}
7	AMS near Kawafusa (extrapolated to 17 March)	3/17 00:00	200–300	1.0×10^{-13}
8	Yamada MP	3/17 00:00	390[a]	8.7×10^{-14}
9	Ohno MP	3/17 00:00	62[a]	3.1×10^{-15}
10	Futatsunuma MP	3/17 00:00	1.9[a]	6.0×10^{-16}
	Yamadaoka MP	3/17 00:00	0.8[a]	6.7×10^{-16}
11	FNPS2 MP	3/17 00:00	9.3[a]	5.9×10^{-15}
12	FNPS2 MP	3/17 00:00	2.9[a]	4.6×10^{-16}
	Futatsunuma MP	3/17 00:00	1.8[a]	1.2×10^{-15}
	Yamadaoka MP	3/17 00:00	1.3[a]	1.5×10^{-15}

[a] Uncertainty of observed ground-shine estimates due to the plume passing through the monitoring place several times.

1 Table 4. The settings for the WSPEEDI-II atmospheric dispersion model used in the coupling of the atmospheric and oceanic dispersion
2 simulations.

	Reverse estimation over the land			Reverse estimation over the ocean
	Domain 1	Domain 2	Domain 3	Domain 1
Study areas	East Japan			North Pacific
Applied GEARN calculations	No	Yes	Yes	Yes
Simulation period for GEARN	5:00 on 12 March–0:00 on 1 April 2011			5:00 on 12 March–9:00 on 31 May 2011
Horizontal grid cell	100×100	190×130	190×190	250×150
Spatial resolutions	9 km	3 km	1 km	80 km
Boundary and initial conditions of MM5	Meso-Scale Model (MSM) by Japan Meteorological Agency (JMA)			Global Spectral Model (GSM) for the global region by JMA
3D/surface analysis nudging	Utilized with wind data at FNPP1 (surface), FNPP2 (120 m) (METI, 2011b), and surface weather stations			Utilized for 3D
Observation nudging	Utilized with wind data at FNPP1 (surface) and FNPP2 (120 m)			No
Release rates and heights	Given by Table 6			
Other parameters for MM5	Same as Katata et al. (2012a, b) and Kobayashi et al. (2013) except for Reisner microphysics scheme			

3
4

Table 5. Characteristics and total inventories of radionuclides for Unit 1-3 at FNPS1 (Nishihara et al., 2012).

Radionuclide	State in atmosphere	Half-life	Boiling point (°C)	Total inventory (PBq)
I-131	Gas/aerosol	8.0 day	180	6.02×10^{6}
I-132	Gas/aerosol	2.3 hour	180	8.85×10^{6}
Te-132	Aerosol	3.2 day	1400	8.68×10^{6}
I-133	Gas/aerosol	21.0 hour	180	1.26×10^{7}
Cs-137	Aerosol	30.0 year	670	6.98×10^{5}
Cs-134	Aerosol	2.1 year	670	7.18×10^{5}

Table 6. Release period, release duration, release rate of total ^{131}I, radioactivity ratio of ^{137}Cs /total ^{131}I, the ratio of gaseous ^{131}I to total ^{131}I, and release height for the period between 5:00 on 12 March to 0:00 on 1 May 2011. Notations of "L" and "O" in the first column represent estimations using land and ocean environmental monitoring data, respectively. In the last column, MP: monitoring post, C: concentration, and AMS: Aerial Measuring System of U.S. Department of Energy/National Nuclear Security Administration (US DOE/NNSA, 2011).

No.	Release period (Japan Standard Time)	Release duration (h)	Release rate of total ^{131}I (Bq h^{-1})	^{137}Cs/ total ^{131}I	Gaseous ^{131}I /total ^{131}I	Release height/volume (m)	Monitoring data for estimation
1O	3/12 05:00-3/12 09:30	4.5	5.8×10^{13}	0.100	0.500	20	Sea water C
2O	3/12 09:30-3/12 14:00	4.5	2.7×10^{13}	0.100	0.500	20	Sea water C
3L	3/12 14:00-3/12 15:00	1.0	2.9×10^{15}	0.100	0.500	120	Kamihatori MP (1 in Table 3)
4O	3/12 15:00-3/12 15:30	0.5	1.3×10^{13}	0.100	0.500	20	Sea water C
5L	3/12 15:30-3/12 16:00	0.5	1.4×10^{16}	0.100	0.500	100×100×100[a]	Shinzan MP (2 in Table 3)
6O	3/12 16:00-3/12 22:00	6.0	1.7×10^{14}	0.100	0.500	120	Sea water C.
7O	3/12 22:00-3/13 04:00	6.0	3.1×10^{14}	0.100	0.500	120	Sea water C
8O	3/13 04:00-3/13 09:00	5.0	2.2×10^{14}	0.100	0.500	120	Sea water C

[a] Volume sources were assumed to hydrogen explosion at Units 1 and 3 (Katata et al., 2012b). The three values indicate the source volume dimension in horizontal and vertical directions x, y, and z. The source center heights are 50 and 150 m above the ground level for Nos.5L and 15O, respectively.

9O	3/13 09:00-3/13 12:30	3.5	2.6×10^{14}	0.100	0.500	120	Sea water C
10O	3/13 12:30-3/13 15:00	2.5	5.0×10^{14}	0.100	0.500	120	Sea water C
11O	3/13 15:00-3/13 23:00	8.0	3.0×10^{14}	0.100	0.500	120	Sea water C
12O	3/13 23:00-3/14 02:30	3.5	8.2×10^{13}	0.100	0.500	120	Sea water C
13O	3/14 02:30-3/14 07:00	4.5	4.4×10^{13}	0.100	0.500	120	Sea water C
14O	3/14 07:00-3/14 11:00	4.0	3.5×10^{13}	0.100	0.500	120	Sea water C
15O	3/14 11:00-3/14 11:30	0.5	3.7×10^{15}	0.100	0.500	100×100×300[a]	Sea water C
16O	3/14 11:30-3/14 18:00	6.5	1.8×10^{13}	0.100	0.500	20	Sea water C
17O	3/14 18:00-3/14 19:00	1.0	1.1×10^{13}	0.100	0.500	20	Sea water C
18O	3/14 19:00-3/14 20:00	1.0	1.0×10^{13}	0.100	0.500	20	Sea water C
19O	3/14 20:00-3/14 21:00	1.0	1.0×10^{13}	0.100	0.500	20	Sea water C
20L	3/14 21:00-3/14 22:00	1.0	2.4×10^{14}	0.066	0.500	20	JAEA-Tokai C (1 in Table 2)
21O	3/14 22:00-3/14 23:00	1.0	1.1×10^{13}	0.100	0.500	20	Sea water C
22L	3/14 23:00-3/15 00:00	1.0	5.4×10^{14}	0.128	0.500	20	JAEA-Tokai C (2 in Table 2)
23O	3/15 00:00-3/15 01:00	1.0	1.3×10^{13}	0.100	0.500	20	Sea water C

24L	3/15 01:00-3/15 02:00	1.0	2.3×10^{15}	0.167	0.500	20	JAEA-Tokai C (3 in Table 2)
25L	3/15 02:00-3/15 03:00	1.0	3.3×10^{14}	0.095	0.500	20	JAEA-Tokai C (3 in Table 2)
26L	3/15 03:00-3/15 04:00	1.0	2.9×10^{14}	0.125	0.500	20	JAEA-Tokai C (3 in Table 2)
27L	3/15 04:00-3/15 07:00	3.0	1.3×10^{14}	0.100	0.500	20	Nasu MP (3 in Table 3)
28L	3/15 07:00-3/15 10:00	3.0	1.2×10^{15}	0.100	0.500	20	Koriyama MP (4 in Table 3)
29L	3/15 10:00-3/15 11:00	1.0	1.0×10^{15}	0.100	0.500	20	Kawauchi, Ohno, & Yamada MPs (5 in Table 3)
30L	3/15 11:00-3/15 16:00	5.0	1.0×10^{14}	0.100	0.500	20	AMS air dose rate map
31L	3/15 16:00-3/15 18:00	2.0	3.3×10^{14}	0.100	0.500	20–120[b]	Iitate MP (6 in Table 3)
32L	3/15 18:00-3/15 20:00	2.0	2.2×10^{15}	0.100	0.500	20–120[b]	AMS near Kawafusa (7 in Table 3)
33L	3/15 20:00-3/15 22:00	2.0	2.3×10^{15}	0.033	0.700	20–120[b]	Yamada MP (8 in Table 3)
34L	3/15 22:00-3/15 23:00	1.0	1.0×10^{16}	0.033	0.700	20–120[b]	Ohno MP (9 in Table 3)
35L	3/15 23:00-3/16 00:00	1.0	2.2×10^{15}	0.033	0.700	20–120[b]	Futatsunuma & Yamadaoka MPs (10 in Table 3)

[b] The situations of both leakage from the Primary Containment Vessel (PCV) and venting at the top of stack with 20 and 120 m height were assumed.

36L	3/16 00:00-3/16 01:00	1.0	1.6×10^{15}	0.033	0.700	20–120[b]	FNPS2 MP (11 in Table 3)
37O	3/16 01:00-3/16 06:00	5.0	2.0×10^{14}	0.033	0.700	20–120[b]	Sea water C
38O	3/16 06:00-3/16 09:00	3.0	2.0×10^{14}	0.100	0.500	20	Sea water C
39L	3/16 09:00-3/16 11:00	2.0	2.8×10^{15}	0.100	0.500	20	FNPS2, Futatsunuma & Yamadaoka MPs (12 in Table 3)
40O	3/16 11:00-3/16 12:00	1.0	1.2×10^{14}	0.100	0.500	20	Sea water C
41O	3/16 12:00-3/16 13:00	1.0	1.5×10^{14}	0.100	0.500	20	Sea water C
42O	3/16 13:00-3/16 14:00	1.0	2.9×10^{14}	0.100	0.500	20	Sea water C
43O	3/16 14:00-3/16 15:00	1.0	5.0×10^{14}	0.100	0.500	20	Sea water C
44O	3/16 15:00-3/17 06:00	15.0	6.2×10^{14}	0.100	0.500	20	Sea water C
45O	3/17 06:00-3/17 21:00	15.0	3.1×10^{14}	0.100	0.500	20	Sea water C
46O	3/17 21:00-3/18 00:00	3.0	3.0×10^{14}	0.100	0.500	20	Sea water C
47O	3/18 00:00-3/18 05:00	5.0	2.1×10^{14}	0.100	0.500	20	Sea water C
48O	3/18 05:00-3/18 08:00	3.0	1.3×10^{15}	0.100	0.500	20	Sea water C
49O	3/18 08:00-3/18 13:00	5.0	1.8×10^{15}	0.100	0.500	20	Sea water C
50O	3/18 13:00-3/18 18:00	5.0	1.5×10^{15}	0.100	0.500	20	Sea water C

51O	3/18 18:00-3/19 05:00	11.0	1.4×10^{15}	0.100	0.500	20	Sea water C
52O	3/19 05:00-3/19 15:00	10.0	1.3×10^{15}	0.100	0.500	20	Sea water C
53L	3/19 15:00-3/21 03:00	36.0	1.6×10^{14}	0.192	0.500	20	MEXT21, 31, 41, 46 & JAEA-Tokai C (4, 6, 7, 8 & 16 in Table 2)
54L	3/21 03:00-3/21 08:00	5.0	1.7×10^{14}	0.242	0.486	20	JAEA-Tokai C (5 in Table 2)
55L	3/21 08:00-3/21 12:00	4.0	4.2×10^{13}	0.125[c]	0.658	20	MEXT44 C (9 in Table 2)
56L	3/21 12:00-3/21 16:00	4.0	5.9×10^{13}	0.007	0.594	20	MEXT71 C (10 in Table 2)
57L	3/21 16:00-3/21 21:00	5.0	4.2×10^{13}	0.125[c]	0.658	20	Assumed same as 55L (9 in Table 2)
58L	3/21 21:00-3/22 23:00	26.0	1.6×10^{14}	0.010	0.671	20	DOE & MEXT 71 C (11 & 19 in Table 2)
59L	3/22 23:00-3/24 00:00	25.0	2.6×10^{14}	0.013	0.495	20	MEXT71 C (12 in Table 2)
60L	3/24 00:00-3/25 00:00	24.0	1.8×10^{13}	0.035	0.605	20	MEXT71 & 80 C (13 & 20 in Table 2)
61L	3/25 00:00-3/26 11:00	35.0	4.1×10^{13}	0.054	0.681	20	MEXT46 & 71 C (14 & 17 in Table 2)
62O	3/26 11:00-3/28 10:00	47.0	1.7×10^{13}	0.042	0.901	20	Sea water & MEXTsea8 C (22 in Table 2)
63O	3/28 10:00-3/29 21:00	35.0	3.9×10^{12}	0.781	0.927	20	Sea water & MEXT80 C (21 in Table 2)

[c] Interporated from the ratios of 55L and 57L due to lack of the data of ^{137}Cs.

64L	3/29 21:00-3/30 11:00	14.0	9.0×10^{12}	0.621	0.544	20	FNPS2 C (23 in Table 2)
65L	3/30 11:00-3/31 00:00	13.0	5.9×10^{13}	0.833	0.688	20	MEXT46 & 61 C (18 & 24 in Table 2)
66O	3/31 00:00-3/31 22:00	22.0	1.4×10^{13}	0.186	0.707	20	Sea water & MEXT71 C (15 in Table 2)
67O	3/31 22:00-4/2 09:00	35.0	9.2×10^{11}	0.970	0.933	20	Sea water & MEXT61 C (25 in Table 2)
68L	4/2 09:00-4/4 09:00	48.0	1.0×10^{13}	0.323	0.894	20	Sea water C
69L	4/4 09:00-4/7 17:00	80.0	3.9×10^{12}	0.204	0.894	20	Sea water C
70L	4/7 17:00-4/13 23:00	150.0	7.0×10^{11}	0.500	0.948	20	Terada et al. (2012)
71L	4/13 23:00-5/1 00:00	409.0	7.0×10^{11}	0.257	0.948	20	Terada et al. (2012)

1

2

Table 7. Statistics of the surface depositions of total ^{131}I and ^{137}Cs, and air dose rate between observations and calculations using any combinations of original and modified WSPEEDI-II (referred as "Old model" and "New model", respectively) and Terada at al. (2012) and the new source terms (referred as "Terada" and "New", respectively). Six statistical parameters were selected to represent different evaluation metrics: the correlation coefficient (CC), the fractional bias (FB), the normalized mean square error (NMSE), and the percent within a factor of two, five, and ten (FA2, FA5, FA10). Regional- and local-scale data were compared with calculations of WSPEEDI-II over domain 2 and 3, respectively.

Source term & model	CC	FB	NMSE	FA2	FA5	FA10
Regional-scale ^{137}Cs surface deposition over East Japan at 0:00 on 1 April 2011						
Terada-Old model	0.56	-0.177	20.0	0.43	0.80	0.94
New-Old model	0.67	0.055	18.7	0.41	0.78	0.92
Terada-New model	0.41	-0.624	55.6	0.39	0.77	0.93
New-New model	0.63	-0.248	42.3	0.42	0.78	0.92
Local-scale ^{137}Cs surface deposition near FNPS1 at 0:00 on 1 April 2011						
Terada-Old model	0.52	-0.103	9.6	0.39	0.82	0.96
New-Old model	0.65	0.111	8.4	0.36	0.75	0.92
Terada-New model	0.29	-0.614	37.7	0.38	0.75	0.91
New-New model	0.53	-0.185	24.7	0.39	0.76	0.90
Local-scale ^{131}I surface deposition near FNPS1 at 0:00 on 1 April 2011						
Terada-Old model	0.52	-0.944	224.1	0.42	0.84	0.95
New-Old model	0.61	-0.967	140.2	0.50	0.89	0.96
Terada-New model	0.59	-0.339	12.5	0.49	0.87	0.97
New-New model	0.67	-0.223	21.4	0.52	0.87	0.95
Local-scale air dose rate at 0:00 on 18 March 2011						
Terada-Old model	0.51	0.078	18.9	0.38	0.83	0.97
New-Old model	0.63	-0.421	23.0	0.46	0.84	0.98
Terada-New model	0.46	-0.159	19.4	0.35	0.74	0.90
New-New model	0.67	-0.386	32.0	0.48	0.89	0.98

1

2

Table 8. Total release amount of total ^{131}I and ^{137}Cs to the atmosphere from 12 March–1 May 2011 using source terms estimated from land data only (referred as "New-land") and from both land and sea data in this study (referred as "New-landsea") and those of past studies. Note that the values of Winiarek et al. (2014) and Stohl et al. (2012) are derived from hourly estimation results using the daily fallout, airborne survey data, and aggregated for all release layers from 0–1000 m, respectively. It is also noted that the release rates of Saunier et al. (2013), when the plume directly flowed to the Pacific Ocean, could not be reconstructed correctly.

Name of source term	Integration period	Total ^{131}I (PBq)	^{137}Cs (PBq)
New-land	12 March–1 May 2011	110.7	9.8
New-landsea	12 March–1 May 2011	151.0	14.5
Terada et al. (2012)	12 March–1 May 2011	123.9	8.8
Kobayashi et al. (2013)	12 March–1 May 2011	200.0	13.0
Saunier et al. (2013)	12 March–27 March 2011	105.9	15.5
Winiarek et al. (2014)	11 March–1 April 2011	–	19.3
Stohl et al. (2012)	10 March–20 April 2011	–	35.9

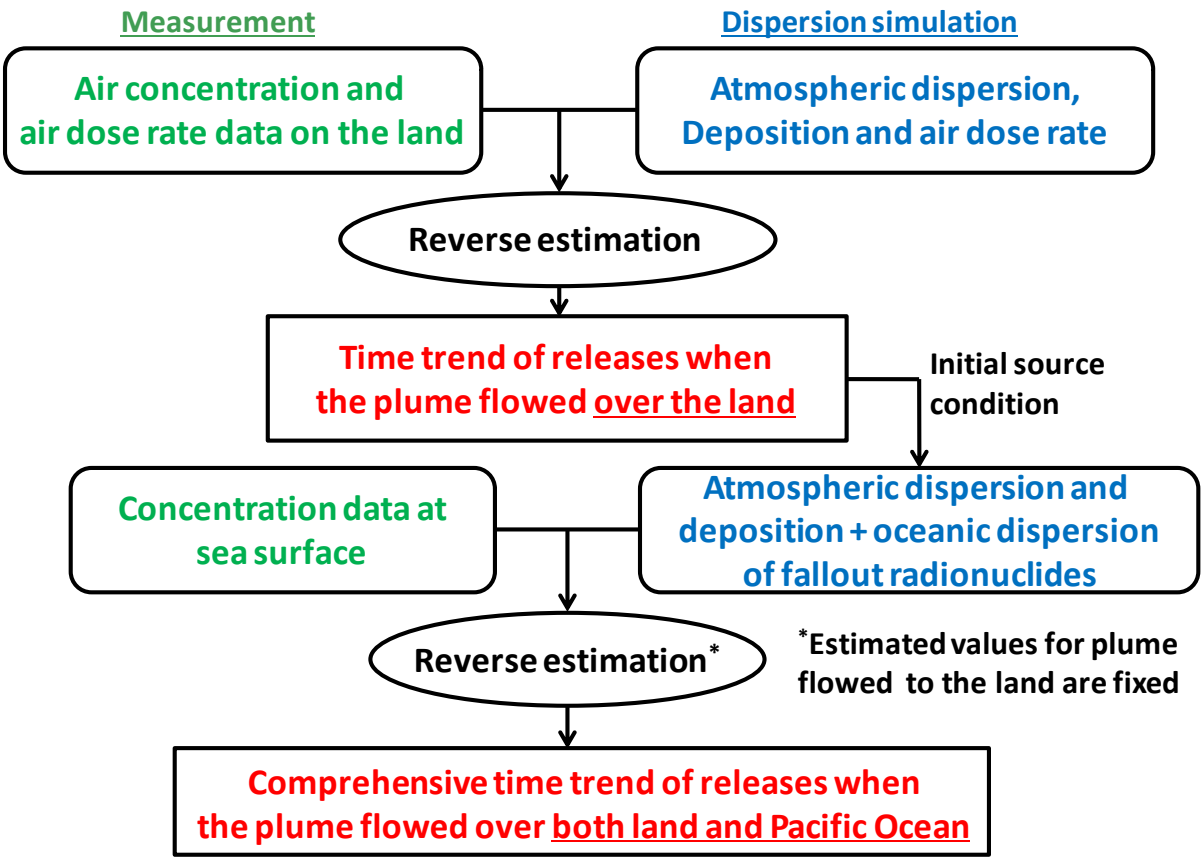

Figure 1. The flowchart of the source term estimation technique based on coupling the atmospheric and oceanic dispersion model simulations.

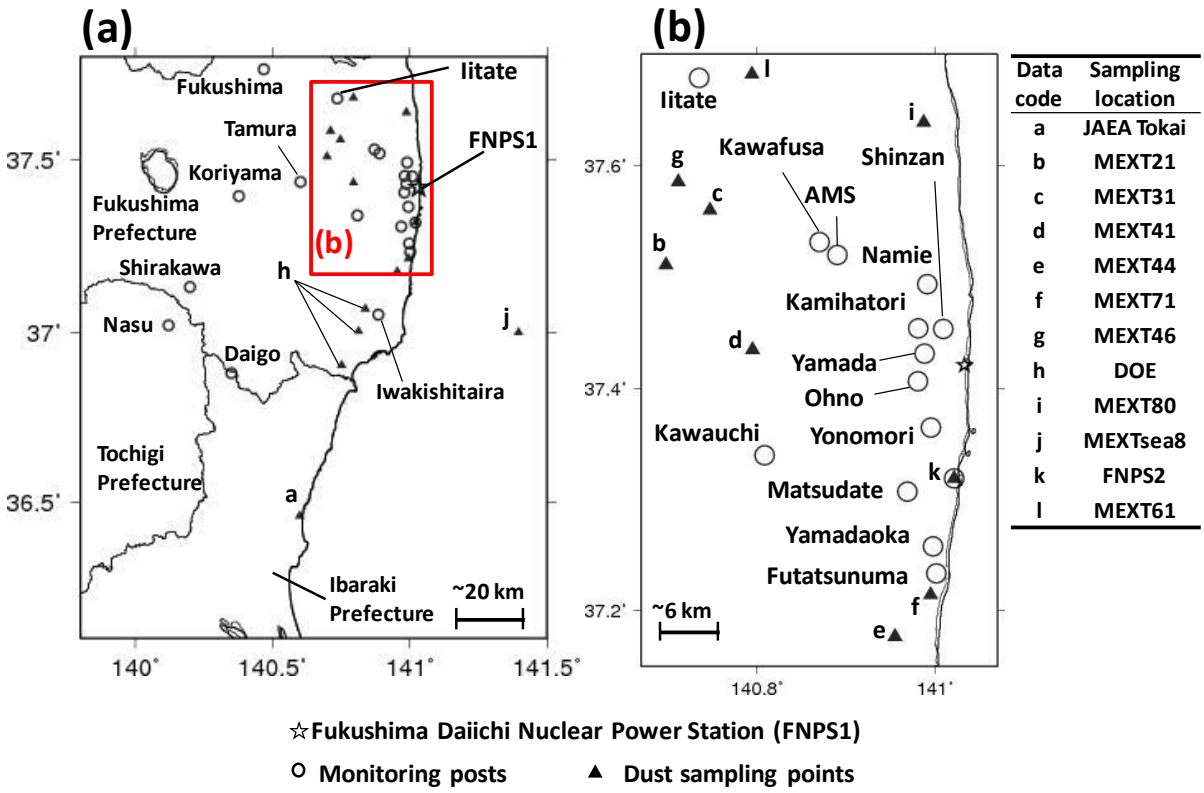

Data code	Sampling location
a	JAEA Tokai
b	MEXT21
c	MEXT31
d	MEXT41
e	MEXT44
f	MEXT71
g	MEXT46
h	DOE
i	MEXT80
j	MEXTsea8
k	FNPS2
l	MEXT61

Figure 2. The sampling locations of the environmental monitoring data over the land used for the source term estimation.

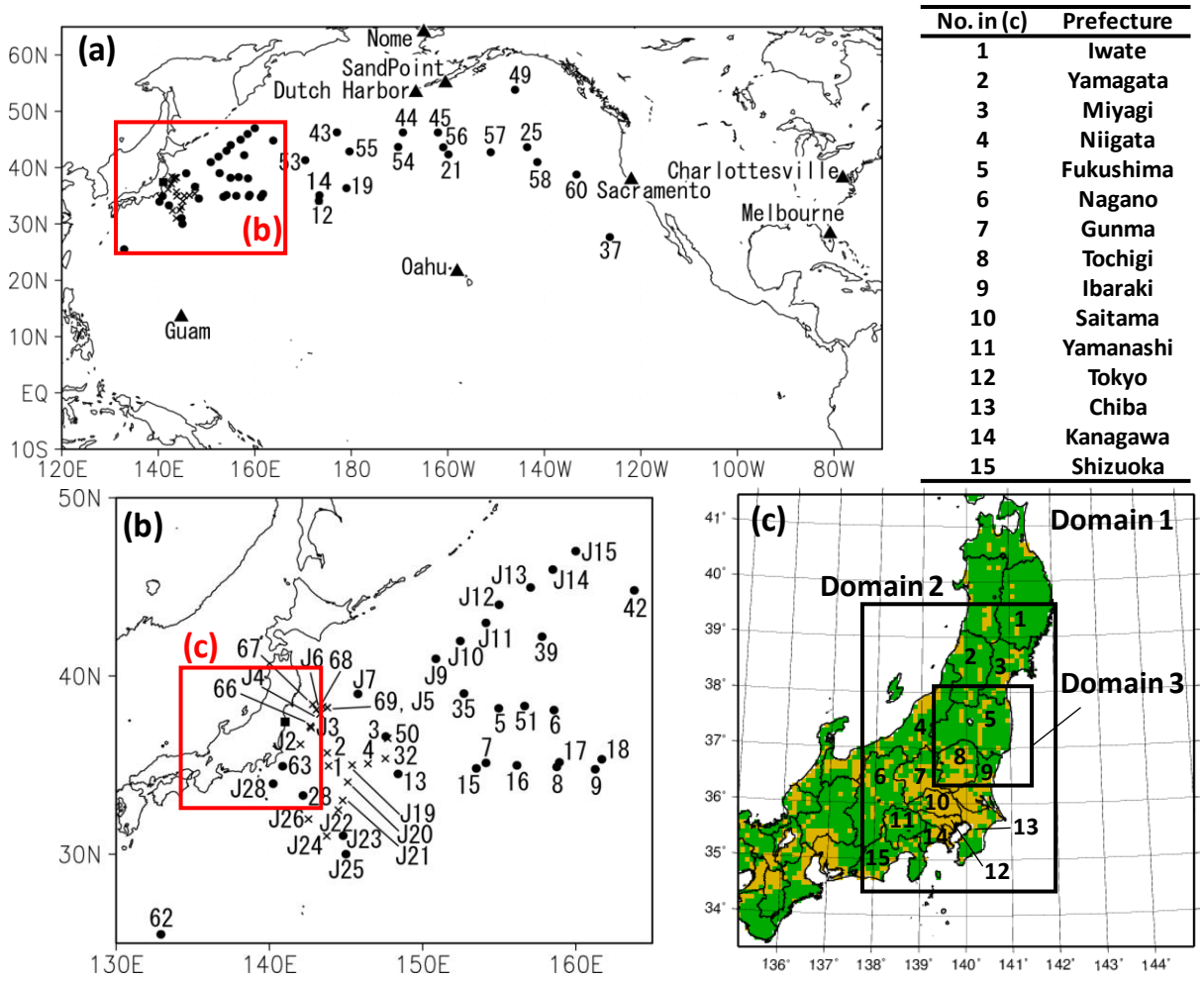

No. in (c)	Prefecture
1	Iwate
2	Yamagata
3	Miyagi
4	Niigata
5	Fukushima
6	Nagano
7	Gunma
8	Tochigi
9	Ibaraki
10	Saitama
11	Yamanashi
12	Tokyo
13	Chiba
14	Kanagawa
15	Shizuoka

Figure 3. The simulation domains for [(a), (b)] the oceanic dispersion and (c) the atmospheric dispersion simulations. The sampling locations of the sea surface concentration data for the source term estimation are plotted in (a) and (b) (black circles), while the sampling points affected by the direct release of radionuclides from the FNPS1 to the ocean were not considered in the reverse estimation (crosses), as indicated by Kobayashi et al. (2013). The prefectures (number) and forest cover (green shaded areas) over East Japan are shown in (c).

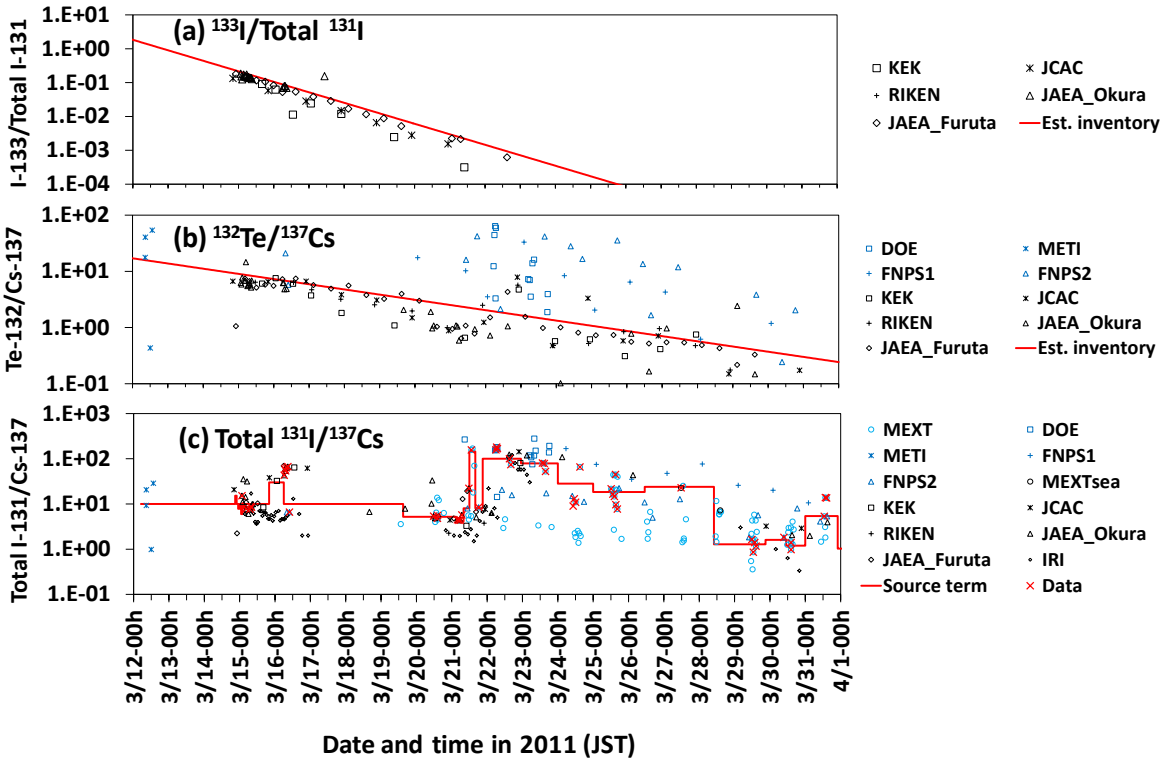

Figure 4. The time series in (a) the ratios of ^{133}I to total ^{131}I, (b) ^{132}Te to ^{137}Cs, and (c) total ^{131}I to ^{137}Cs in atmosphere for the data sampled at each station [blue symbols: METI, FNPS1, FNPS2, MEXT, MEXTsea, and DOE] and at offsite monitoring sites in Eastern Japan [black symbols: JAEA-Tokai, KEK, RIKEN, JCAC, and Tokyo Metropolitan Government (IRI)] from 12-31 March 2011. The red solid lines in (a) and (b) are the curves derived from the inventories and radioactive decay with the value of ^{132}Te/^{137}Cs=20 at the shutdown time. The red solid line in (c) represents the ratio of total ^{131}I to ^{137}Cs for the source term estimated in this study, which is assumed or determined from the data shown as the red symbols in (c).

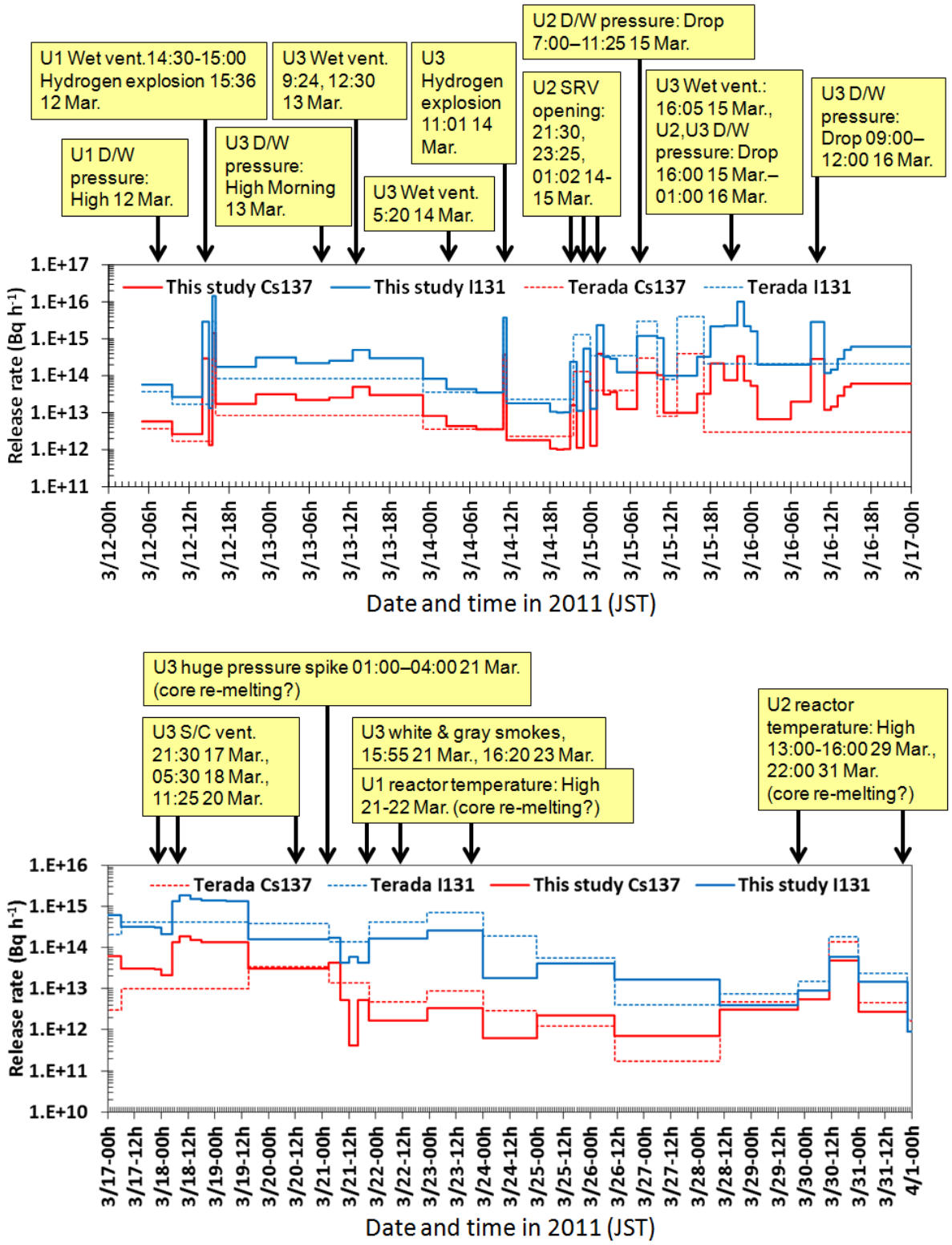

Figure 5. Temporal changes in release rate of total ^{131}I and ^{137}Cs from 12 March to 1 April 2011 reconstructed in this study (solid lines) and Terada et al. (2012) (dashed lines). The recognized events in the reactors (Prime Minister of Japan and His Cabinet, 2011; TEPCO, 2011a; 2012) are shown above the figure.

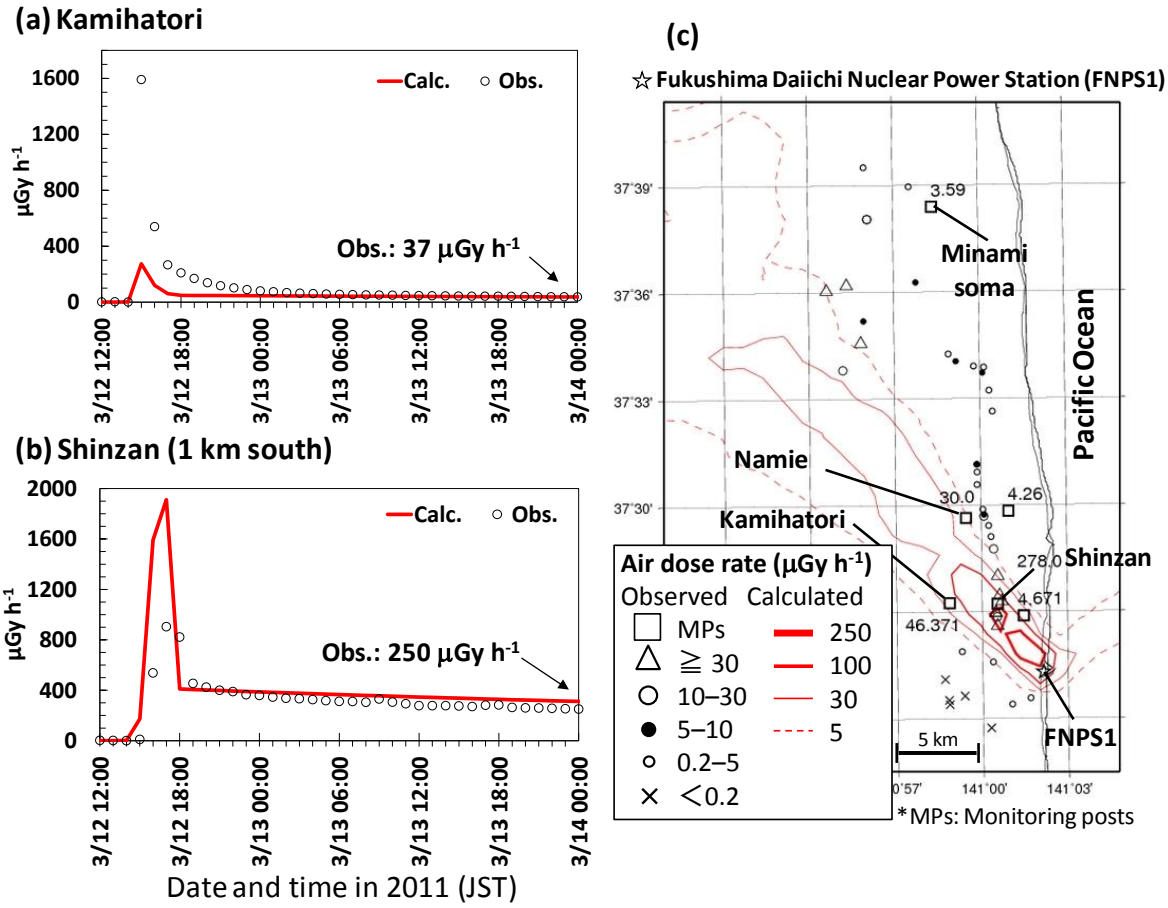

Figure 6. Time series of calculated (solid lines) and observed air dose rates (open circles) at the automated monitoring posts (a) Kamihatori and (b) Shinzan (1-km south of the actual monitoring post of Shinzan), and (c) comparison of the calculated air dose rates at 12:00 on 13 March 2011 in the north-northwest area of the FNPS1 versus measurements from 6:00 to 15:00. In (b), the calculated air dose rate at 1-km south of Shinzan was compared with the observed one because the principal axis of the calculated plume seemed to be several kilometers further west from that of the observed one.

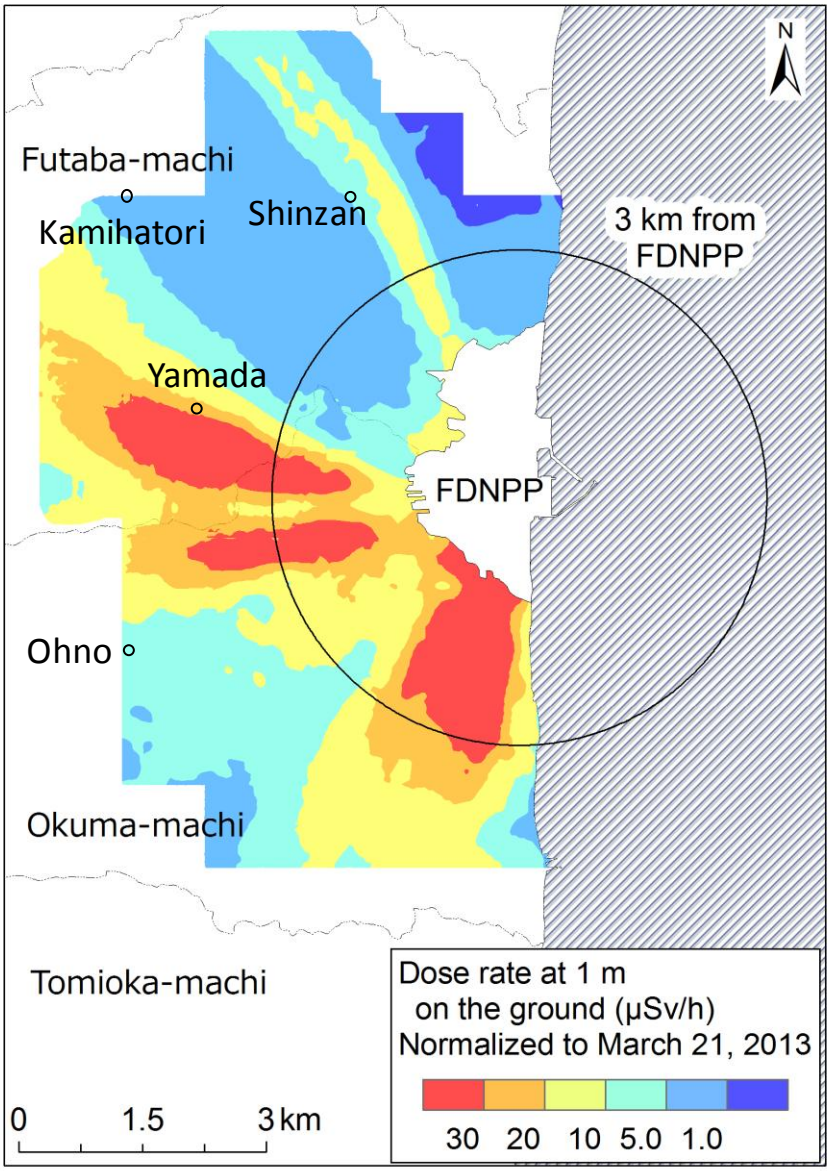

Figure 7. Spatial distributions of the air dose rate within the 5-km area around FNPS1 observed by airborne survey from 28 January to 20 March 2013 (Sanada and Torii, 2014).

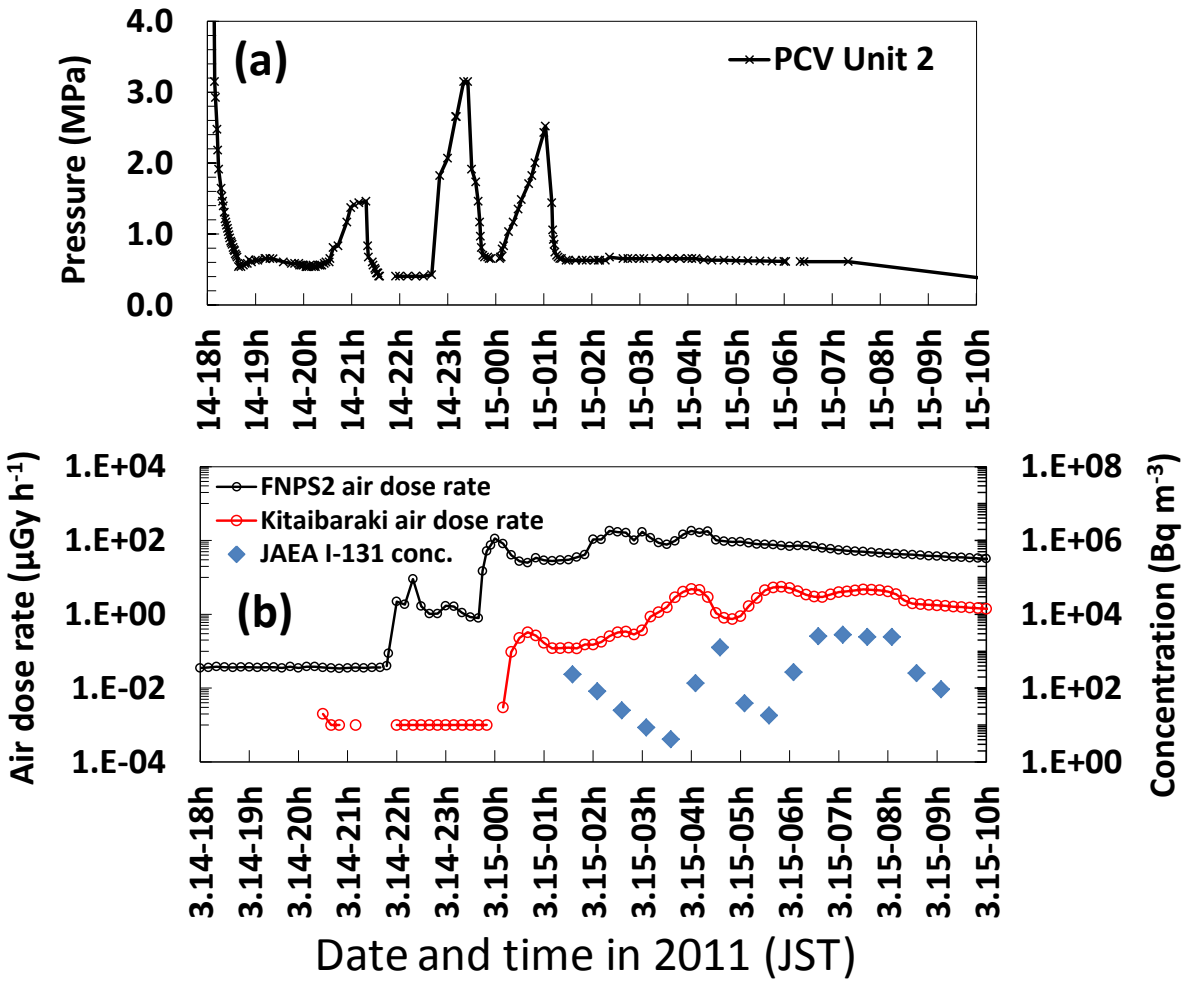

Figure 8. Temporal changes in measurements of (a) the pressures of the reactor pressure vessel (RPV) at Units 2 of FNPS1, and (b) the air dose rates and total ^{131}I concentration at several monitoring posts and JAEA-Tokai, respectively, from 14–15 March. The location of monitoring posts is depicted in Fig. 2.

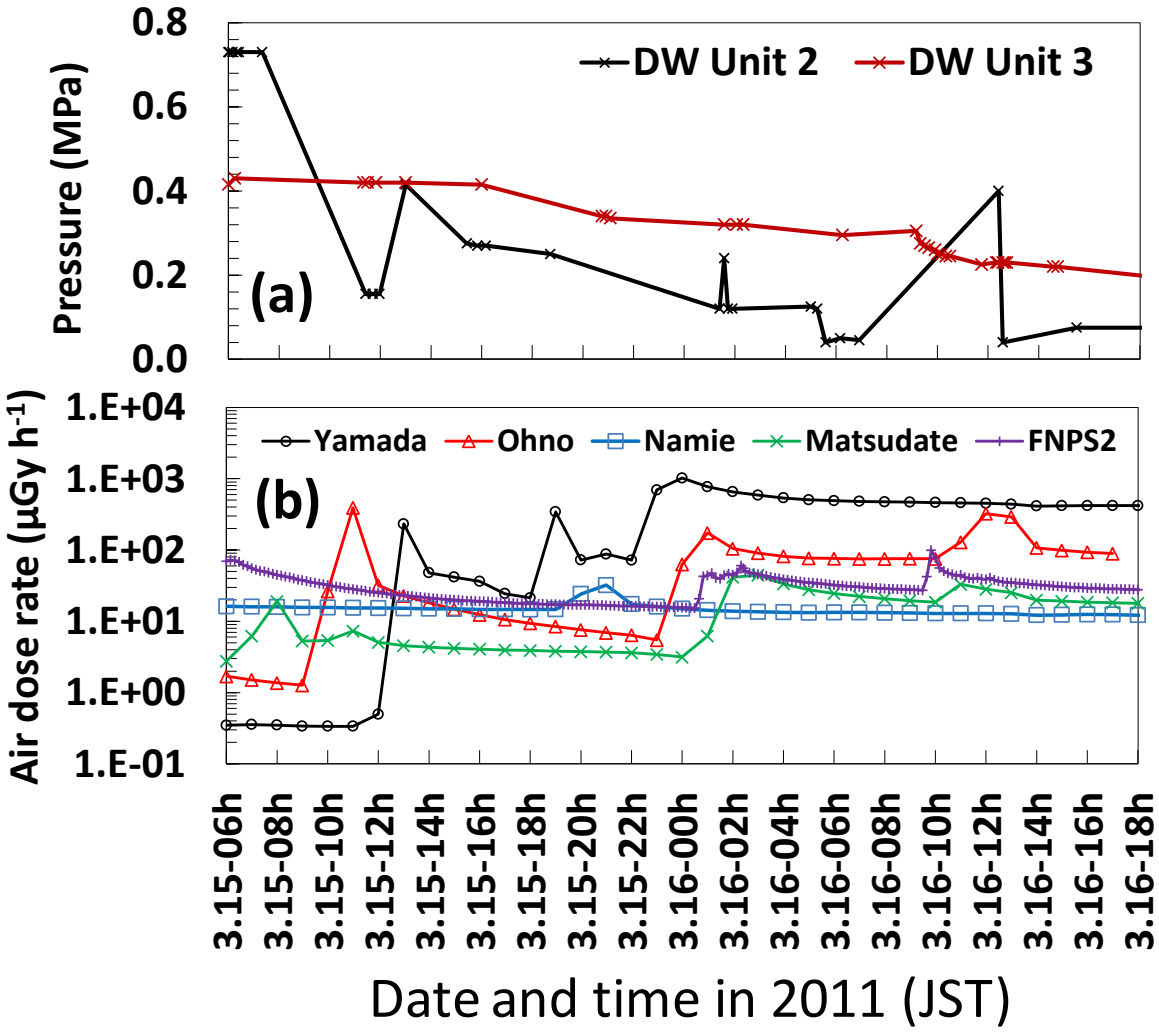

Figure 9. Temporal changes in measurements of (a) the pressures of the drywell (DW) at Units 2 and 3 of FNPS1, and (b) the air dose rates at several monitoring posts from 15–16 March 2011. The location of monitoring posts is depicted in Fig. 2.

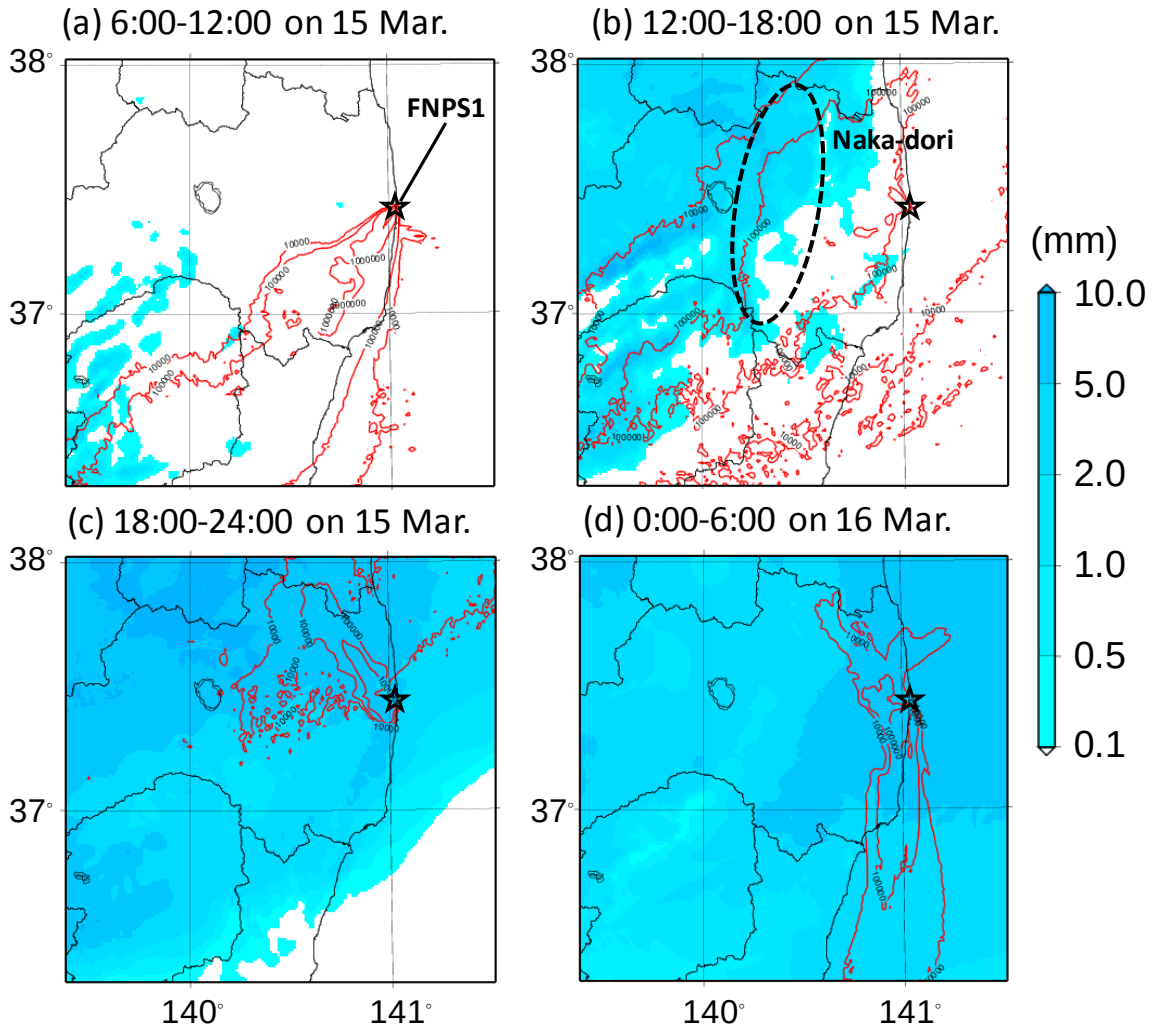

Figure 10. Spatial distributions of the vertical cumulative air concentration of ^{137}Cs (Bq m^{-3}, red contour lines) and precipitation amount (mm, shaded areas) accumulated from (a) 6:00–12:00 on 15 March, (b) 12:00–18:00 on 15 March, (c) 18:00–24:00 on 15 March, and (d) 0:00–6:00 on 16 March calculated by WSPEEDI-II using the new source term. The dashed ellipse in (b) represents Naka-Dori area in Fukushima Prefecture (section 3.4).

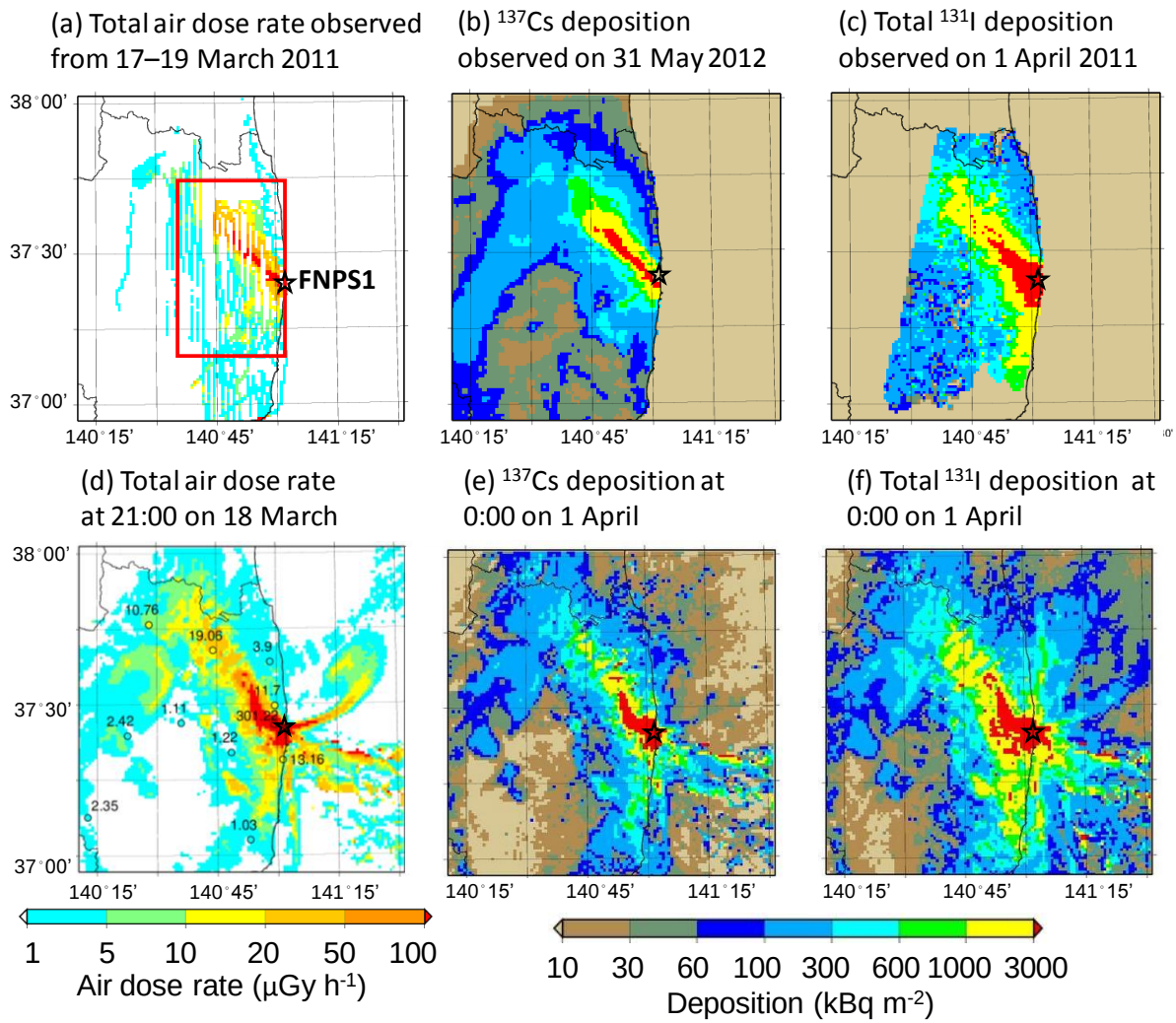

Figure 11. Spatial distributions of [(a), (d)] air dose rates (US DOE/NNSA, 2011), [(b), (e)] ^{137}Cs deposition (NRA, 2012a), and [(c), (f)] total ^{131}I deposition (Torii et al., 2013) comparing [(a)-(c)] the measurements and [(d)-(f)] calculations using the modified WSPEEDI-II with the new source term for Domain 3. The red-colored square in (a) represents the area compared with calculation results in Fig. 16d. Values and colors of circles in (d) represent observed air dose rates at monitoring posts with the minimum significant digit is 0.01.

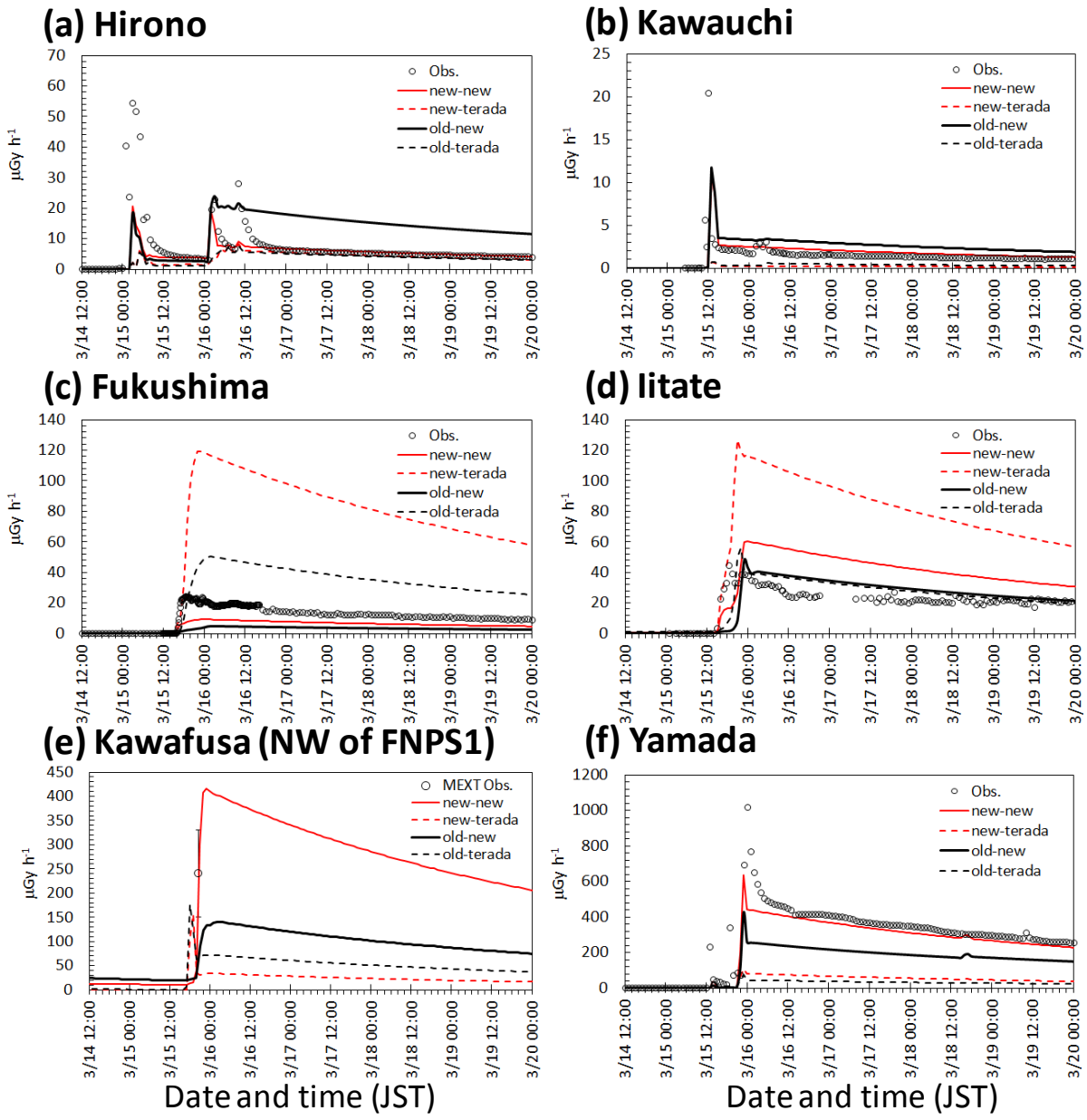

Figure 12. Temporal changes in the air dose rates in Fukushima Prefecture from 15–16 March 2011 in the four simulations using original and modified WSPEEDI-II (referred as "Old" and "New", respectively) and Terada at al. (2012) and the new source terms (referred as "Terada" and "New", respectively). Locations of the monitoring points are shown in Fig. 2. The error bar with observational data in (e) represents the range of values measured by Geiger-Mueller survey meters and ionization chambers at three locations from 20:40–20:50 on 15 March (MEXT, 2011).

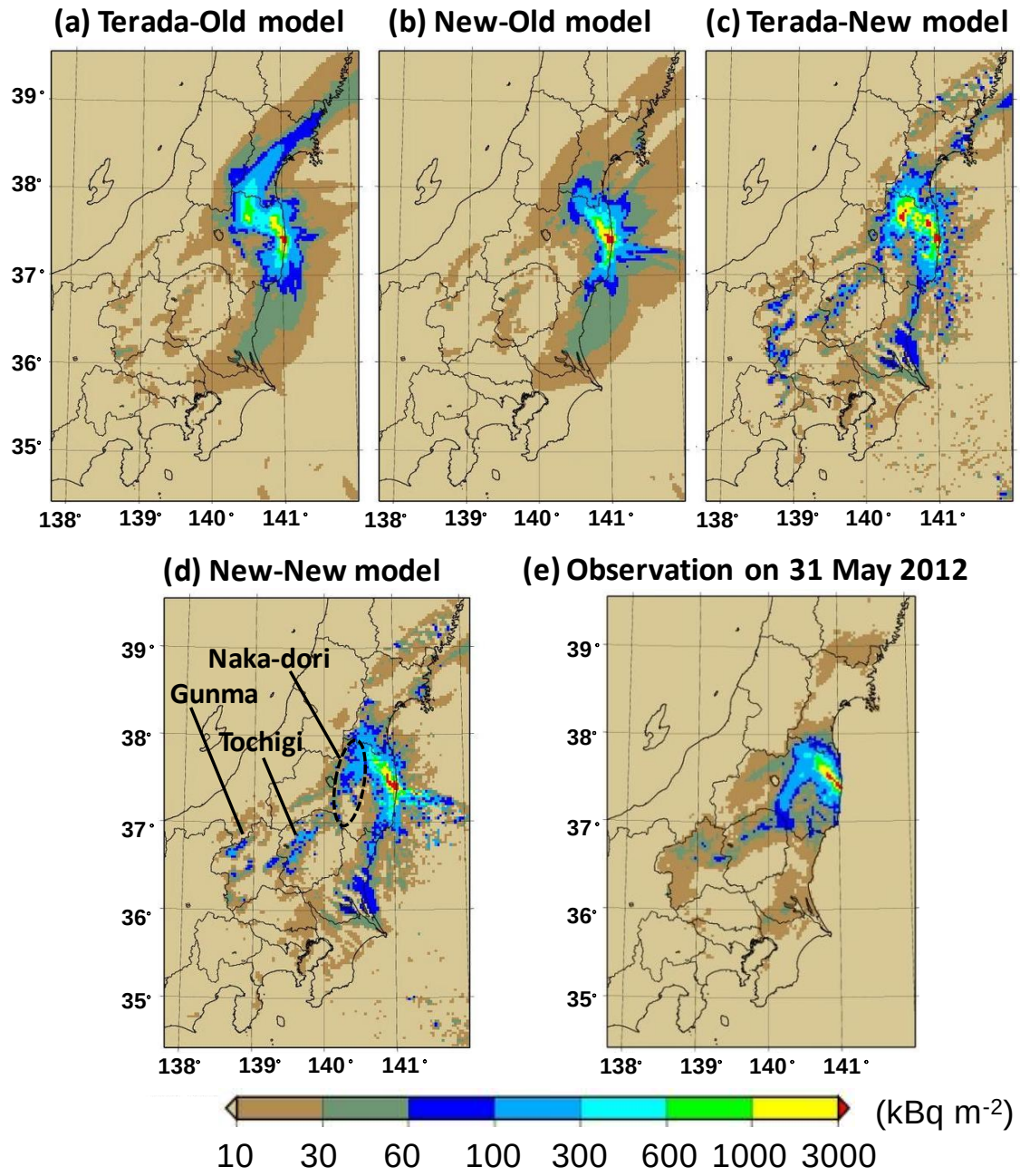

Figure 13. Spatial distributions of surface deposition of ^{137}Cs over East Japan (Domain 2) in [(a)–(d)] the four simulations using original and modified WSPEEDI-II (referred as "Old model" and "New model", respectively) and Terada at al. (2012) and the new source terms (referred as "Terada" and "New", respectively) and (e) observations (NRA, 2012a) and at 0:00 on 1 April 2011. The dashed ellipse in (d) represents Naka-Dori area in Fukushima Prefecture (subsection 4.1.1).

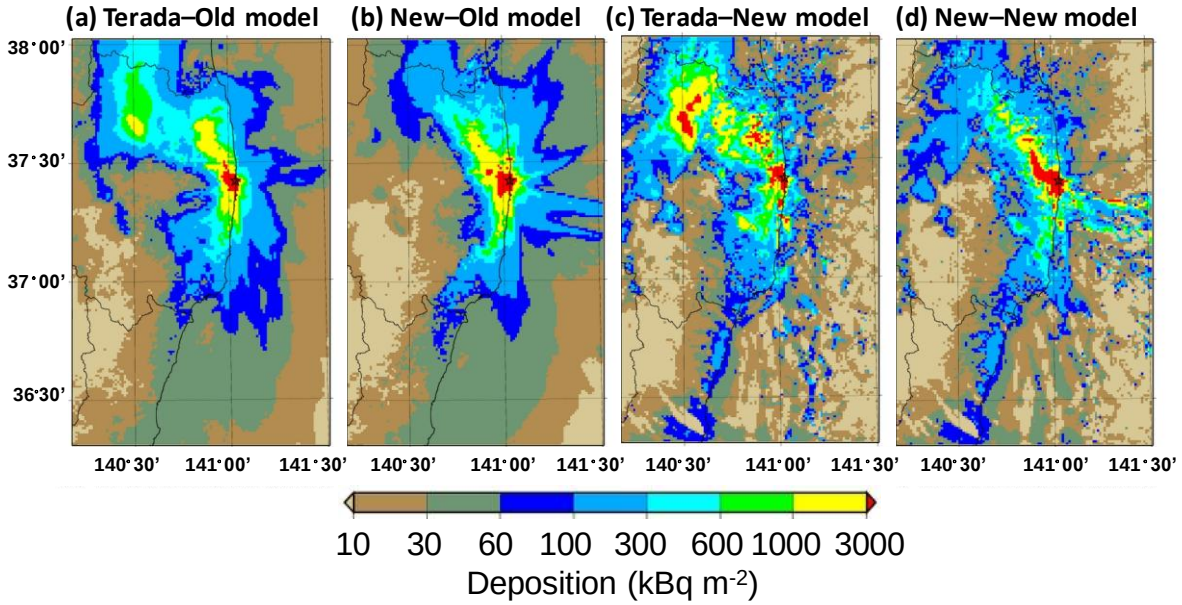

Figure 14. Local-scale spatial distributions of surface deposition of ^{137}Cs (Domain 3) in the four simulations using original and modified WSPEEDI-II (referred as "Old model" and "New model", respectively) and Terada at al. (2012) and the new source terms (referred as "Terada" and "New", respectively) at 0:00 on 1 April 2011.

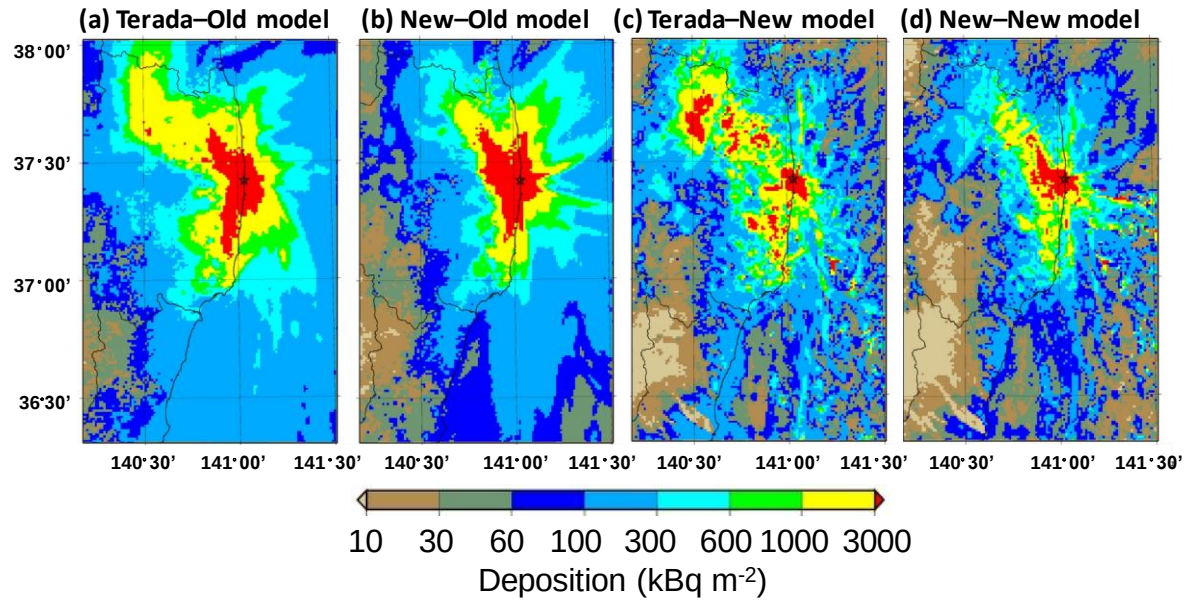

1

2 Figure 15. Local-scale spatial distributions of surface deposition of ^{131}I (Domain 3) in the four
3 simulations using original and modified WSPEEDI-II (referred as "Old model" and "New
4 model", respectively) and Terada at al. (2012) and the new source terms (referred as "Terada"
5 and "New", respectively) at 0:00 on 1 April 2011.

6

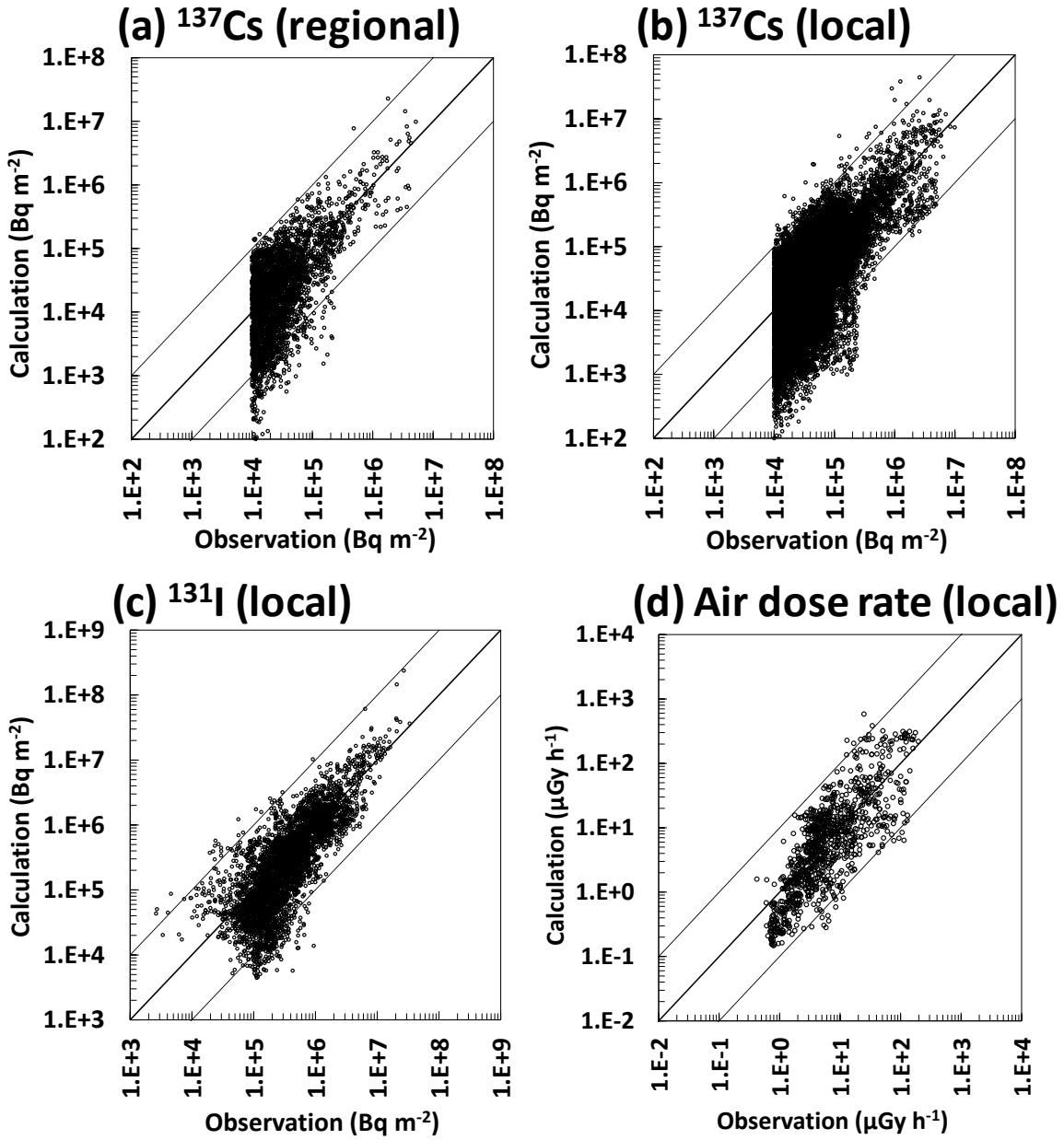

Figure 16. Scatter diagrams of the surface deposition of [(a)–(b)] ^{137}Cs and (c) total ^{131}I (Bq m^{-2}) on 1 April 2011 and of (d) the total air dose rate (μGy h^{-1}) on 18 March 2011 comparing the measurements (US DOE/NNSA, 2011; NRA, 2012a; Torii et al., 2013) and calculations using the modified WSPEEDI-II with the new source term for (a) Domain 2 and [(b)–(d)] Domain 3. The black solid lines show 1:1 correspondence, and the bands within a factor of 10. The region for the air dose rate comparison is depicted in Fig. 11a.

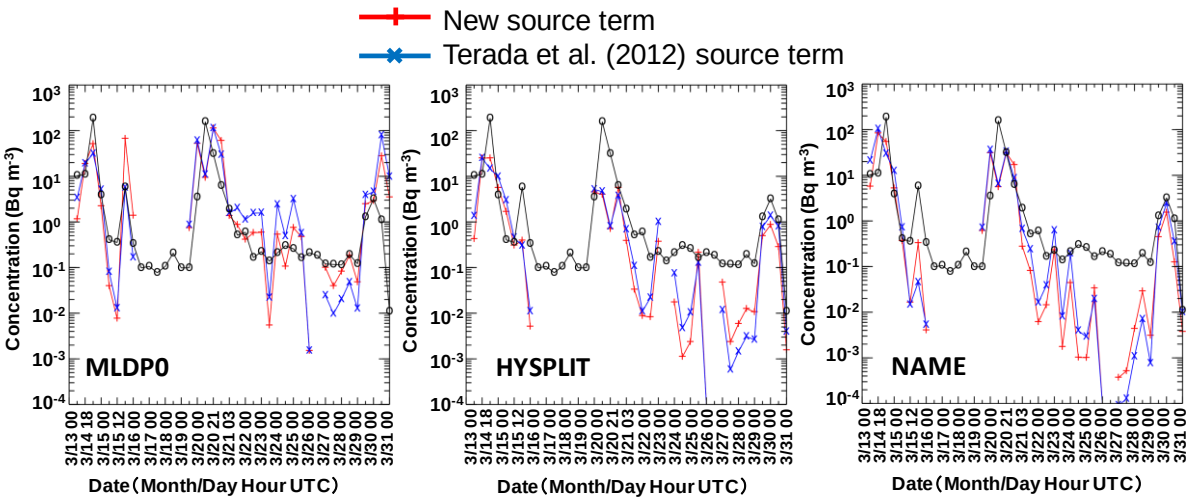

Figure 17. Temporal changes in observed (lines with open circles) and modeled air concentrations (Bq m^{-3}) using three WMO models (MLDP0, HYSPLIT, and NAME) with the source terms of this study (red lines with pluses) and Terada et al. (2012) (blue lines with crosses) for ^{137}Cs at JAEA-Tokai in Ibaraki Prefecture from 13–31 March 2011.

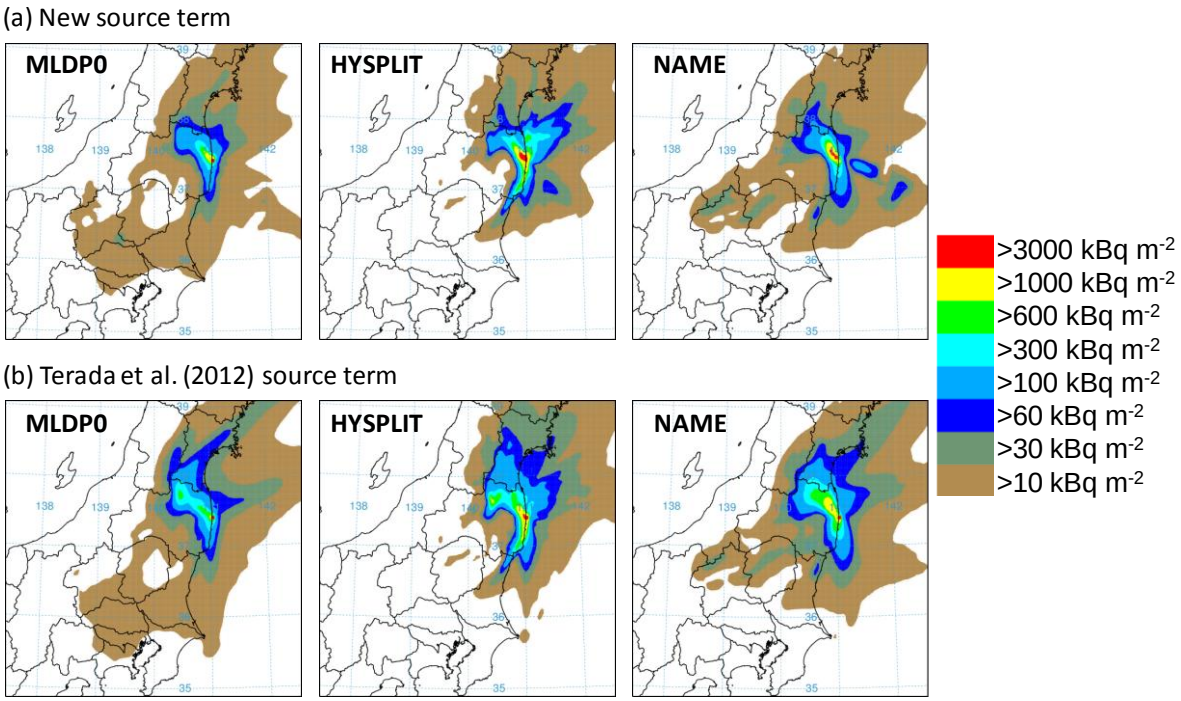

Figure 18. Spatial distributions of surface depositions of ^{137}Cs (kBq m^{-2}) on 1 April 2011 calculated by three WMO models (MLDP0, HYSPLIT, and NAME) using (a) the new source term and (b) Terada et al. (2012).

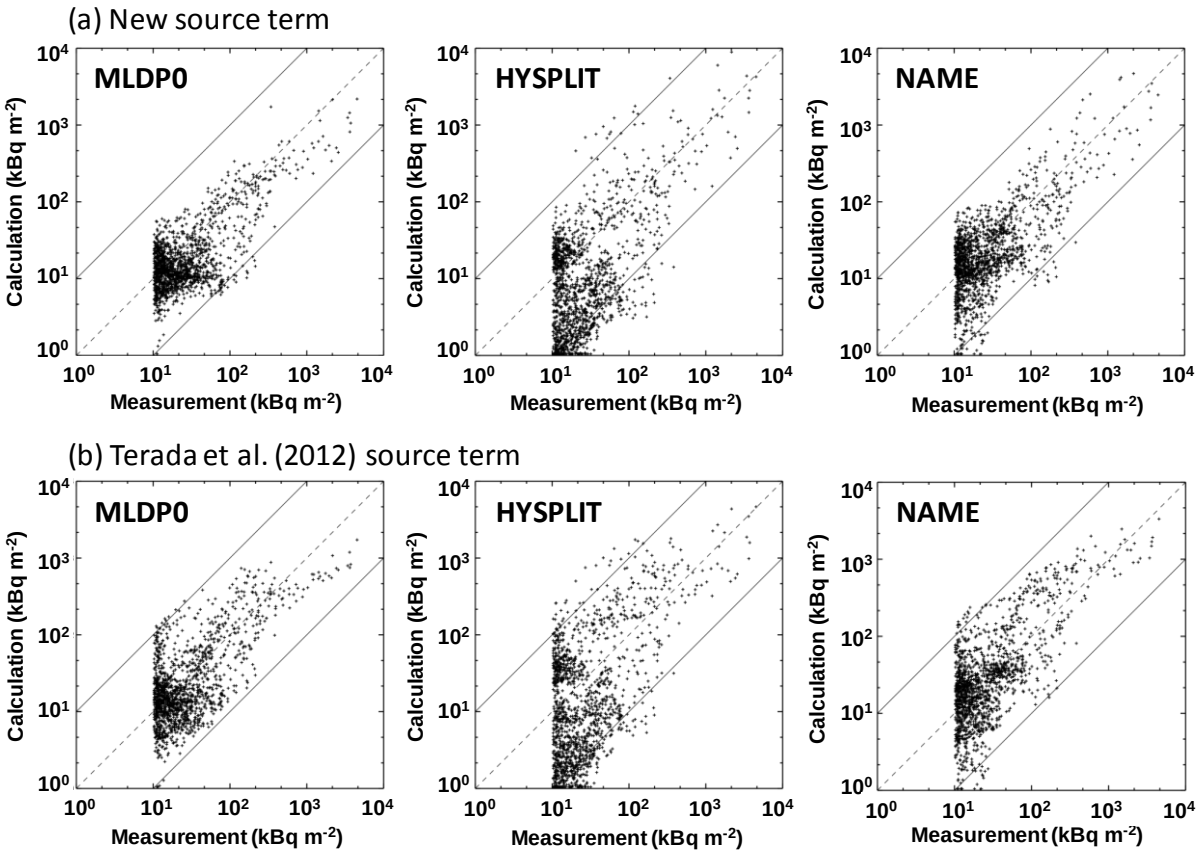

Figure 19. Scatter diagrams of surface deposition (kBq m^{-2}) comparing measurements and calculations using three WMO models (MLDP0, HYSPLIT, and NAME) with the source term of (a) this study and (b) Terada et al. (2012) on 1 April 2011. The black dashed lines show the 1:1 correspondence.

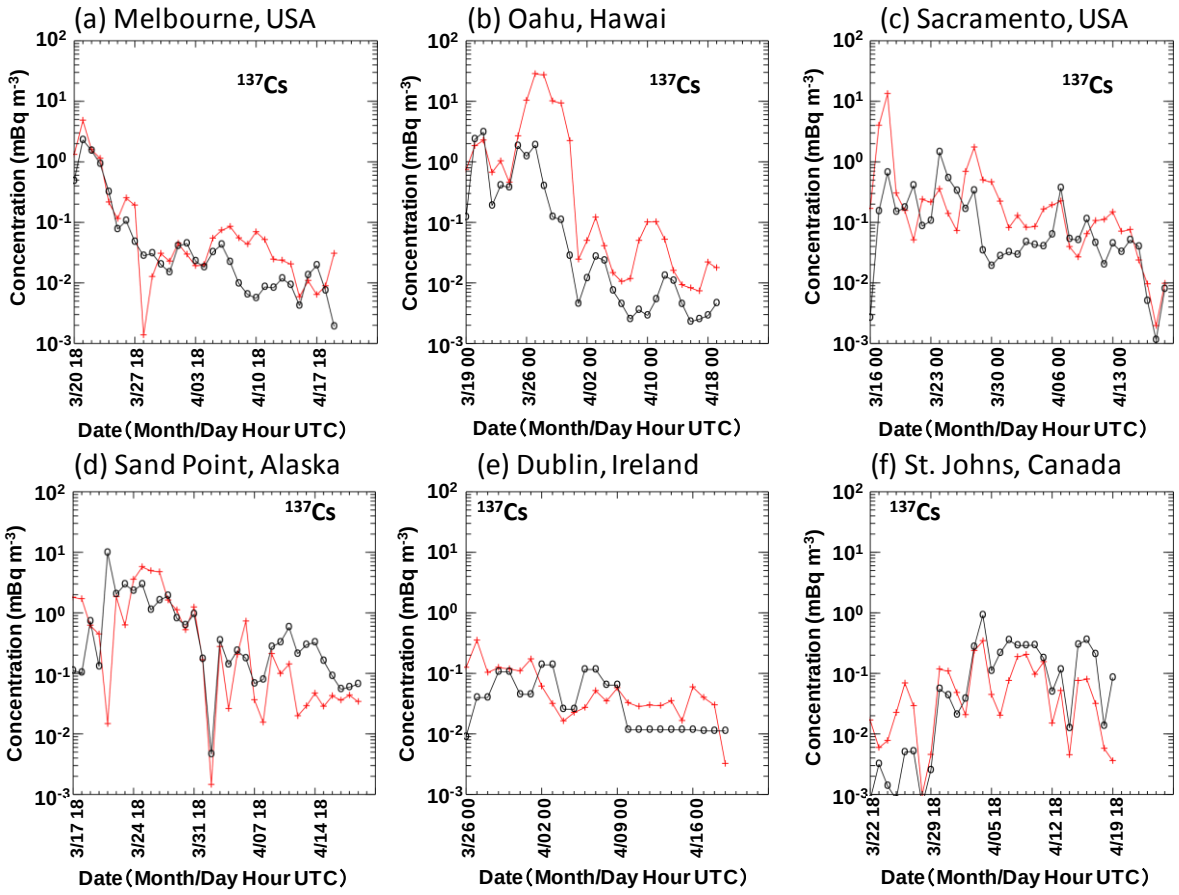

Figure 20. Temporal changes in observed (lines with open circles) and modeled (lines with crosses) air concentrations (mBq m^{-3}) using HYSPLIT with the new source term for air concentration of ^{137}Cs at selected CTBTO, U.S. EPA, and European stations from 13–31 March 2011.

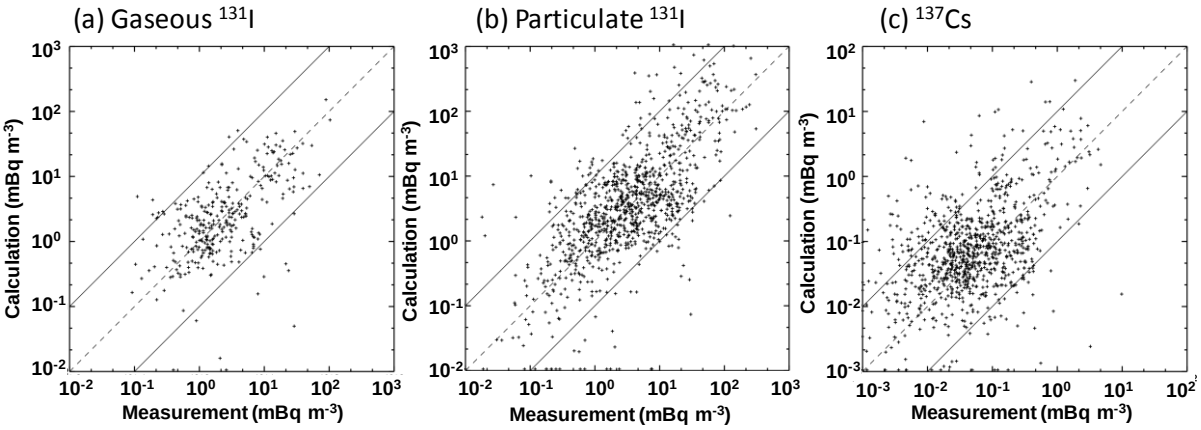

Figure 21. Scatter diagrams of air concentrations (mBq m^{-3}) comparing measurements and calculations using HYSPLIT with the new source term for (a) gaseous and (b) particulate ^{131}I, and (b) ^{137}Cs in the CTBTO, US-EPA, and European monitoring stations for the period of 15 March through 20 April. The black dashed lines show the 1:1 correspondence.

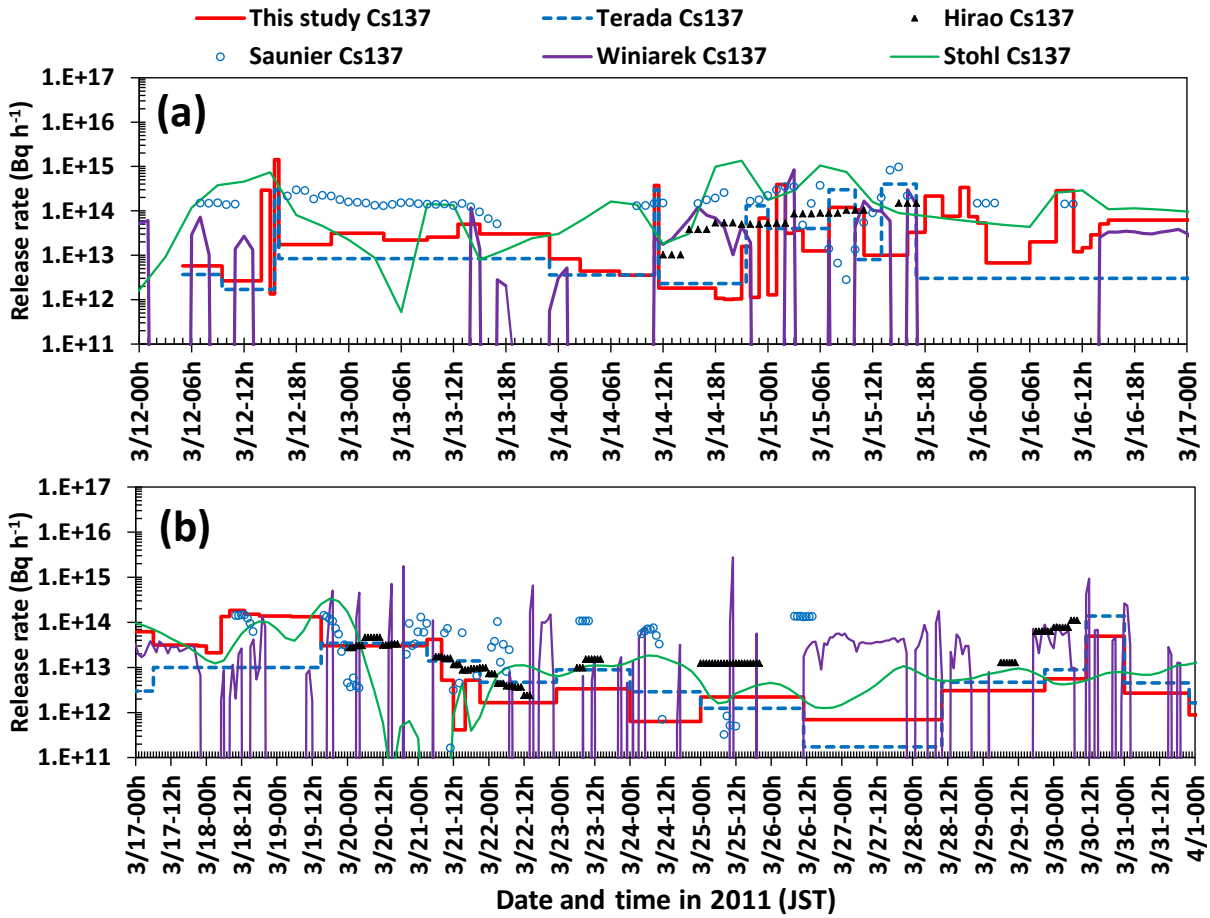

Figure 22. Comparisons of the time varying release rates for ^{137}Cs from 12 March to 1 April 2011 between this study and past studies (Terada et al., 2012; Stohl et al., 2012; Hirao et al., 2013; Saunier et al., 2013; Winiarek et al., 2014). Note that the values of Winiarek et al. (2014) and Stohl et al. (2012) are derived from hourly estimation results using the daily fallout, airborne survey data, and aggregated for all release layers from 0–1000 m, respectively. It is also noted that the release rates of Saunier et al. (2013), when the plume directly flowed to the Pacific Ocean, could not be reconstructed correctly.

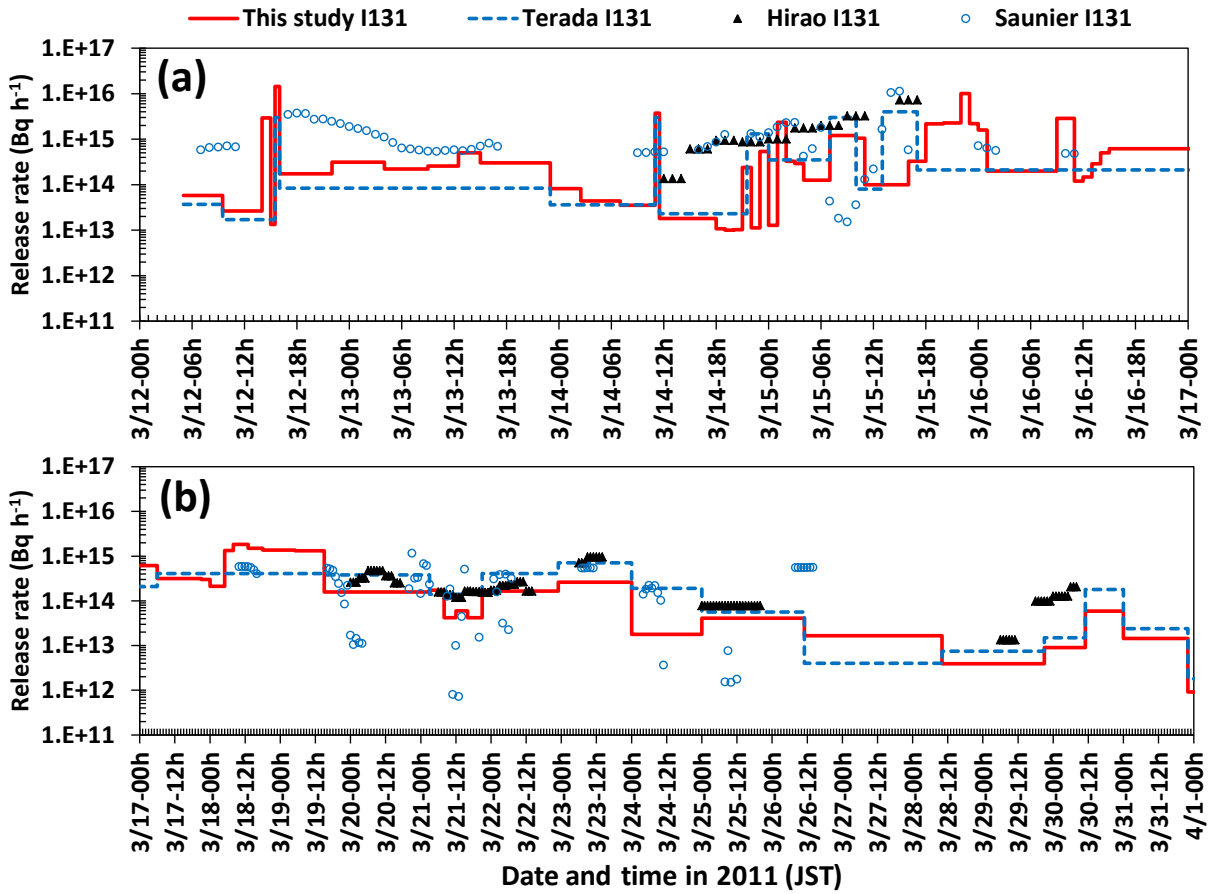

Figure 23. Comparisons of the time varying release rates for total ^{131}I from 12 March to 1 April 2011 between this study and past studies (Terada et al., 2012; Hirao et al., 2013; Saunier et al., 2013). It is noted that the release rates of Saunier et al. (2013), when the plume directly flowed to the Pacific Ocean, could not be reconstructed correctly.

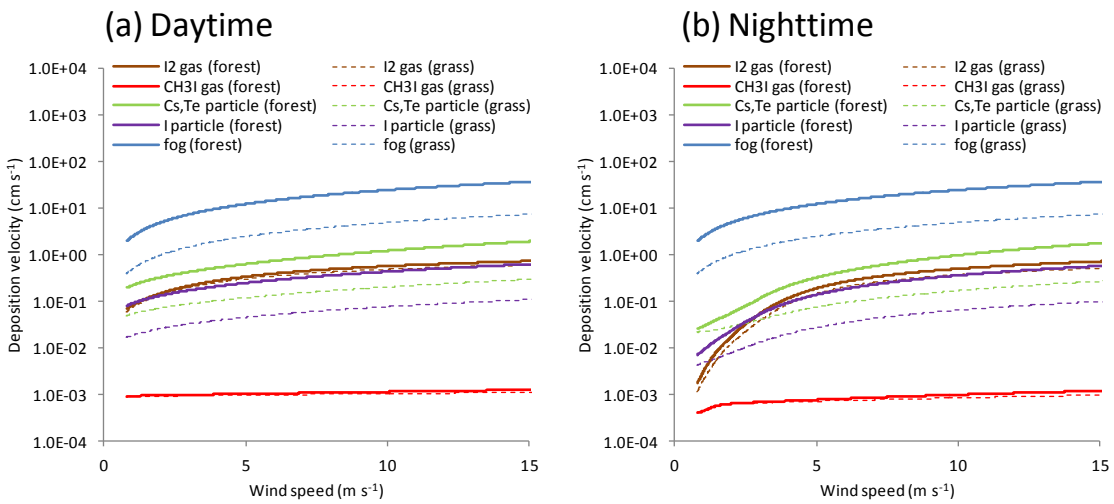

Figure A1. Changes in the modeled deposition velocity (V_d) of gaseous and particulate radioactive substances and of fogwater versus the horizontal wind speed over forest (solid lines) and grassland (dashed lines) surfaces (a) during the daytime and (b) nighttime for typical clear condition. Input meteorological data are mainly from the surface weather stations in Fukushima Prefecture from 12–15 March, 2011 and show the following: 16 and –1.5 °C for air temperature, 21 and –5 °C for ground surface temperature, 800 and 0 W m^{-1} for solar radiation, 30 and 70 % for relative humidity during the daytime and nighttime, respectively.

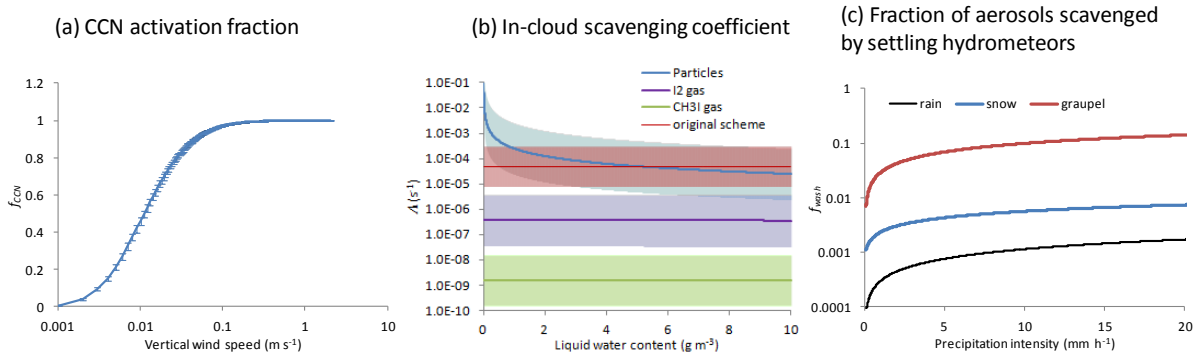

Figure A2. (a) Changes in the CCN activation fraction, f_{ccn}, versus the vertical wind speed, (b) in the modeled in-cloud scavenging coefficient, Λ, of gaseous and particulate radioactive substances versus the vertical mean liquid water content, $\overline{W_L}$ in Eq. (A7), and (c) in the modeled fraction of aerosols scavenged by settling hydrometeors (f_{wash}) for rain, snow, and graupel versus the precipitation rate. Input meteorological data are mainly from the surface weather stations in Ibaraki and Fukushima Prefectures from 12–15 March, 2011 and show the following: 5 °C for air temperature and 950 hPa for air pressure in (a) and (c), and 15 °C for air temperature, 1 km for cloud thickness, 1 mm h^{-1} for precipitation rate with f_{ccn}, f_{ice}, and f_{qc} = 1 in (b). The vertical bars in (a) show the deviation in f_{ccn} when air temperature and pressure were changed from 0–15 °C and 900-1000 hPa, respectively. The shaded areas in (b) represent the range of Λ when precipitation rate changes from 0.1–10 mm h^{-1}.